Phosphorylation of the Smc4 N-terminus regulates DNA binding during condensin-mediated chromosome morphogenesis in *Saccharomyces cerevisiae*

Annahat Singh Kochhar

Thesis submitted to the University of Ottawa
in partial Fulfillment of the requirements for the
Master of Science in Cellular and Molecular Medicine

Department of Cellular and Molecular Medicine
Faculty of Medicine
University of Ottawa

Abstract

Effective transmission of genetic material during mitosis has long been known to be essential for cell survival. A key mitotic regulator in eukaryotes is the condensin complex, responsible for condensing genomic DNA for its equal division between two daughter cells. Importantly, the Smc4 subunit of condensin contains an intrinsically disordered N-terminal region (Smc4-NT) unique to the Smc4 members of the conserved SMC protein family. Deletion of the entire Smc4-NT causes lethality in yeast, suggesting a unique functional role for this region. Our laboratory has previously shown that Smc4-NT phosphorylation by cyclin-dependent kinase 1 (Cdk1) at the onset of mitosis activates condensin function, but the exact role of the Smc4-NT is unknown. We have now established that the Smc4-NT has intrinsic DNA binding activity that is abrogated upon phosphorylation by Cdk1. We have also discovered that the conserved casein kinase 2 (CK2) phosphorylates the Smc4-NT *in vitro* and may serve to inhibit the activity of the Smc4-NT. We established the positive and negative phosphorylation of the Smc4-NT as an important regulator of condensin function.

Acknowledgements

First and foremost, I'd like to sincerely thank my supervisor, Dr. Damien D'Amours, for giving me the opportunity to work in his laboratory. I remember the very first lecture he gave our Cellular Basis of Disease class in the third year of my undergrad. He pulled out a bag of loosely tied pairs of socks and had 2 students reach into the bag without looking to try to pull individual pairs apart: a model for sister chromatid separation during mitotic division. This demonstration and the work being done in his lab inspired me so much that I joined his lab 4 years ago as an undergraduate student for a 6-week rotation and haven't left since. Damien, thank you for always encouraging me to push myself, for teaching me perseverance and focus, for helping me develop my critical thinking and analysis skills, and for truly sparking my passion for science. Working in this lab helped me grow into myself not just as a scientist, but as a person.

A huge thank you as well to my committee members, Dr. Mike Downey and Dr. Marjorie Brand, for their insightful comments and discussions that helped my project take shape. Thank you as well to Dr. Julie St-Pierre for her helpful guidance in statistical analysis. I acknowledge with gratitude that my master's work was supported in part by the CIHR CGS-M scholarship.

I am extremely grateful to all the members of the D'Amours laboratory for helping me through all my ups and downs (of which there were plenty) over the last few years. Thank you all for helping me through my mental breakdowns and giving me pep talks that helped me keep going, for scientific discussions that led to "what is the meaning of life" discussions, and for being the best group of people I've ever had the opportunity to work with. To my bench neighbour, Shamayita Roy, you're the big sister that I never had, thank you for always looking out for me and

keeping me sane. Most notably, thank you to my mentor Alyssa Pastic – I will forever be indebted to you for taking me on as a little undergraduate student with no lab experience. I am the scientist that I am today because of your training, and I won't ever forget it!!

I would not have been able to get through the last few years without the most supportive group of friends and my wonderful family. Manasvita, Krisha, Noor, Petra, Marianne – thanks for always being there for me and for making sure I took the time to be proud of all my little accomplishments. To my brother, Harman, thanks for being my best friend. I always turn to you in happy moments and in sad ones, because you always know exactly what to say to get through to me (even though it sometimes gets on my nerves). To my parents, who inspired me to enter academia, thank you for believing in me when I told you that I wanted to pursue graduate studies. Thank you for giving me every opportunity that you never had, and for encouraging me and supporting me when I didn't have the strength to support myself. You are the reason I have gotten this far and all I've ever wanted to do is make you proud.

Table of Contents

List of Abbreviations

α = alpha

Ade = adenine

AEBSF = 4-(2-aminoethyl) benzenesulfonyl fluoride hydrochloride

ANOVA = analysis of variance

APS = ammonium persulfate

ATP = adenosine triphosphate

β = beta

bp = base pair

BCA = bicinchoninic acid

BPB = bromophenol blue

BSA = bovine serum albumin

BV = bed volumes

Can = canavanine

CAP = chromosome-associated protein

CBX2 = Chromobox protein homolog 2

Cdc = cell division control

Cdk = cyclin dependent kinase

CFTR = cystic fibrosis transmembrane conductance regulator

CK2 = casein kinase 2

Ckb = casein kinase beta subunit

Clb = cyclin B

Cryo-EM = cryogenic electron microscopy

CV = column volume

DNA = deoxyribonucleic acid

dsDNA = double stranded deoxyribonucleic acid

DTT = dithiothreitol

ECL = enhanced chemiluminescence

EDTA = ethylenediaminetetraacetic acid

EMSA = electrophoretic mobility shift assay

FPLC = fast protein liquid chromatography

G1 phase = Gap 1 phase

G2 phase = Gap 2 phase

GSH = glutathione

GST = glutathione S-transferase

H1 = histone 1

H2A = histone 2A

H2B = histone 2B

H3 = histone 3

H4 = histone 4

HCl = hydrochloric acid

HEAT (repeat) = Huntingtin, elongation factor 3, A subunit of protein phosphatase 2A, TOR1

HEPES = 4-(2-hydroxyethyl)-1-piperazineethanesulfonic acid

HIS = histidine

H_2O = water

HPLC = high-performance liquid chromatography

HRP = horseradish peroxidase

IDPR = intrinsically disordered protein region

Ipl = increase in ploidy

IPTG = isopropylthio-β-galactoside

K = lysine

KCl = potassium chloride

K_D = dissociation constant

kDa = kiloDalton

KH_2PO_4 = potassium phosphate monobasic

K_2HPO_4 = potassium phosphate dibasic

L = leucine

LB = lysogeny broth

LC-MS/MS = liquid chromatography with tandem mass spectrometry

Leu = leucine

LMP = low melting point

mAU = milli absorbance unit

$MgCl_2$ = magnesium chloride

mg/mL = milligrams per milliliter

mL = millilitre

mM = millimolar

MOPS = 3-(N-morpholino)propanesulfonic acid

M phase = mitosis phase

MW = molecular weight

MWCO = molecular weight cut-off

NaCl = sodium chloride

Na_2HPO_4 = disodium phosphate

ng = nanogram

Ni-NTA = nickel-nitrilotriacetic acid

NLS = nuclear localization signal

nm = nanometres

nt = nucleotide

OD = optical density

ORC = origin recognition complex

ORF = open reading frame

P = proline

PAGE = polyacrylamide gel electrophoresis

PBS = phosphate-buffered saline

PCR = polymerase chain reaction

pH = potential hydrogen

PK buffer = protein kinase buffer

PP = protein phosphatase

Psmc4 = *SMC4* promoter

PTM = post-translational modification

PVDF = polyvinylidene difluoride

R = arginine

rDNA = ribosomal deoxyribonucleic acid

RNA = ribonucleic acid

RPM = revolutions per minute

RxL = arginine-any amino acid-leucine

S = serine

SC- = synthetic complete

SDS = sodium dodecyl-sulfate

SEC = size-exclusion chromatography

SMC = structural maintenance of chromosomes

Smc4-NT = Smc4 N-terminus

S phase = synthesis phase

ssDNA = single-stranded deoxyribonucleic acid

STII = Strep-tag

T = threonine

TADH1 = alcohol dehydrogenase 1 terminator

TAE = Tris base, acetic acid, EDTA

TBS = Tris-buffered saline

TBS-T = Tris-buffered saline Tween-20

TCA = trichloroacetic acid

TEMED = N,N,N′,N′-Tetramethylethylenediamine

TEV = Tobacco Etch virus

Tris = tris(hydroxymethyl)aminomethane

Trp = tryptophan

Tsmc4 = *SMC4* terminator

URA = uracil

v/v = volume/volume

w/v = weight/volume

X = any amino acid

YEP = yeast extract peptone

YEPD = yeast extract peptone dextrose

YPA = yeast extract peptone adenine

YCplac = yeast centromeric plasmid

YIplac = yeast integrative plasmid

$Zn(NO_3)_2$ = zinc nitrate

Zn^{2+} = zinc

µg = microgram

µg/mL = micrograms per millilitre

µM = micromolar

µL = microlitre

List of Figures

List of Tables

Introduction

The cell cycle

It has long been known that the transmission of genetic material from parent to progeny cells, a process that is essential for survival, occurs via compaction of amorphous chromatin and segregation of resulting chromosomes (1). This observation was first accurately described by Walther Flemming in 1882, who observed the emergence of "threadlike" structures he dubbed "chromatin", followed by the breakdown of the nuclear envelope and scaffolding (2). He described the separation of the "threads" into two groups, followed by the reforming of the scaffolding of the nuclei, a process he named "mitosis" (3). The cell cycle has been the target of countless studies since Flemming's fateful discovery. Although chromosome condensation is an early cytological landmark of the mitotic process, the exact mechanism by which it occurs eludes scientists to this day (4, 5).

Eukaryotic cells undergo a cycle consisting of 4 phases: G1 (gap 1), S (synthesis), G2 (gap 2), and M (mitosis) (6) (Figure 1). Briefly, during G1, generally the longest phase of the cell cycle, the cell is biochemically active and undergoes extensive growth, despite little visual change under a microscope (7). Importantly, at this stage, the cell evaluates its environment to determine if conditions are favourable for mitosis. If the cell determines that conditions are unfavourable, it exits the cycle and enters a stage called G0, during which the cell cycle is arrested until a further signal initiates re-entry into mitosis (8). Otherwise, the cell moves on to S phase, during which DNA replication occurs, and the cell duplicates its centrioles in preparation for cell division (9). In the last phase before mitotic division, the G2 phase, the cell makes final preparations to divide by duplicating organelles and other protein machinery that will be essential for chromosome manipulation (10). The cytoskeleton is also dismantled. In yeast, this phase is quite short and often

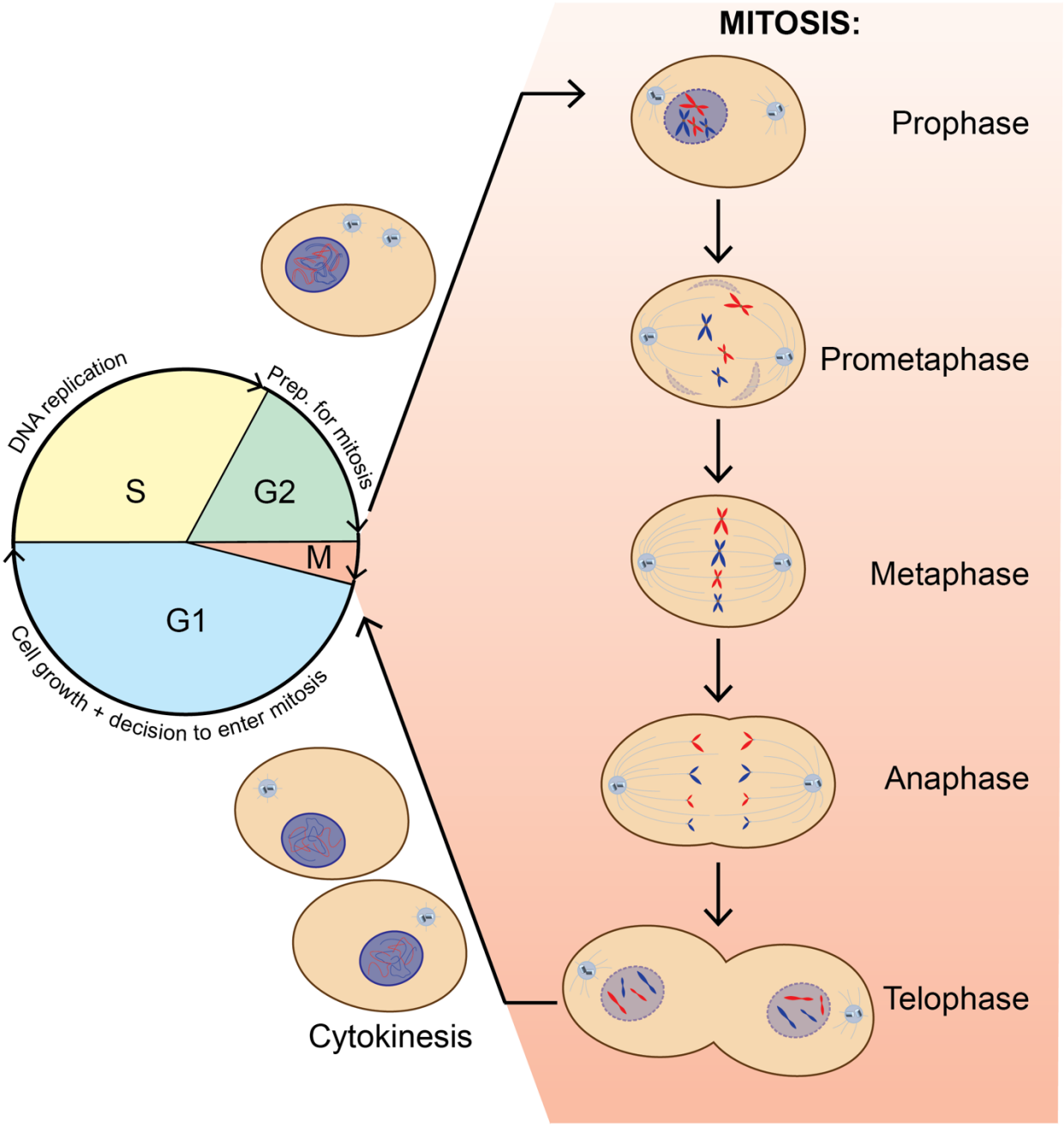

Figure 1. The eukaryotic cell cycle. Graphical representation of the approximate durations of different stages of the cell cycle in a typical human cell (left) and depiction of the major cytological changes during each stage of mitosis (right).

blurs with the M phase of the cell cycle (11).

Finally, the mitotic phase of the cell cycle is the stage during which the cell divides into two identical daughter cells. Mitosis consists of the following stages [reviewed in (12, 13)]:

Prophase: The nuclear envelope begins to break down and chromatin begins to condense to form visible chromosomes. Centrosomes begin to move towards opposite ends of the cell.

Prometaphase: The nuclear envelope completes breakdown and microtubules begin binding to kinetochores of the centromere that connects sister chromatids.

Metaphase: Centrosomes complete their migration to opposite poles of the cell and chromosomes are aligned at the metaphase plate in the center of the cell. All chromosomes are attached to microtubules by their kinetochores.

Anaphase: The sister chromatids are separated and migrate towards opposite poles, led by mitotic spindles. By the end of this stage, both bodies that will form daughter cells contain an equal number of chromosomes.

Telophase: The nuclear envelope begins to reform, now consisting of 2 separate envelopes around two daughter cells with equivalent genetic material. Spindle microtubules begin to depolymerize and chromosomes de-condense to return to chromatin form. All other cell organelles begin to reappear.

Cytokinesis: The cytoplasm divides to pinch off into 2 identical daughter cells. With the completion of this last stage, the cell cycle recommences.

Interphase chromatin

During interphase, DNA of about 147 bp in length wraps around core histones (2 each of H2A, H2B, H3 and H4) to form nucleosomes about 10nm in diameter (14). Nucleosomes are linked together by small segments of linker DNA, giving the appearance of “beads on a string” (15). Histone H1 binds to the entry and exit sites of DNA on the surface of the nucleosomal core to further stabilize the particle (16). Regions of low gene expression can be further compacted by

histone modifications that allow certain regions to be held closer together (17). RNA has also been shown to interact with histone tails to neutralize their charges and reduce the electrostatic compaction of DNA, promoting open chromatin and increased gene expression (18). It has been proposed that nucleosomes are further compacted via histone tail and RNA interactions to form 30nm diameter fibers, though due to lack of *in vivo* evidence, it has been posited that these forms may be rare in intact chromatin (19). Beyond this point, while it is known that several proteins are implicated in binding and further compacting chromatin, the specifics are still not fully understood (Figure 2).

Mitotic chromosomes

Attempting to equally divide spools of chromatin between daughter cells would be like trying to divide a bowl of spaghetti into 2 exact portions – extremely complex and prone to misdistribution. A myriad of different diseases are characterized by erroneous chromosome segregation, reaffirming the importance of chromosome compaction ahead of segregation to ensure sustainable growth and development of organisms (20). During mitosis, chromatin is compacted into visible, rodlike structures of genetic material called chromosomes, that are divided equally between daughter cells (21). The general structure of a chromosome consists of two condensed, replicated halves of the cell's genetic content, called sister chromatids, held together by a point of attachment called the centromere (1) (Figure 2). After the core histones that make up the majority of chromatin scaffolding, the most abundant protein enriching chromosomal regions is a protein complex called condensin (22). While thousands of proteins have been shown to associate with mitotic chromosomes, condensin and topoisomerase II are indispensable for chromatid assembly in eukaryotic cells (23). Even in the absence of nucleosomes, condensin and

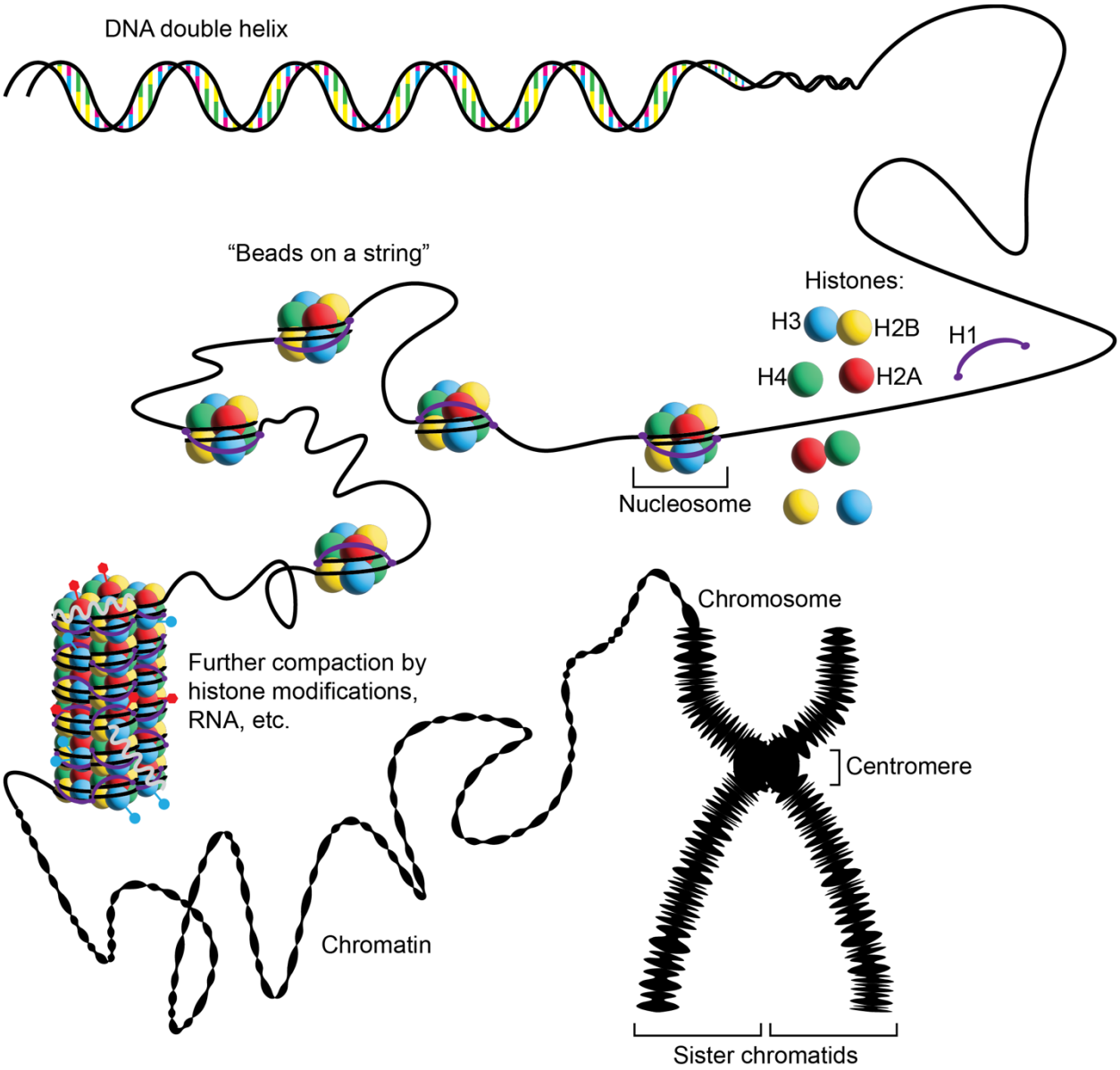

Figure 2. Levels of DNA compaction in eukaryotic cells. Simplified graphical representation of the levels of compaction of the DNA double helix backbone that lead to the formation of visible chromosomes.

topoisomerase II are able to form mitotic chromatid structures, albeit with slightly diffuse formations (24).

Identification of condensin

The study of mitotic chromosomes was limited for a long time due to their fragile structure

that is easily perturbed when isolated from an *in vivo* system (25). Condensin was first identified through the reconstitution of mitotic chromosomes using *Xenopus laevis* egg extracts in a cell-free environment. The use of this *in vitro* system permitted the identification of 8s condensin, consisting of a heterodimer formed by XCAP-C and XCAP-E (Xenopus Chromosome-Associated-Polypeptides) (23). Further studies using this cell-free model resulted in the identification of 13s condensin, consisting of the previously identified heterodimer plus three additional subunits (26). Condensin is a pentameric, highly conserved ATPase that has been shown to associate with chromatin to alter its configuration during the cell cycle (23, 27). Condensin belongs to the Structural Maintenance of Chromosomes, or SMC, family of proteins, which also includes cohesin and the Smc5/6 complex. Together, SMC proteins play different roles in the maintenance of genomic integrity [reviewed in (28–30)].

Condensin structure

The general architecture of SMC proteins consists of two SMC subunits that are joined by three regulatory subunits to form a ring-like structure [reviewed in (28)]. In condensin, the SMC subunits are referred to as Smc2 and Smc4 in yeast, or hCAP-E and hCAP-C in humans, respectively (31, 32) (Table 1). The Smc2/Smc4 subunits heterodimerize, with their respective N- and C- terminal segments pairing together to form ATPase head domains that are important for regulating condensin's turnover on chromosomes (23, 26). Antiparallel coiled-coil regions separate the ATPase head domain region at one extremity of the heterodimer from a "hinge" domain at the other end (33, 34). A kleisin subunit bridges the ATPase head domains together to form the central ring structure and recruits 2 additional HEAT repeat subunits (35–37). In yeast, the kleisin subunit is known as Brn1 and the HEAT repeat subunits are Ycs4 and Ycg1 (31) (Figure 4A).

Table 1: Overview of condensin subunits in different species.

	S. cerevisiae	*S. pombe*	Vertebrates, including *H. sapiens*
SMC subunits	Smc2	Cut14	CAP-E
	Smc4	Cut3	CAP-C
Kleisin	Brn1	Cnd2	CAP-H (I) CAP-H2 (II)
HEAT repeat subunits	Ycs4	Cnd1	CAP-D2 (I) CAP-D3 (II)
	Ycg1	Cnd3	CAP-G (I) CAP-G2 (II)

Loop extrusion model

Initial work on condensin hypothesized that condensin made up part of a scaffold that anchored DNA loops on top of each other to permit compaction. As structural and functional analyses of condensin progressed, alternate theories proposed that condensin functioned as a stochastic crosslinker between different 10nm fibres of chromatin (28). However, mathematical modelling predictions and emerging Hi-C data started to point towards a "loop extrusion" model of chromosome condensation, which is currently the most widely accepted model of condensin function (19). During loop extrusion, DNA is thought to be pulled through the condensin ring structure to create compact loops that progressively stack on top of each other to form condensed chromosomes (38). Polymer dynamics simulations have shown that ATP hydrolysis by condensin provides the motor activity it requires to translocate along DNA substrates moving in relation to each other, fulfilling the key expectation of the loop extrusion model (39). Molecular dynamics simulations of a coarse-grained polymer model have shown that both loop formation and inter-condensin interactions must be carefully co-regulated to achieve active mitotic chromosome assembly (40).

A big breakthrough supporting the loop extrusion mechanism of condensin came through the development of single molecule loop extrusion assays using *S. cerevisiae* condensin. By

tethering both ends of a fragment of dsDNA to a passivated surface flushed with condensin and ATP, researchers observed the local compaction of DNA. No compaction was observed with ATPase defect condensin mutants or in the absence of ATP, reaffirming that ATP hydrolysis is required for condensin loop creation and is the rate limiting step in loop extrusion (41). These assays initially proposed that loop extrusion occurs in a one-sided, asymmetric fashion, with one site in condensin remaining stably anchored to DNA (Figure 3A). However, this assumption could not explain the different forms of chromosome compaction that have been observed across all organisms. Condensin was later shown to act in a two-sided manner to remove unlooped chromatin gaps, forming an "effectively two-sided" model (42) (Figure 3B). Additionally, condensins were shown to influence each others' function in budding yeast, even if individual loops produced were not proximally located (43) (Figure 3C). While these experiments studied condensin function at a local level, this local activity is responsible for global chromosome conformation changes (40–42, 44). Loop extrusion has been shown to be the primary method of DNA organization in a cellular context, with this process being regulated in a cell cycle-dependent manner (45). The presence of nucleosomes or other DNA binding molecules may serve to prevent the reverse reaction/slippage of DNA, without contributing directly to DNA compaction (44).

Condensin I vs. II

Vertebrates are known to possess two types of condensin complexes, condensin I and II, whereas invertebrates possess only one condensin complex homologous in structure and function to condensin I (46). While it was initially proposed that condensin II evolved from condensin I in higher eukaryotes, lineage mapping has since shown that several species independently lost condensin II throughout evolution (29). Even bacteria and archaea possess a "condensin-like"

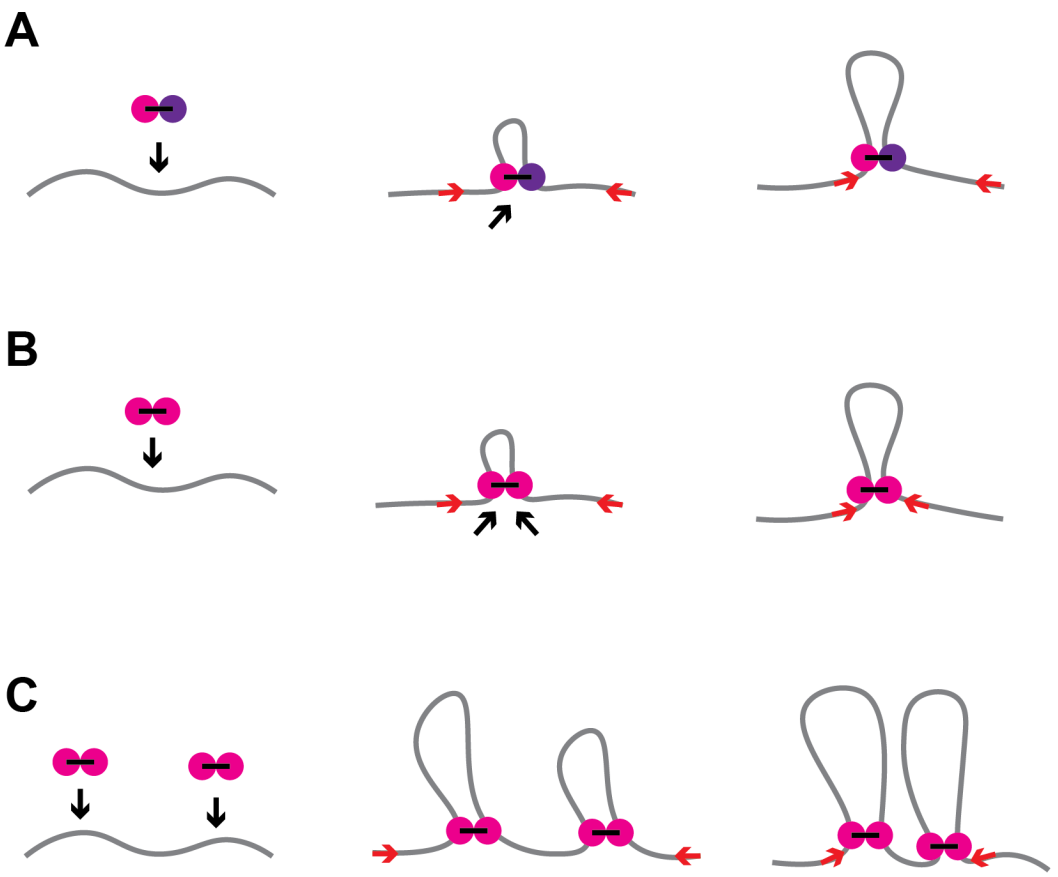

Adapted from Banigan et al., 2020

Figure 3. Proposed mechanisms of loop extrusion. Grey lines represent DNA. **(A)** One-sided model of loop extrusion, where one side of condensin (purple) remains firmly anchored to DNA, while the other side (pink) freely translocates along the DNA backbone. **(B)** Two-sided model of loop extrusion, where both sides of condensin translocate along DNA as needed to resolve unlooped structures. **(C)** Neighbouring condensins can influence each other's function and work together to extrude DNA in what appears to be a "two-sided" mechanism.

cellular structure composed of 3 subunits (47). Researchers have proposed that condensin I acts to laterally compact chromatin loops, whereas condensin II establishes the chromosome axis (48). This would suggest that the behaviours of condensins I and II are spatiotemporally regulated *in vivo* (24). Importantly, the loss of any condensin subunit inhibits chromosome condensation to a varying degree in any organism studied to date (49–51). In lower eukaryotes, this is generally characterized by a complete lack of chromosome morphogenesis, whereas higher eukaryotes tend

to experience a delay in chromosome reorganization that does not generate functional chromosomes (52).

Spatiotemporal regulation of condensin

Cellular localization of condensin complexes seems to be the biggest difference amongst different species. In budding yeast, the sole condensin complex homologous to condensin I localizes to the nucleus throughout the cell cycle. In humans, condensin II is bound to chromosomes throughout interphase and participates in early condensation, with condensin I mostly translocating to the nucleus at the onset of prometaphase and maintaining a more dynamic interaction with chromosomes (27, 53, 54). It has also been shown that in many organisms, such as humans and chickens, condensin I is present in interphase nuclei, despite earlier evidence suggesting it was only able to bind to chromosomes after nuclear envelope breakdown (55). In fission yeast, condensin stays in the cytoplasm during interphase and only localizes to the nucleus during mitosis.

Despite varying cellular localization across different species, condensin acts primarily during metaphase to reorganize loose chromatin into densely packed chromosomes (45). Perturbation of normal condensin activity can lead to defects in the timing of or the extent of chromosome condensation, both of which can be detrimental to cell cycle progression and lead to genomic instability, the hallmark of many diseases (56, 57). As such, condensin activity must be tightly spatiotemporally regulated through mechanisms such as post-translational modifications (PTMs) (5). PTMs alter the structure and function of proteins to allow them to respond to different cellular signals (58). A key PTM responsible for the kinetics of many enzymes, including condensin, is phosphorylation (59). The pattern of condensin phosphorylation throughout the cell

cycle varies and helps to promote chromosome condensation events at the right time, suggesting a cyclic mechanism of phospho-regulation (60, 61). To understand how phosphorylation by different enzymes and at different target sites allows condensin to restructure chromosomes, it is important to understand when condensin phosphorylation leads to activation and inhibition of its function (60, 62, 63).

SMC4

Though putative phosphorylation sites for Cdk1, a key cell cycle regulator, have been identified in all subunits of condensin, our laboratory has shown that the ablation of these sites in *SMC4* specifically causes severe growth defects in yeast (64). Interestingly, seven out of the ten possible Cdk1 sites identified in Smc4 are found to be clustered in its disordered, N-terminal extension (Smc4-NT) (Figure 4A, Figure 4B, blue), and ablation of these seven sites leads to dramatic defects in chromosome condensation and segregation. Among the 6 conserved SMC protein families, only Smc4 family members carry an N-terminal extension. Importantly, the presence of Cdk1 phosphorylation sites contained within these extensions is conserved among most eukaryotes, including humans (52). While the sequence of the Smc4-NT in yeast covers the first 163 residues of Smc4, the first 149 residues are predicted to be a region of intrinsic disorder. Deletion of the Smc4-NT region causes lethality in yeast, suggesting a unique functional role for this region that remains to be explored.

Intrinsically disordered protein regions

The Smc4-NT is predicted to be an intrinsically disordered protein region (IDPR) (64). Despite the absence of a stable, three-dimensional structure, IDPRs can play functional roles in

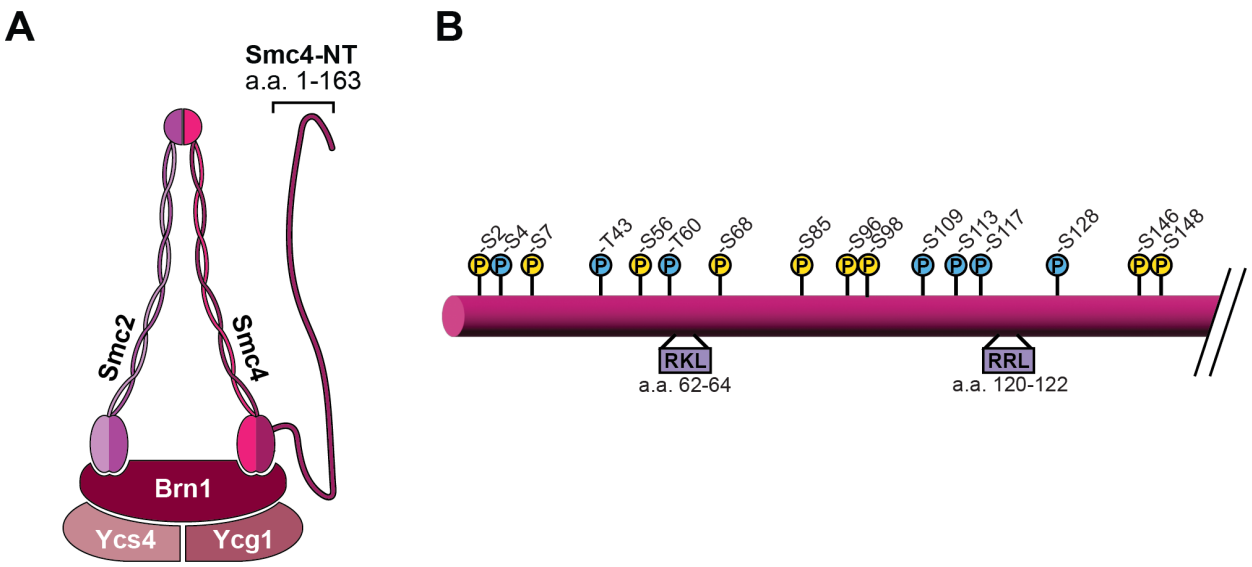

Figure 4. Graphical representation of yeast condensin and the Smc4 N-terminus region. (A) A diagram of the pentameric condensin complex, showing the ATPase subunits (Smc2 and Smc4) and regulatory subunits (Brn1, Ycs4, Ycg1). The Smc4-NT is bracketed. **(B)** Depiction of linearized Smc4-NT showing the relative locations of putative phosphorylation sites and cyclin-binding RxL motifs. Minimal consensus Cdk1 phosphorylation sites are noted by blue annotations, mass spectrometry-identified phosphorylation sites are shown by yellow annotations, and RxL motifs are indicated by purple annotations.

vital cellular processes such as signal transduction, cell cycle regulation, or transcription (65–67). Interestingly, about 70% of DNA-binding proteins possess intrinsically disordered tails, whereas such tails are found in only 50% of non-DNA binding protein counterparts (68). While IDPRs may play a role in protein-DNA interactions, the detailed aspects of how disordered regions function in protein-DNA recognition are not completely understood (65). A proposed model for this interaction is the "monkey bar" model, in which the disordered region of a protein assists in intersegment transfer between two DNA molecules to enhance the specificity of the overall protein's interaction with DNA (68). Another model is the "fly casting" hypothesis, in which the disordered tail structure reaches relatively distant regions of DNA that lie beyond the structured areas of the protein (65). Importantly, the structure of IDPRs has been shown to be modified by PTMs, such as phosphorylation. In fact, most phosphorylation sites throughout the proteome are

located within IDPRs (67, 69, 70). Phosphorylation at key sites is known to regulate function of IDPRs, often by inducing a "disorder to order" structural change that affects the IDPR's interactions with different target substrates (71–73). This transition is thought to help improve the specificity of DNA binding and has possibly been evolutionarily selected to have a charge pattern that optimizes DNA search by changing the bulk electrostatics of the protein (67, 74).

ATP-dependent and independent functions of condensin

Condensin possesses DNA-stimulated ATPase activity, with an affinity for structured or long DNA fragments. The induction of supercoils into relaxed circular DNA in the presence of ATP and topoisomerase II requires ATP hydrolysis by the SMC subunits of condensin (75, 76). Interestingly, DNA-binding by condensin appears to be a phosphorylation-independent event (54, 75, 77). Several regions of condensin have been shown to possess DNA binding activity in different model organisms. In budding yeast, the Smc2/4 heterodimer has DNA binding activity that is not affected by ATP but requires a high molar ratio of protein to DNA regardless of DNA substrate size (78, 79). The HEAT repeat subunits of budding yeast condensin have also been shown to directly bind DNA with a high affinity, a function that is hypothesized to play a role in initial condensin loading onto chromatin (80).

It has been proposed that phosphorylation of condensin modifies its interactions with DNA substrates with which it has been shown to associate *in vitro* (61). In fission yeast, autophosphorylation of condensin's hinge domain has been shown to cause condensin's dissociation from DNA and its resulting mobility along chromosomes, suggesting that phosphorylation antagonizes DNA binding activity (81). Condensin has been shown to maintain a

dynamic association with chromosomes throughout mitosis, possibly due to a requirement for an optimal condensin turnover rate regulated by cell cycle-dependent phosphorylation (54, 64, 82).

Cdk1 activation of condensin

Cyclin-dependent kinases (Cdks) are the master regulators of the cell cycle (83). It is well established that in eukaryotes, an increase in the activity of Cdk1 is the primary trigger for the onset of mitosis and subsequent chromosome condensation events (84). Cdk1 is a proline-directed serine/threonine kinase that phosphorylates the consensus motif S/T-P-X-K/R or the minimal sequence S/T-P [reviewed in (85, 86)]. Cdk1 has also been shown to phosphorylate non-S/T-P motifs *in vitro* (87, 88). The major mitotic form of Cdk1 is in complex with cyclin B, whose degradation is required for mitotic exit (89). The function of Cdk1 is conserved across many species, including humans and yeast (where it is referred to as Cdc28). This is demonstrated through the normal proliferation and activity of yeast strains with the yeast Cdk1-encoding gene, *CDC28*, replaced by the human gene, *CDC2/CDK1* (90). Cdk1 has many targets throughout the cell cycle, and it is hypothesized that enzymes targeted earlier in the cell cycle are responsible for events that occur at the beginning of mitosis (52).

Such is the case for the condensin complex, as Cdk1 phosphorylation of condensin is essential and required for condensin activation (51, 60, 64, 76, 91, 92). Many phosphorylation sites in condensin are contained within shorter regions, thought to be part of flexible peptide loops. These peptide loops are thought to increase accessibility of substrate target sites to their respective kinases (61). Interestingly, mass spectrometry analysis of over 500 Cdk1 phosphorylation sites revealed that more than 90% are predicted to be in loops or disordered structures (93). These sites tend to be clustered within regions that may have been evolutionarily conserved for biological

function, such as causing or eliminating interactions between substrates (93, 94). Knowing that condensin is highly regulated by Cdk1 phosphorylation and that it possesses DNA binding activity at many regions such as the hinge domain of Smc2/4 heterodimer, we sought to understand if the Smc4-NT, an intrinsically disordered region containing many Cdk1 phosphorylation sites, exhibits similar DNA binding properties.

RxL motifs in Cdk substrates

Regulation of Cdk1 substrate specificity is modulated by the abundance of different cyclins at different stages of the cell cycle (95, 96). Premature mitotic entry is prevented by weaker Cdk1 specificity for substrates that are active at later stages of the mitotic process. Targets of Cdks, including the Smc4-NT, often contain "RxL" or "Cy" motifs which bind to the hydrophobic patch of cyclins (97, 98). These motifs act as docking sites to mediate Cdk phosphorylation at key substrates. Most studies have focused on the importance of RxL motifs for substrate interaction with cyclin E (G1 phase) or A (S phase) in humans (97, 99–101). In yeast, it has been shown that mutation of the hydrophobic patch of S phase cyclin Clb5 abrogates substrate binding and phosphorylation, but a similar mutation of M phase cyclin Clb2 does not produce any effects (96). While RxL motifs facilitate substrate phosphorylation by S and G2 phase cyclin complexes (Clb5, Clb3), it has recently been shown that M phase cyclin Clb2 recognizes an LxF motif (96, 98, 102). RxL motifs can also serve as anchor points for the assembly of multi-protein hubs required for certain mitotic events (103). Interestingly, Robellet et al. showed that ablation of the two RxL motifs from the Smc4-NT resulted in a dramatic reduction of cell cycle dependent phosphorylation (64). While the Smc4-NT of condensin is thought to be more directly implicated in M phase, we

wondered whether the removal of these supposed S phase docking motifs would impact DNA binding by the Smc4-NT (Figure 4B, purple).

Interphase regulation of condensin by CK2

While condensin has been reported to be constitutively phosphorylated in human cells, its phosphorylation patterns differ throughout the cell cycle (61). Cdk1 is sufficient to drive the cell cycle in yeast, but its functions are supported and antagonized by many other kinases throughout the cell cycle (52, 104). This suggests that mitotic phosphorylation at specific sites of condensin is responsible for the initiation of chromosome condensation (64). Interphase regulation of chromosomes by condensin seems likely, as condensin has been shown to be associated with active tRNA genes through chromatin immunoprecipitation in yeast (105, 106). Additionally, in fission yeast, Cnd2 (a Brn1 homolog) plays a role in mitotic chromosome condensation and interphase by differential binding to chromatin (107).

Casein kinase 2 (CK2) is thought to play a major role in cell cycle regulation, including condensin phosphorylation during interphase (108–110). CK2 has been shown to be responsible for the majority of interphase condensin phosphorylation. While CK2 depletion does not affect chromosome condensation in mitotic cell extracts, condensation does not occur in interphase cell extracts under any conditions. This suggests that CK2 phosphorylation of condensin during interphase catalytically inhibits its function (62). CK2 phosphorylation is also dominant over Cdk1 phosphorylation (62, 111, 112). For full condensin activation by Cdk1, it has been proposed that CK2 phosphorylation must be completely removed by phosphatases such as PP6 and PP2A, suggesting condensin activation and inactivation by a highly regulated mechanism of phosphorylation (113, 114). Interphase phosphorylation of condensin could be implicated in

regulating other condensin-mediated processes besides chromosome condensation. Condensin functions are now known to not be limited to chromosome condensation and segregation – condensin also contributes to genome stability, cell differentiation, and development. Condensin II has also been found to enrich at transcriptionally active regions in embryonic stem cells (115). As the Smc4-NT is enriched in phosphorylation sites for Cdk1, we wondered whether it also contains phosphorylation sites for CK2 that could serve to negatively regulate condensin function.

Yeast as a model

Saccharomyces cerevisiae, or budding yeast, is the catalyst for the production of bread and beer, but also serves as an excellent model organism for research. Yeasts are an incredibly useful model organism as their natural homologous recombination process allows for easy genetic manipulation (116). Recessive phenotypes caused by gene mutations can be specifically visualized through the dissection of haploid organisms, created by growing yeast on nutrient-starved media to stimulate meiosis (117) (Figure 5). Mutants in essential genes, such as cell cycle regulators, can be studied using temperature sensitivity, a phenomenon in which a mutant gene will confer a normal phenotype at a permissive temperature (23°C) but will reveal a mutant phenotype at a restrictive temperature (37°C) (118). Inducing specific phenotypes at restrictive temperature permits the observation of various cellular processes regulated by essential genes (119). In addition to these techniques, which are not as easily conducted in mammalian cells, Cdk1 activity and the structure of condensin are well conserved between humans and yeast (76, 90). Altogether, yeast presents an advantageous model organism to evaluate aspects of the cell cycle and how they apply to humans.

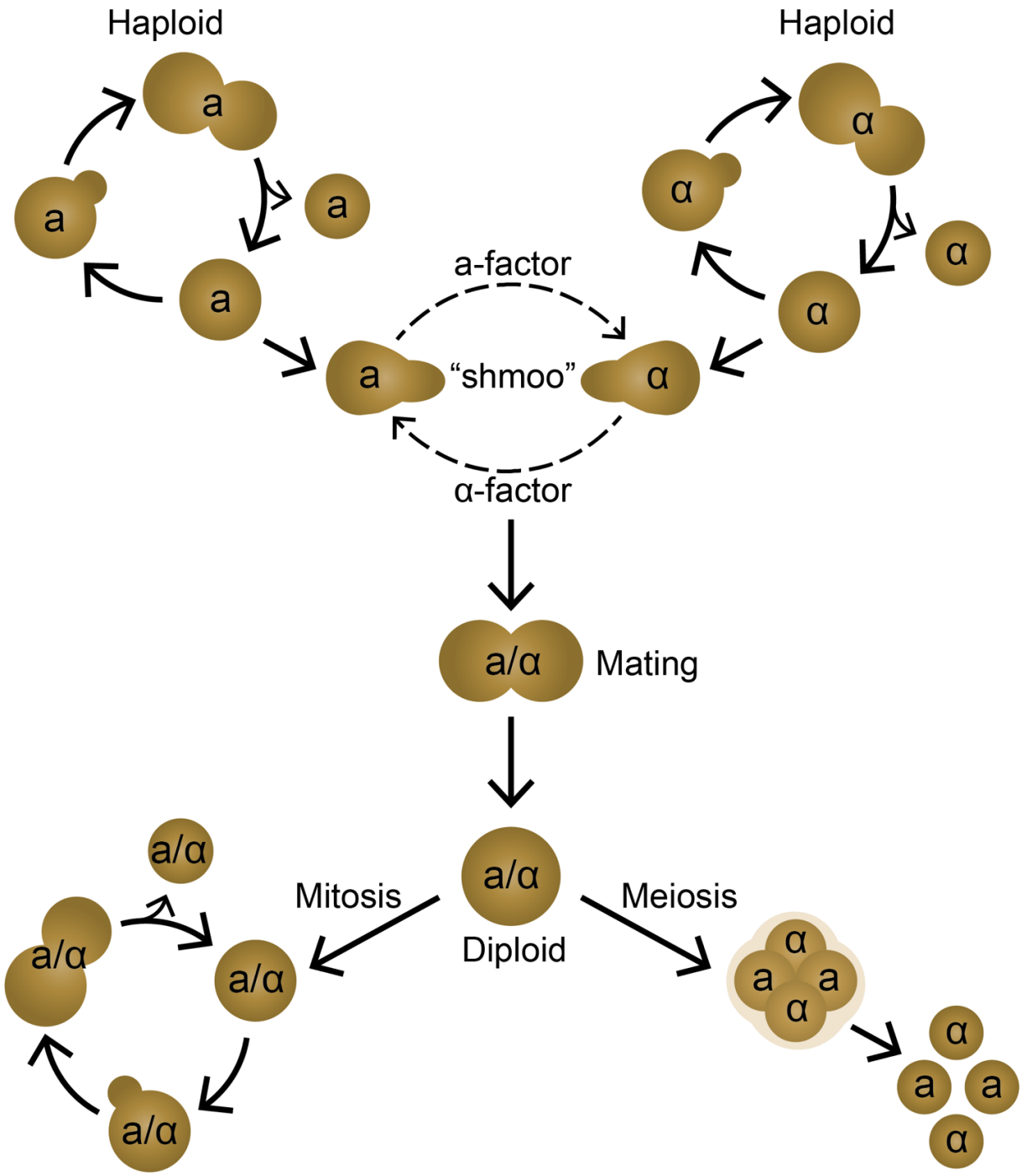

Figure 5. Simplified model of the life cycle of budding yeast. Haploid strains with mating types *MAT***a** (a) and *MAT***α** (α) can undergo mitotic division to produce identical offspring (top, left and right). Cells of one mating type respond to the pheromone released by cells of the opposite mating type to initiate "shmoo" formation and mate, ultimately producing the stable diploid cell with a mating type of *MAT***a**/*MAT***α** (a/α, middle, center). Diploid cells can undergo mitotic division to produce genetically identical daughter cells (left), or, in nutrient-poor conditions, sporulate and undergo meiosis, to produce 4 haploid spores which will germinate into two *MAT***a** and two *MAT***α** cells.

Hypothesis and Objectives

Our central hypothesis is that the Smc4-NT regulates the association of the condensin complex with DNA in a phosphorylation-dependent mechanism. Understanding how this regulation occurs will provide crucial biochemical and genetic insights into the broader mechanism of chromosome condensation.

Through electrophoretic mobility shift assay (EMSA), we discovered that purified Smc4-NT, a predicted IDPR, is a strong DNA binding domain. Robellet et al. have previously shown that the Smc4-NT is phosphorylated by Cdk1 and essential for the proper formation of chromosomes (64). We aimed to determine how Cdk1 phosphorylation of the Smc4-NT affects its DNA binding activity specifically. Additionally, through mass spectrometry analysis, we identified nine novel phosphorylation sites in the Smc4-NT that we hypothesized might be targets for CK2, which has been shown to be important for negatively regulating human condensin (Figure 4B, yellow). Finally, we wondered whether ablation of the two cyclin binding motifs in the Smc4-NT would affect its Cdk1-dependent phosphorylation effects (Figure 4B, purple). We used various *in vivo* and *in vitro* assays to determine that the DNA binding activity of the Smc4-NT is regulated by phosphorylation. My project consisted of the following specific aims:

Objective 1: Purify Smc4-NT construct and establish baseline DNA binding activity of this region.

Objective 2: Determine the effects of the ablation of mass spectrometry-identified phosphorylation sites in the Smc4-NT on cell proliferation, cell cycle-dependent phosphorylation, and DNA binding.

Objective 3: Assess the effects of Cdc28-Clb2 phosphorylation on the DNA binding activity of the Smc4-NT.

Objective 4: Combine Smc4-NT phospho-mutants with the deletion of CK2 and evaluate effects on cell proliferation and cell cycle-dependent phosphorylation.

Objective 5: Determine if CK2 phosphorylates the Smc4-NT *in vitro*.

Objective 6: Determine the effects of the ablation of the cyclin binding motifs in the Smc4-NT on cell proliferation and DNA binding.

Determining the link between the phosphorylation of the essential Smc4-NT and its ability to bind DNA will provide important insights into the exact mechanism by which condensin interacts with chromatin to promote chromosome condensation. My project represents an important first step in the development of novel therapeutic approaches focusing on the inhibition of cell division.

Materials and methods

Cloning of full length SMC4 mutants in yeast shuttle vectors

The alleles *smc4-9A* and *smc-16A* were generated in part by custom gene synthesis (BioBasic Inc.), for insertion into a *YCplac111-Psmc4-BamHI-SMC4=L=3xSTII::TADH1::HIS3MX6::Tsmc4* plasmid backbone. Recipient vectors and synthesized vectors containing gene inserts were digested with 20U of BamHI-HF and EagI-HF (New England Biolabs) for 2 hours at 37°C. Digestion products were separated on a 0.8% agarose gel (0.8% agarose in 1xTAE [40mM tris acetate, 1mM EDTA], run with 100V of current for 65 minutes) and the appropriate bands were gel extracted using the MinElute Gel Extraction Kit (250) (Qiagen) following the manufacturer's instructions. Following DNA quantification by NanoDrop One (ThermoFisher Scientific), digested insert and plasmid were combined at a 5:1 molar ratio of insert: vector with 150ng total DNA in a ligation reaction containing 1 unit/µL T4 DNA ligase (New England Biolabs). After overnight incubation at room temperature, ligation products were transformed into XL10-Gold ultracompetent *Escherichia coli* cells (Agilent) by heat shock and grown overnight at 37°C on LB plates containing 1X ampicillin (Sigma-Aldrich). Single colonies were selected and propagated in liquid LB-AMP media overnight, and plasmids were extracted using the QIAprep Spin Miniprep Kit (250) (Qiagen) using the manufacturer's instructions. 6 colonies were screened by diagnostic digest with BlpI for each desired vector. Positive clones were sent for sequencing at the StemCore Laboratories DNA Sequencing Facility (Ottawa Hospital Research Institute). Sequenced clones containing the mutation of interest and no unwanted background mutations were preserved and used for further experiments. Resulting gene products express full length Smc4 with desired mutations followed by a 3xStrep-tag, and grow on yeast media lacking the essential amino acid histidine.

The allele *ura3-1::smc4-rxlA::URA3* was created by subcloning the *smc4-rxlA* sequence from the vector *YCplac111-Psmc4-BamHI-smc4-rxlA=L=3xSTII::TADH1::HIS3MX6::Tsmc4* into the vector *YIplac211-Psmc4-smc4-7A=L=3xSTII::TADH1::HIS3MX6::Tsmc4* using the restriction sites SphI and EagI (New England Biolabs). The same methodology for subcloning and screening was used as described above; 10 potential positive clones were screened by diagnostic digest with BamHI-HF and XhoI (New England Biolabs).

The alleles *smc4-S40A,S67A,S68A* and *smc4-7A[S40A,S67A,S68A]* were created by mutagenesis of *YCplac111-Psmc4-BamHI-SMC4=L=3xSTII::TADH1::HIS3MX6::Tsmc4* or *YCplac111-Psmc4-BamHI-smc4-7A=L=3xSTII::TADH1::HIS3MX6::Tsmc4*, respectively. Two mutagenic primers introducing the mutations of interest were designed for each vector, one to incorporate the S40A mutation, and another to incorporate the S67A and S68A mutations. Primers were manufactured by Integrated DNA Technologies. Manual site-directed mutagenesis was performed with the QuikChange Lightning Multi site-directed mutagenesis kit (Agilent). Following mutagenesis, plasmids were transformed into XL10-Gold ultracompetent *E. coli* cells (Agilent) and sequenced to confirm presence of desired mutations as described above.

Cloning of Smc4-NT phospho-mutants for time course assays in yeast shuttle vectors

Centromeric plasmids expressing Smc4-NT phospho-mutants were constructed by subcloning mutant *smc4* sequences into the vector *YCplac111-SMC4[1-142]::NLS::13xMYC::TADH1::HIS3MX6*. Primers were designed to amplify the region of *smc4[1-142]* from the *YCplac111-Psmc4-BamHI-SMC4=L=3xSTII::TADH1::HIS3MX6::Tsmc4* mutant plasmids created as described above. Forward primers annealed ~500bp upstream of the gene start and included an SphI restriction site. Reverse primers added a BglII site after residue 142 of the *smc4*

gene followed by a sequence encoding the SV40 large T antigen NLS (PKKKRK) (120) and the beginning of a 13xMYC tag. Primers were manufactured by Integrated DNA Technologies. Amplified inserts were sequentially digested with SphI and BglII (New England Biolabs) and the recipient vector *YCplac111-SMC4[1-142]::NLS::13xMYC::TADH1::HIS3MX6* was digested with SphI and BamHI-HF (New England Biolabs). The identical 4 nucleotide overhangs created by digestion with BglII and BamHI allowed the insert and vector to be ligated with a change in one nucleotide and amino acid in the linker sequence connecting *smc4* to the NLS, without a direct effect on the sequence of *smc4* or the NLS. The same methodology for subcloning was used as described above and potential clones were screened by diagnostic digest with NcoI (New England Biolabs). Plasmids providing the correct digestion products were fully sequenced by the StemCore Laboratories DNA Sequencing Facility (Ottawa Hospital Research Institute).

Yeast growth strains and conditions

All *Saccharomyces cerevisiae* strains are derived from W303 background strains with a wild-type genotype of *leu2-3,112 trp1-1 can1-100 ura3-1 ade2-1 his3-11,15.* Standard yeast culture conditions were used in this study (121).

To insert full length *smc4* phospho-mutant alleles at their endogenous loci, mutant *smc4* plasmids created as described above were linearized with SphI-HF and KpnI-HF (New England Biolabs) and transformed into diploid yeast strains to allow mutations to be incorporated via the natural homologous recombination process of yeast. Yeast transformation was performed using the classic method described in Schiestl and Gietz (122) with the modification described in Gietz et al. (123). Colonies that grew on synthetic complete media lacking the essential amino acid histidine (SC-HIS) were screened for integration of the desired mutations by extraction of yeast

genomic DNA using our laboratory's "Smash and Grab" protocol, followed by genotyping by PCR. Transformants providing a PCR product of the correct size were sent for sequencing at the StemCore Laboratories DNA Sequencing Facility (Ottawa Hospital Research Institute). Strains containing the mutation of interest and no unwanted background mutations were preserved and used for further experiments. Haploid yeast strains were created by sporulation and dissection of heterozygous diploid strains, followed by replica plating and scoring of yeast spores to select for spores growing on SC-HIS plates. Haploid strains growing on SC-HIS plates were preserved as mutant strains of interest and sequenced to confirm the presence of the desired mutations at the StemCore Laboratories DNA Sequencing Facility (Ottawa Hospital Research Institute).

Yeast strains containing mutations in multiple genes (ie., *ckb1Δ* and *ckb2Δ* combined with mutations in *SMC4*) were created by mating and dissection of sporulated heterozygous diploid strains, followed by replica plating and scoring yeast growth at restrictive temperature and on various selectable markers.

Strains expressing *smc4-rxlA* at the *URA3* locus were created by linearization of the vector *YIplac211-Psmc4-smc4-rxlA=L=3xSTII::TADH1::HIS3MX6::Tsmc4* (created as described above) with StuI (New England Biolabs). The linearized vector was transformed into haploid *MAT***a** wild-type yeast or yeast bearing the *smc4-22* mutations at its endogenous locus.

Strains for phosphorylation time courses were created by transformation of centromeric *YCplac111* derivative plasmids (created as described above) into haploid *MAT***a** yeast with a genotype of *cdc15-2*. As plasmids express the *LEU2* gene, individual colonies growing on SC-LEU media were colony purified and preserved. Plasmids were maintained in yeast using SC-LEU selective medium.

All strains used in this study underwent at least one backcross with wild-type haploid yeast and were sequenced at the region of mutation to confirm the presence of the mutations of interest and absence of unwanted mutations.

TCA extraction to evaluate mutant Smc4 protein expression

Total protein extracts were prepared using a protocol adapted from Foiani et al (124). Cells from 10mL of culture at an OD_{600} of 0.3 (early log phase) were resuspended in 200µL of ice cold 20% TCA and combined with an equal volume of glass beads in locking lid tubes. Cells were lysed by shaking on a Vibrax VXR Orbital Shaker (IKA) at 1500RPM for 45 minutes. Supernatant was transferred to a new tube and glass beads were washed with 300µL of 5% TCA. Wash was combined with supernatant and centrifuged at 13000RPM for 5 minutes in a tabletop centrifuge (Centrifuge 5424, Eppendorf). The resulting pellet was resuspended in 200µL of 2X sample buffer (100mM Tris-HCl pH 9.5, 20% glycerol, 4% SDS) and boiled at 100°C for 5 minutes. Following centrifugation for 5 minutes at 13000RPM, supernatant was aliquoted and stored at -80°C.

Protein concentration was quantified by Pierce BCA Protein Assay Kit (ThermoFisher Scientific). 10µg of each sample was loaded on a 4-12% Criterion XT Bis-Tris precast polyacrylamide gel (BioRad) and run in MOPS running buffer (50mM MOPS, 50mM Tris base, 0.1% SDS, 1mM EDTA) for 90 minutes with 150V of current. Protein expression was verified through Western blot with α-Strep as described below.

Serial dilution temperature sensitivity assays

Haploid *MAT***a** control and mutant strains were inoculated into YPD complete media and incubated at 23˚C, shaking at 250RPM overnight. After at least 16 hours of growth, cultures were

diluted to an OD_{600} of 0.2 in YPD and grown at 23˚C, 250RPM for at least 4 hours to an OD_{600} of 0.4-0.8. Strains were then diluted to an OD_{600} of 0.2 in 200µL of fresh YPD in a Corning Falcon 96-well, non-treated, U-shaped bottom sterile microplate (Fisher Scientific). A 5-fold serial dilution set was prepared to a final dilution of 1:3125. 5µL of each dilution was spotted onto solid YPD medium and grown at 23°C and 37°C for approximately 30-36 hours. Plates were scanned using the Epson Perfection V850 Pro scanner.

Cloning of Smc4-NT mutants for protein purification in E. coli shuttle vectors

Plasmids expressing wild-type and mutant forms of the Smc4-NT were created for bacterial overexpression and purification. Gene inserts were amplified from the mutant *YCplac111* vectors created as described above. Forward primers were designed to incorporate an SpeI restriction site, followed by a TEV protease cleavage site flanked by flexible linkers, immediately upstream of the *SMC4* ORF. Downstream primers introduced an XhoI site after residue 163 of *SMC4*. Primers were manufactured by Integrated DNA Technologies. Following amplification, inserts were subcloned using SpeI and XhoI (New England Biolabs) into the *pET41a* vector to introduce a GST tag at the N-terminus of the Smc4-NT to facilitate protein overexpression. The same methodology for subcloning was used as described above, but following transformation in XL10-Gold ultracompetent *Escherichia coli* cells (Agilent) by heat shock, cells were pre-grown for 1 hour in LB media and then plated on LB containing 1X kanamycin (ThermoFisher Scientific). Potential clones were screened by diagnostic digest with HpaI (New England Biolabs). Plasmids providing the correct digestion products were sequenced by the StemCore Laboratories DNA Sequencing Facility (Ottawa Hospital Research Institute). The resulting constructs express the fusion protein GST-linker-TEV-linker-Smc4[1-163]-8xHIS.

Small scale overexpression test

Wild-type Smc4-NT-6xHIS from our laboratory's collection and the fusion protein, GST-linker-TEV-linker-Smc4[1-163]-8xHIS, were overexpressed side by side to determine if fusion protein would improve protein yield for use in downstream assays. Plasmids encoding for kanamycin resistance, expressing either the empty vectors or the proteins of interest were transformed into *E. coli* BL21 competent cells by heat shock and pre-grown for 1 hour in LB media. Cells were then plated on LB plates containing 1X kanamycin and grown at 37°C overnight. The following day, an individual colony from each plate was inoculated into 5mL of liquid LB-KAN media and grown at 37°C, shaking at 250RPM overnight. After approximately 16 hours of growth, the overnight cultures were used to inoculate 30mL of LB-KAN (in a 125mL flask) to an OD_{600} of 0.05. After growth at 37°C for approximately 2 hours, cultures reached an OD of 0.6-0.8. 10mL of each culture was harvested as the "uninduced" fraction by centrifugation at 3700RPM for 30 minutes at 4°C (Centrifuge 5920R, Eppendorf) and pellet was frozen at -20°C. Remaining 20mL of each culture was induced for protein overexpression with 1mM IPTG (Fisher Scientific) and grown overnight at 18°C, 160RPM. Following growth for at least 16 hours, each culture was split into 2x10mL "induced" fractions and cells were collected by centrifugation at 3700RPM for 30 minutes at 4°C. Pellets were frozen at -20°C until lysis.

Prior to cell lysis, each cell pellet from 10mL of culture was resuspended in 5mL of resuspension buffer (50mM K_2HPO_4/KH_2PO_4, 300mM NaCl, 1mM imidazole, 2mM β-mercaptoethanol, pH 8.0), supplemented with 0.225mg/mL lysozyme and protease inhibitors (0.5mM AEBSF, 10μM Pepstatin A, and 10μM E-64). Lysates were incubated on ice for 30 minutes, until slurries were opaque and a bit viscous. Cells were lysed by sonication on ice using Sonifier SFX550 (Branson) in bursts of 10 seconds on/5 seconds off for a total of 30 seconds on

at intensity 30%. Each lysate underwent 2-4 rounds of sonication, until the sample consistency became translucent and less viscous. 1mL of each sonicated sample was kept as a "total protein" fraction and remaining lysates were centrifuged for 35 minutes at 13,000 RPM at 4°C. Supernatants of centrifuged samples were saved as "soluble protein" fractions.

Samples were loaded in duplicate on a 4-12% Criterion XT Bis-Tris precast polyacrylamide gel (BioRad) and run in MOPS running buffer (50mM MOPS, 50mM Tris base, 0.1% SDS, 1mM EDTA) for 90 minutes with 150V of current. Gel was cut in half and processed in parallel for Coomassie staining and α-HIS Western blot as described below.

Western blotting

Following separation of proteins on a polyacrylamide gel, proteins were transferred to a nitrocellulose membrane using the iBlot 2 system (Invitrogen). Membranes were blocked with 2% milk and 1% BSA in TBS-T (20mM Tris base, 150mM NaCl, [pH 7.6], 0.1% Tween-20) for 1 hour at room temperature on an orbital shaker at ~100RPM. Blots were probed with the following primary antibodies for 1 hour: 1:1000 α-HIS (Qiagen) for detection of the Smc4-NT or GST-Smc4-NT, 1:1000 α-Strep (Qiagen) for the detection of the Clb2 subunit of Cdc28-Clb2 and full-length Smc4, and 1:2500 α-PGK1 (Abcam) for the Pgk1 loading control. Secondary antibody used was 1:5000 HRP-conjugated α-mouse antibody (VWR). Blots were rinsed in TBS-T 3 times for 10 minutes at ~100 RPM on an orbital shaker after blocking and antibody incubation steps.

All antibodies were diluted in TBS-T and incubation steps were carried out at room temperature on a variable speed rocker. Protein-antibody conjugates were revealed by chemiluminescence through film imaging following manufacturer's instructions (Clarity Western ECL substrate [BioRad], Hyperfilm ECL films [Sigma-Aldrich]).

Coomassie staining

Following separation of proteins on a polyacrylamide gel, gel was rinsed briefly in water and covered in ~20mL of Coomassie Brilliant Blue stain (50% v/v methanol, 10% v/v glacial acetic acid, 1% w/v Coomassie Brilliant Blue R-250). Gel was microwaved for 30 seconds and then incubated, covered, in heated stain for 2 minutes. To destain, gel was microwaved for 3 minutes and 30 seconds in ~250mL of water containing a paper towel to absorb the stain. Gel was covered and incubated in water for 2 hours to overnight until fully destained.

Overexpression of GST-linker-TEV-linker-Smc4[1-163]-8xHIS

All wild-type and mutant forms of the Smc4-NT were overexpressed as a fusion protein, GST-linker-TEV-linker-Smc4[1-163]-8xHIS. Plasmids expressing the protein of interest and a kanamycin resistance marker were transformed into *E. coli* BL21 competent cells by heat shock and pre-grown for 1 hour in LB media. Cells were then plated on LB-KAN and grown at 37°C overnight. The following day, an individual colony was inoculated into 500mL of liquid LB-KAN media and grown at 37°C, shaking at 250RPM overnight. After approximately 16 hours of growth, the overnight culture was used to inoculate 4L of LB-KAN media (split into 4 x 4L flasks, 1L media each) to an OD_{600} of 0.05. Cells were grown at 37°C for 2 hours, to an OD_{600} of approximately 0.6-0.8. Cells were induced for protein overexpression with 1mM IPTG and grown overnight at 18°C, 160RPM. Following growth for at least 16 hours, cells were collected by centrifugation at 4200RPM for 45-60 minutes at 4°C (J6-MI low-speed centrifuge, Beckman Coulter). Following centrifugation, cell pellet from 1L of culture was resuspended in 25mL of resuspension buffer (50mM K_2HPO_4/KH_2PO_4, 300mM NaCl, 1mM imidazole, pH 8.0, supplemented with 2mM β-mercaptoethanol) and frozen at -20°C until purification.

Protein purification

Wild-type and mutant forms of Smc4-NT were overexpressed as a fusion protein, GST-linker-TEV-linker-Smc4[1-163]-8xHIS, following which the GST tag was removed by TEV cleavage during purification. After every round of purification, 10µL of flow-through, washes and elutions were collected and combined with 4xLaemmli sample buffer (BioRad) supplemented with β-mercaptoethanol. Samples were run on a 4-12% Criterion XT Bis-Tris precast polyacrylamide gel (BioRad) in MOPS running buffer (50mM MOPS, 50mM Tris base, 0.1% SDS, 1mM EDTA) for 90 minutes with 150V of current and Coomassie stained as described above. All purification steps were carried out at 4°C.

Cell Lysis

Cell pellet from 1L of culture, resuspended in 25mL of resuspension buffer (50mM K_2HPO_4/KH_2PO_4, 300mM NaCl, 1mM imidazole, pH 8.0, supplemented with 2mM β-mercaptoethanol) was thawed and topped up to a final volume of 200mL with resuspension buffer. Lysozyme was added to the lysate to a final concentration of 0.225mg/mL, as well as protease inhibitors: 0.5mM AEBSF, 10µM Pepstatin A and 10µM E-64. Bacterial slurry was incubated, rocking, at 4°C for 30 minutes, until slurry was a bit viscous. Cells were lysed by sonication on ice using Sonifier SFX550 (Branson) using a program consisting of cycles of 1 minute on/1 minute off, for 3 minutes on in total. 4 rounds of sonification were performed at increasing intensities: first at 30%, followed by intensity 35%, 40%, and 45%. Lysate was split into 50mL Falcon tubes and centrifuged at 13,000 RPM for 45 minutes at 4°C in a Sorval Legend XFR floor centrifuge (ThermoFisher Scientific). Supernatants were pooled and further clarified by filtration with 0.2µM Nalgene Rapid-Flow sterile single use bottle top filters (ThermoFisher Scientific).

Round 1: Ni-NTA purification

10mL of cOmplete His-Tag Purification Resin (Sigma-Aldrich), equivalent to about 5mL of beads, was washed thrice with 25mL of filtered milliQ water (Reference A+ Q-POD Milli-Q Water System, Millipore) and then equilibrated with 3 washes in 25mL resuspension buffer (50mM K_2HPO_4/KH_2PO_4, 300mM NaCl, 1mM imidazole, pH 8.0, supplemented with 2mM β-mercaptoethanol). Equilibrated Ni-NTA beads were combined with the protein lysate and incubated at 4°C, rocking, for 30 minutes. Lysate slurry was incrementally poured into a 75mL gravity chromatography column and collected, then run incrementally through the column a second time to ensure maximal binding of protein of interest to beads. Beads were washed twice with 5 bed volumes (BV) of wash buffer 1A (50mM K_2HPO_4/KH_2PO_4, 750mM NaCl, 5mM imidazole, pH 8.0, supplemented with 2mM β-mercaptoethanol), and twice with 10BV of wash buffer 1B (50mM K_2HPO_4/KH_2PO_4, 300mM NaCl, 10mM imidazole, pH 8.0, supplemented with 2mM β-mercaptoethanol). Washes were briefly incubated with beads before collection. Protein of interest was collected in 5 elutions of 3BV of elution buffer 1 (50mM K_2HPO_4/KH_2PO_4, 300mM NaCl, 200mM imidazole, pH 8.0, supplemented with 2mM β-mercaptoethanol); buffer was incubated with beads for ~5 minutes before each elution.

Round 2: GSH purification and TEV cleavage

Elutions from the first round of Ni-NTA purification were pooled into two groups, one containing more concentrated elutions, and the second containing less concentrated elutions. A GSTrap HP 5mL column (Cytiva) connected to an ÄKTA pure 25 FPLC (GE Healthcare) was equilibrated at 5mL/min with 5CV of GSTrap wash buffer (50mM K_2HPO_4/KH_2PO_4, 300mM NaCl, pH 8.0, supplemented with 2mM β-mercaptoethanol). Following equilibration, pooled elutions were loaded onto the GSTrap column from most to least concentrated at a flow rate of

1.5mL/min to allow maximal binding of the protein of interest. Column was washed with 10CV of GSTrap wash buffer (50mM K_2HPO_4/KH_2PO_4, 300mM NaCl, pH 8.0, supplemented with 2mM β-mercaptoethanol) to remove non-specific binding. Protein was eluted at 2.5mL/min with 5CV of GSTrap elution buffer (50mM Tris-HCl, 300mM NaCl, 5% glycerol, 10mM L-glutathione, pH 8.0, supplemented with 2mM β-mercaptoethanol), in 2mL fractions. Based on the peak observed in the ÄKTA chromatograph, elutions containing the protein of interest were pooled and concentrated to a final volume of ~1mL with an Amicon Ultra-15 Centrifugal Filter Unit, 10kDa MWCO (MilliporeSigma). For GST tag cleavage, protein was diluted to 1mg/mL in TEV cleavage buffer (50mM Tris-HCl, 0.5mM EDTA, 5% glycerol, pH 8.0, supplemented with 1mM DTT). GST tag was cleaved by overnight digestion at 4°C with 200μL of HaloTEV protease (Promega).

Round 3: Ni-NTA purification

To remove the cleaved GST tag from the protein of interest, which both have a size of about 25kDa, digestion products were subjected to a second round of Ni-NTA. 1mL of cOmplete His-Tag Purification Resin (Sigma-Aldrich), equivalent to about 0.5mL of beads, was washed thrice with 10mL of filtered milliQ water (Reference A+ Q-POD Milli-Q Water System, Millipore) and then equilibrated with 3 washes of 10mL TEV cleavage buffer (50mM Tris-HCl, 0.5mM EDTA, 5% glycerol, pH 8.0, supplemented with 1mM DTT). Equilibrated Ni-NTA beads were combined with the digestion mixture and incubated at 4°C, rocking, for 30 minutes. Protein slurry was poured into a 25mL gravity chromatography column. Collected flow-through was run through the column a second time to ensure maximal binding of the protein of interest to the beads. Beads were washed twice with 0.5CV of wash buffer 2A (50mM K_2HPO_4/KH_2PO_4, 750mM NaCl, 5mM imidazole, 5% glycerol, pH 8.0, supplemented with 2mM β-mercaptoethanol), and twice with 1CV of wash buffer 2B (50mM K_2HPO_4/KH_2PO_4, 300mM NaCl, 10mM imidazole, 5% glycerol, pH 8.0,

supplemented with 2mM β-mercaptoethanol). Washes were briefly incubated with beads before collection. Protein was collected with 5 elutions of 1BV elution buffer 2 (50mM K_2HPO_4/KH_2PO_4, 300mM NaCl, 200mM imidazole, 5% glycerol, pH 8.0, supplemented with 2mM β-mercaptoethanol). Beads were incubated with elution buffer 2 for ~5 minutes before each elution was collected.

Round 4: Size exclusion chromatography

TEV protease and contaminant at 70kDa were separated from the protein of interest by size exclusion chromatography. A HiLoad 16/600 Superdex 75 prep grade column (Cytiva) connected to an ÄKTA pure 25 FPLC (GE Healthcare) was washed with 2CV of filtered water and equilibrated with 2CV of SEC buffer (50mM K_2HPO_4/KH_2PO_4, 300mM NaCl, pH 8.0). Elutions from the third round of purification were pooled and concentrated down to a final volume of ~300µL with an Amicon Ultra-0.5 Centrifugal Filter Unit, 3kDa MWCO (MilliporeSigma). Concentrated protein was injected onto the column and eluted with 1CV of SEC buffer, the first 0.35CV of which was discarded. Elutions were collected in 1mL increments with the remaining 0.65CV of SEC buffer. Elutions containing highly purified protein of interest were further concentrated, aliquoted, snap-frozen in liquid nitrogen and stored at -80°C.

Quantification of purified proteins

Purified proteins were run alongside BSA standards on a 4-12% Criterion XT Bis-Tris precast polyacrylamide gel (BioRad). Gel was Coomassie stained as described above and proteins were quantified by band intensity analysis using ImageJ software (125). The band intensity of the BSA standards with known concentrations was used to generate a standard curve. The intensity of the band corresponding to each protein sample was used to interpolate each protein's concentration from the equation of the standard curve.

Electrophoretic mobility shift assay (EMSA)

EMSAs were performed based on a protocol established by our laboratory to determine the DNA binding affinity of wild-type and mutant Smc4-NT proteins.

EMSA reactions were separated on 150mL UltraPure agarose gels (1% Ultrapure agarose [Invitrogen], 10X UltraPure TAE [Invitrogen] in filtered milliQ H_2O [Reference A+ Q-POD Milli-Q Water System, Millipore]). Gels were cast using the Hoefer Sub15 gel electrophoresis kit with 16-well combs and placed at 4°C when solidified until right before reactions were loaded. Reactions were set up in rigid 8-tube strip PCR tubes with individual attached flat caps (BrandTech Scientific). Increasing molar amounts of purified Smc4-NT protein were incubated with 0.2nM of single-stranded ΦX174 Virion DNA (New England Biolabs) in a final reaction volume of 25µL in EMSA buffer (10mM HEPES [pH 7.5], 7mM $MgCl_2$ [pH 7.0], 75mM-117.36mM NaCl [pH 8.0], 2mM β-mercaptoethanol). NaCl concentration was matched between different proteins compared on the same gel. Reactions were incubated at 30°C for 35 minutes, following which 1µL of 5x GelPilot DNA Loading Dye (Qiagen) was added to each tube. Each reaction was quickly combined at a 1:1 ratio with UltraPure LMP agarose mixture (0.0012% UltraPure LMP agarose [Invitrogen], 10X UltraPure TAE [Invitrogen] in filtered milliQ H_2O) and then loaded one well at a time onto the UltraPure agarose gel prepared earlier. Protein-DNA complexes were separated by agarose gel electrophoresis in 1XTAE running buffer (40mM Tris, 1mM EDTA, 20mM glacial acetic acid) with a current of 40V for 960 minutes at 4°C. Gel was stained with 20µL SYBR Gold nucleic acid stain (ThermoFisher) in 200mL reused 1X TAE running buffer for 1 hour and 15 minutes with 80RPM of agitation on an orbital shaker. Gel was washed 3 times for 10 minutes in 200mL 1xTAE and imaged with the D-Diget gel imager (LI-COR). At least 3 replicates were performed for each gel shown.

Quantification was done using ImageJ software (125). The intensity of each band (corresponding to the amount of free DNA per lane) was measured. The intensity of the band for each molar excess of protein was taken as a fraction of the band intensity corresponding to the no protein reaction band, to determine the percentage of free DNA left per well. Each percentage of free DNA was subtracted from 100% to obtain the amount of bound DNA per well.

Cdc28-Clb2 kinase assays and EMSAs

1.5µg of purified Smc4-NT protein was combined with 20ng of purified Cdc28-Clb2 in a final reaction volume of 25µL in kinase buffer (25mM Tris-HCl [pH 7.5], 10mM $MgCl_2$, 0.5mM EDTA, 2mM DTT, 1mM AEBSF, 10µM E-64, 10µM pepstatin A, 200µM tungstate). Buffer was supplemented with 1mM ATP as needed. For reactions performed with inactivated Cdc28-Clb2, kinase was boiled for 5 minutes at 95°C prior to addition to kinase reaction. For all reactions, kinase and ATP were added last. Due to the limited amount of kinase present in each reaction, reactions were set up in duplicate and combined prior downstream use in EMSAs. This left enough kinase in the reaction mixture to be detected through Western blot. Phosphorylation reactions were incubated at 30°C for 30 minutes. To verify phosphorylation, kinase reactions were combined with 4xLaemmli sample buffer (BioRad) supplemented with β-mercaptoethanol, separated on a 14% SDS-PAGE gel (made with 30% acrylamide/bis-acrylamide [37.5:1] solution), and processed for Western blot as described above.

EMSA reactions were performed as described above, with kinase reactions used to reach desired molar excesses of proteins. All salt carryover from kinase assay to EMSA was accounted for and equilibrated. Kinase reactions containing ATP and reactions without ATP were loaded on separate gels.

CK2 phosphorylation of Smc4-NT

750ng of purified Smc4-NT protein was combined with 500 units of human Casein Kinase II (New England Biolabs) in a final reaction volume of 25µL in 1X PK Buffer (50mM Tris-HCl, 10mM $MgCl_2$, 0.1mM EDTA, 2mM DTT, 0.01% Brij 35 [New England Biolabs]), supplemented with 1mM ATP. CK2 phosphorylation reaction was set up in duplicate. A control reaction was set up using the same conditions with 750ng of purified Smc4-NT protein and 10ng purified Cdc28-Clb2. For all reactions, kinase and ATP were added last. Phosphorylation reactions were incubated at 30°C for 30 minutes. After reaction completion, duplicate reactions were combined, and all reactions were stopped with the addition of 4xLaemmli sample buffer (BioRad) supplemented with β-mercaptoethanol. Reactions, along with stock Smc4-NT protein, were run on a 4-12% Criterion XT Bis-Tris precast polyacrylamide gel (BioRad) in MOPS running buffer (50mM MOPS, 50mM Tris base, 0.1% SDS, 1mM EDTA) for 90 minutes with 150V of current. CK2 reaction was loaded evenly between 2 wells, one of which was Coomassie stained as described above.

Gel portion containing stock Smc4-NT, Cdc28-Clb2 reaction, and CK2 reaction was stained for phosphorylation as follows. All incubation steps were carried out at room temperature on an orbital shaker at ~80RPM. Following gel run, proteins were fixed twice in gel fixing solution (50% methanol, 10% glacial acetic acid) for 30 minutes and then overnight. Gel was washed 3 times for 15 minutes in milliQ H_2O. Following washes, gel was stained in a foil-wrapped container (to exclude light) for 75 minutes in 50mL Pro-Q Diamond Phosphoprotein gel stain (ThermoFisher Scientific). Gel was destained 3 times for 30 minutes in Pro-Q Diamond Phosphoprotein Gel Destaining Solution (ThermoFisher Scientific) and then washed 3 times for 10 minutes with milliQ H_2O. Gel was imaged using Pro-Q Diamond imaging program of a Gel Doc XR+ Imager (BioRad). Following imaging, gel was transferred to a new foil-wrapped staining container and immersed in

50mL SYPRO Ruby Protein Gel Stain (ThermoFisher Scientific) overnight. The next day, gel was transferred to a new foil-wrapped destaining container and washed with 10% methanol, 7% acetic acid for 30 minutes. Gel was washed 3 times for 15 minutes in milliQ H_2O and then imaged using the SYPRO Ruby imaging program of a Gel Doc XR+ Imager (BioRad).

Mass spectrometry of CK2-phosphorylated Smc4-NT

Samples were processed for mass spectrometry analysis to identify CK2 phosphorylation sites in the Smc4-NT *in vitro*. Phosphorylated Smc4-NT protein was excised from Coomassie-stained gel, cut in half, and stored in 1% glacial acetic acid. Half of the stained band was submitted for mass spectrometry analysis at the Ottawa Hospital Research Institute Proteomics Core Facility, where it was processed by the facility as follows. Proteins were digested in-gel using trypsin (Promega) according to the method of Shevchenko et al. (126). Peptide extracts were concentrated by Vacufuge (Eppendorf). LC-MS/MS was performed using a Dionex Ultimate 3000 RLSC nano HPLC (Thermo Scientific) and Orbitrap Fusion Lumos mass spectrometer (Thermo Scientific). 5% of sample was injected. MASCOT software version 2.8.1 (Matrix Science, UK) was used to perform peptide-spectrum matching. Observed spectra were matched against UniProt reference proteome *S. cerevisiae* UP000002311 (version 2022-05-24) and against a database of common contaminants. The results were exported to Scaffold (Proteome Software, USA) for further validation and viewing. The data was analyzed to determine potential phosphorylated residues.

Phosphorylation time courses

Yeast cells with a genotype of *cdc15-2*, containing a yeast centromeric plasmid encoding the Smc4-NT, were synchronized in G1 using α-factor and released at a restrictive temperature of

37°C to evaluate phosphorylation of Smc4-NT phospho-mutants throughout the duration of one cell cycle. Strains were grown overnight at 250RPM at room temperature in SC-LEU media to maintain selective pressure and prevent loss of the plasmid encoding the Smc4-NT. The following morning, fresh YPD media was inoculated to an OD_{600} of 0.225 using overnight culture and grown for about 3 hours at 250RPM at room temperature until an OD_{600} of 0.3 (early log phase). 11mL of culture was taken as a "log" phase time point sample and processed as described below. Following time point removal, α-factor was added to the culture to a concentration of 5μg/mL and culture was grown at room temperature at 160RPM. 1.5 hours and 2.5 hours after the initial addition of α-factor, culture was supplemented with an additional 2μg/mL of α-factor. Cells were monitored for synchronization in G1 using a Nikon Eclipse 50i light microscope with a 40X objective until 90% of cells were unbudded with a mating projection, approximately 150-180 minutes after the initial addition of α-factor. Just prior to release, "T=0" time point was taken but processed after release, as described below. Cells were released by pouring culture into filtering apparatus and washing with at least 1L of pre-filtered, YPA wash medium prewarmed to 37°C. Filter containing yeast was placed in a pre-warmed release flask in a water bath at 37°C. Once all strains were released, yeast was resuspended in YPD medium prewarmed to 37°C. Cultures were grown at 180RPM in a water bath at 37°C and time points were taken every 30 minutes after resuspension until 150 minutes.

Time point samples were processed as follows. After centrifugation for 3 minutes at 3700RPM at 4°C, pellets were resuspended in 1mL of H_2O. 200μL was transferred to a microcentrifuge tube for budding index and the remaining volume was transferred to a microcentrifuge tube for TCA extraction. Both tubes were centrifuged at 4000RPM for 3 minutes and supernatants were removed by aspiration. Pellet for budding index was resuspended in 1mL

of 70% EtOH and stored at 4°C until budding index analysis. Just prior to analysis, samples were centrifuged at 5000 RPM for 5 minutes and pellets were resuspended in 200-600µL 1X PBS (137mM NaCl, 2.7mM KCl, 10mM Na_2HPO_4, KH_2PO_4 [pH 7.2]). At least 100 total cells were counted per time point (Nikon Eclipse 50i light microscope, 40X objective) to determine the percentage of budded cells. Pellet for TCA extraction was resuspended in 20% TCA and processed as described above, but samples were resuspended in 100µL-250µL of 2X complete sample buffer (100mM Tris-HCl [pH 9.5], 20% glycerol, 4% SDS, 0.2% BPB, 715mM β-mercaptoethanol).

Evaluating phosphorylation throughout cell cycle with 8% Zn^{2+} Phos-tag gels

Phosphorylation-induced gel shift of the Smc4-NT was visualized by separating protein lysates on an 8% 20µM Zn^{2+} Phos-Tag gel. A neutral Bis-Tris buffer system was used to prepare separating and stacking gels. Separating gel buffer consisted of 350 mM Bis-Tris (pH 6.8), 8% acrylamide/bis-acrylamide 30% solution (37.5:1), 20µM Ready-to-Use Phos-Tag acrylamide aqueous solution (Cedarlane), 40µM $Zn(NO_3)_2$, 0.13% v/v TEMED, and 0.046% w/v APS. Stacking gel buffer consisted of 350 mM Bis-Tris (pH 6.8), 4.5% acrylamide/bis-acrylamide 30% solution (37.5:1), 0.13% v/v TEMED, and 0.046% w/v APS. Gel running buffer consisted of 100mM Tris base, 100mM MOPS, and 0.1% w/v SDS, to which 5mM sodium bisulfite was added immediately before electrophoresis. 3 gels were run together under a constant current of 40mA at 4°C for approximately 800 minutes for optimal separation of phosphorylated and non-phosphorylated protein species.

Prior to transfer of separated proteins to PVDF membranes for immunoblotting, gels were washed at ~80 RPM, 4 times for 10 minutes each with methanol-free transfer buffer containing EDTA (25mM Tris base, 192mM glycine, 10mM EDTA). This permitted removal of zinc cations

that would prevent effective protein transfer to membranes. Gels were then washed 4 times for 10 minutes with methanol-free transfer buffer (25mM Tris base, 192mM glycine) to remove EDTA. Gels were transferred to 0.45μM PVDF membranes (ThermoFisher Scientific) by semi-dry transfer (TE77X semi-dry transfer unit, Hoefer). Gels were transferred in transfer buffer (25mM Tris base, 192mM glycine, 10% v/v methanol) at 1mA/cm^2 constant current for 60-80 minutes. Following electrophoretic transfer, membranes were allowed to fully dry.

For immunoblotting, membranes were reactivated in methanol, rinsed with milliQ H_2O, and blocked in 3% w/v BSA in TBS-T (20mM Tris base, 150mM NaCl, [pH 7.6], 0.1% Tween-20) for 1 hour at room temperature (Figure 7) or 4.5% w/v BSA in TBS-T overnight at 4°C (Figure 11). Membranes were probed with 1:1000 α-Myc 9E10 primary antibody (Cedarlane) in 3% BSA in TBS-T and 1:10 000 HRP-conjugated secondary α-mouse antibody (VWR) in TBS-T, each for 1 hour at room temperature on a variable speed rocker. Blots were rinsed in TBS-T 3 times for 10 minutes at ~100 RPM on an orbital shaker after blocking and antibody incubation steps. Protein-antibody conjugates were revealed by chemiluminescence through film imaging following manufacturer's instructions (Clarity Western ECL substrate [BioRad], Hyperfilm ECL films [Sigma-Aldrich]).

Statistical analysis of DNA binding through EMSA

Each compared dataset contained all replicates of DNA binding measured at each molar excess point. Sample distribution for each dataset was calculated with Shapiro-Wilk normality testing, with a significance level of 0.05. Statistical significance was calculated using parametric tests, only for sample sets that were found to follow normal (Gaussian) distribution. Statistical analyses and graphs were generated using Prism 9.0 (GraphPad).

Figure 6: DNA binding of wild-type Smc4-NT

Statistical significance was calculated with one sample t-tests, to compare Smc4-NT DNA binding at each molar excess point to the absence of any DNA binding (ME = 0), with a significance level of 0.05.

Figures 8 and 13: DNA binding of mutants compared to wild-type Smc4-NT

Statistical significance was calculated with two-tailed, paired t-tests with a confidence level of 95%, to compare wild-type Smc4-NT to mutant Smc4-NT DNA binding at each molar excess point.

Figure 9: DNA binding of phosphorylated Smc4-NT

Statistical significance was calculated using repeated measures one-way ANOVA tests with assumed sphericity and Tukey's multiple comparisons test with a 95% confidence interval. The mean of each column was compared with the mean of every other column, to compare the DNA binding of Smc4-NT in the presence and absence of active Cdc28-Clb2, inactive Cdc28-Clb2, and ATP.

Figures 10 and 13: DNA binding of phosphorylated Smc4-NT mutants

Statistical significance was calculated by performing two-tailed, paired t-tests with a confidence level of 95%, to compare the DNA binding of Smc4-NT alone to the binding in the presence of active Cdc28-Clb2, in the presence and absence of ATP.

Results

The Smc4-NT binds ssDNA

It has previously been shown that several key regions of Smc4, such as the hinge domain and ATPase heads, bind DNA (33, 34, 77–79). The Smc4-NT is indispensable in yeast and evolutionary conserved, suggesting it confers an important role to condensin function. The Smc4-NT region is predicted to be disordered (64), and it has been shown that DNA binding proteins often possess intrinsically disordered protein "tails" (74). As such, we wondered whether the Smc4-NT is also implicated in DNA binding.

Although our laboratory has previously successfully overexpressed and purified the Smc4-NT through the incorporation of a C-terminal hexahistidine tag (64), this method has not yielded large amounts of protein. We designed the fusion protein GST-Smc4-NT-8xHIS to overexpress and purify sufficient Smc4-NT protein for use in *in vitro* DNA binding assays. The incorporation of a GST tag just upstream of the Smc4-NT promoted the stability of the protein and increased overexpression (Figure 6A). However, the GST-tag is a large, 26kDa affinity tag that tends to dimerize (127). As the Smc4-NT protein itself is only ~25kDa, we wondered if the presence of the GST tag would interfere with the DNA binding activity of the Smc4-NT. We determined that the GST tag must be removed from the Smc4-NT as lower molar excesses of GST-Smc4-NT were required to achieve the same binding as Smc4-NT alone (Figure S1).

To evaluate the affinity of exclusively the Smc4-NT for DNA, we designed a workflow to efficiently purify Smc4-NT from the fusion protein GST-Smc4-NT-8xHIS (Figure 6B). Using four consecutive rounds of purification, we removed all contaminants, as well as the cleaved GST tag and HaloTEV protease, from the protein lysate to obtain pure Smc4-NT (Figure 6C, Figure S2).

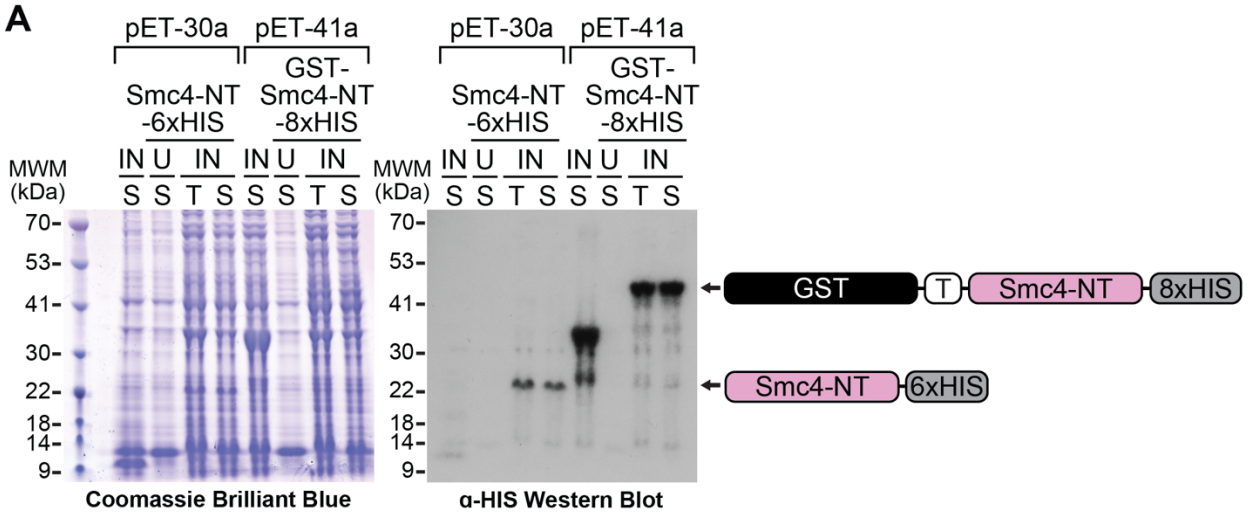
A
pET-30a
pET-41a
Smc4-NT -6xHIS
GST-Smc4-NT -8xHIS
IN U IN IN U IN
S S T S S S T S
MWM (kDa)
70-
53-
41-
30-
22-
18-
14-
9-
Coomassie Brilliant Blue
α-HIS Western Blot
GST
T
Smc4-NT
8xHIS
6xHIS

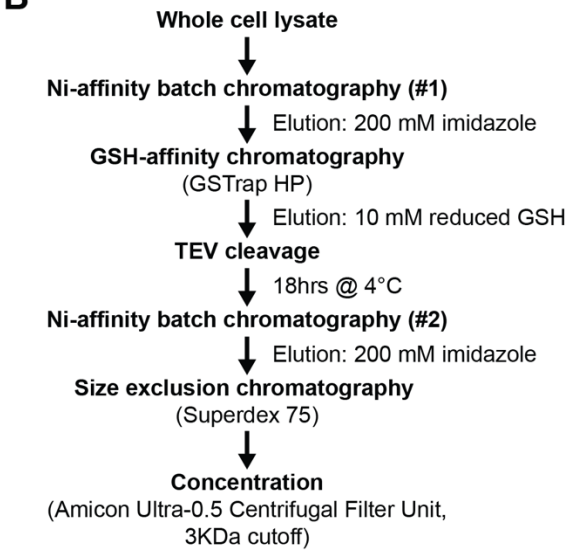
B
Whole cell lysate
Ni-affinity batch chromatography (#1)
Elution: 200 mM imidazole
GSH-affinity chromatography
(GSTrap HP)
Elution: 10 mM reduced GSH
TEV cleavage
18hrs @ 4°C
Ni-affinity batch chromatography (#2)
Elution: 200 mM imidazole
Size exclusion chromatography
(Superdex 75)
Concentration
(Amicon Ultra-0.5 Centrifugal Filter Unit, 3KDa cutoff)

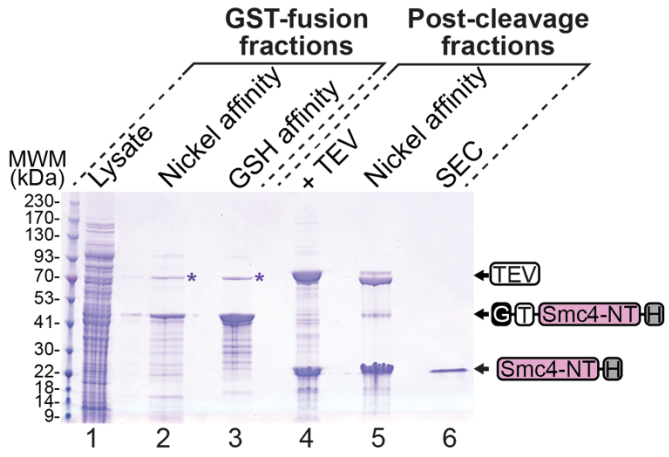
C
GST-fusion fractions
Post-cleavage fractions
Lysate
Nickel affinity
GSH affinity
+ TEV
Nickel affinity
SEC
MWM (kDa)
230-
170-
130-
93-
70-
53-
41-
30-
22-
18-
14-
9-
TEV
GST
T
Smc4-NT
H
1 2 3 4 5 6

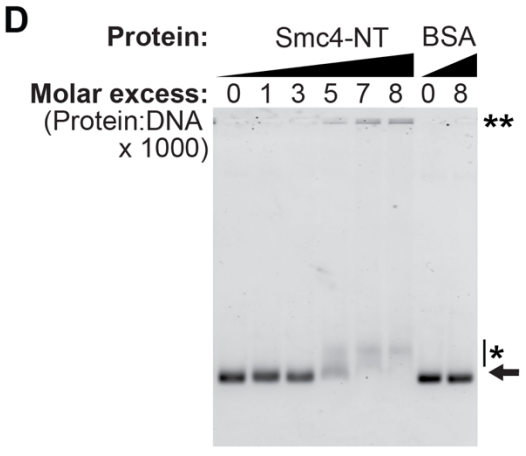
D
Protein:
Smc4-NT
BSA
Molar excess:
0 1 3 5 7 8 0 8
(Protein:DNA x 1000)
**
*

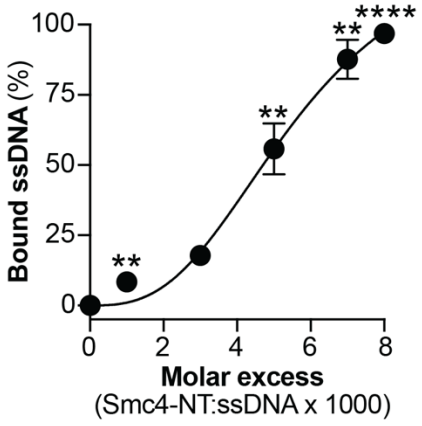
E
Bound ssDNA (%)
100
75
50
25
0
**
**
**
****
0 2 4 6 8
Molar excess
(Smc4-NT:ssDNA x 1000)

Figure 6. Purified Smc4-NT binds DNA *in vitro*. (A) Coomassie stained gel (left) and α-His Western blot (middle) showing relative expression levels of GST-Smc4-NT-8xHIS and Smc4-NT-8xHIS. Relative positions of proteins are indicated on the right; IN = induced fraction, U = uninduced fraction; S = soluble protein; T = total protein. **(B)** Workflow used to purify Smc4-NT from GST-Smc4-NT-8xHIS. **(C)** Representative gel showing the different chromatography steps used to purify Smc4-NT. The positions of the recombinant HaloTEV protease (TEV), uncleaved GST-Smc4-NT-8xHIS (G-T-Smc4-NT-H), and TEV-cleaved Smc4-NT-8xHIS (Smc4-NT-H) are indicated on the right. In the fusion protein, "T" refers to a TEV cleavage site flanked by flexible linkers. Asterisks (*) on gel indicate a contaminant band that co-migrates at the same molecular weight as HaloTEV protease, present in the purification sample prior to and following the addition of HaloTEV protease. **(D)** EMSA with increasing molar concentrations of Smc4-NT protein relative to 0.2nM ssDNA. DNA-protein complexes were resolved on a 1% agarose gel and visualized using SYBR Gold nucleic acid stain. BSA control lane shows a reaction of DNA substrate incubated with an equivalent amount of BSA to the highest molar excess of Smc4-NT used. Arrow (←) points to free DNA, single asterisk (*) indicates partially bound DNA, and double asterisk (**) shows fully bound DNA. **(E)** Binding curve for wild-type Smc4-NT binding to ssDNA. Band intensity of free DNA was calculated using ImageJ and subtracted from 100% free DNA to determine amount of bound ssDNA at each molar excess point of Smc4-NT. Nonlinear regression was performed to determine the specific binding of the Smc4-NT using Hill slope. The data reported in the graph shows the mean DNA binding +/- SEM of n=4. Statistical significance was calculated with one-sample t-tests to compare the DNA binding of Smc4-NT at each molar excess point to the absence of binding (ME = 0); no symbol = statistics not calculated; **$p<0.01$; ****$p<0.0001$.

We employed electrophoretic mobility shift assays (EMSAs) in which we incubated increasing molar excesses of purified Smc4-NT protein with a constant amount of DNA substrate. Unpublished work from our laboratory has shown that the Smc4-NT has higher affinity for ssDNA over dsDNA substrates (data not shown). As such, we decided to use ΦX174 Virion ssDNA to test the DNA binding activity of purified Smc4-NT *in vitro*. We quantitatively separated and visualized Smc4-NT-bound DNA and free DNA by gel electrophoresis, expecting to observe a retardation in ssDNA band migration if protein-bound DNA was present (Figure 6D). We observed a significant retardation in migration of ssDNA when the molar ratio of Smc4-NT to DNA exceeded a 1000-fold excess of protein to DNA (Figure 6E). Interestingly, based on the Hill slope, the molar excess

point at which about half the available binding sites on the Smc4-NT were bound to ssDNA, or the dissociation constant, K_D, was ~5666 fold excess of protein. To confirm that it was indeed binding of the Smc4-NT to ssDNA that was affecting the migration of ssDNA through the agarose gel, we ran a control reaction using BSA at the maximum molar excess value of Smc4-NT used. This did not result in a gel shift of the ssDNA, indicating that the gel migration pattern of ssDNA is due to binding by Smc4-NT, rather than unspecific molecular crowding effects.

Mass spectrometry identified key phosphorylation sites in the Smc4-NT

Our laboratory has previously shown that while deletion of the Smc4-NT region is lethal in yeast, removal of the seven minimal consensus Cdk1 phosphorylation sites from the Smc4-NT in *smc4-7A* results in viable yeast that exhibits growth defects at a restrictive temperature of 37°C (64). Since *smc4-7A* is still viable, we wondered if the Smc4-NT contains any additional phosphorylation sites that do not follow the minimal Cdk1 consensus phosphorylation sequence (S/T-P-X) that may contribute to the phospho-regulation of the Smc4-NT.

We phosphorylated Smc4-NT and Smc4-7A-NT (in which all minimal consensus Cdk1 phosphorylation sites were mutated to alanine) with Cdc28-Clb2 *in vitro*. After verifying the phosphorylation reactions, we sent the phosphorylated proteins for mass spectrometry analysis to identify any additional phosphorylation sites. Of important note, Smc4-NT proteins were overexpressed and purified in *E. coli* cells and should not contain any baseline phosphorylated residues. Mass spectrometry analysis of purified and phosphorylated Smc4-NT and Smc4-7A-NT identified nine additional phosphorylation sites in both proteins (Figure 4B: blue = minimal consensus Cdk1 phosphorylation sites, yellow = mass spectrometry-identified sites). Of these nine

sites, some have previously been identified as *in vivo* phosphorylation sites for various kinases by other research groups (128).

We wondered whether removal of the mass spectrometry-identified phosphorylation sites would have any proliferative effects on yeast. We created *smc4-9A*, in which we mutated the nine mass spectrometry-identified phosphorylation sites in *SMC4* to alanine, and *smc4-16A*, which combines the mutations in *smc4-9A* with those in *smc4-7A* (the Cdk1 phospho-site-deficient allele). We introduced the phospho-mutant *smc4* alleles into a wild-type diploid yeast strain for genomic integration at one allele only. After confirming the presence of the mutations by DNA sequencing, we assessed the viability of each haploid strain by tetrad spore dissection; all resulting haploid strains were viable. To further investigate the proliferative effects of these mutations, we performed cell viability serial dilution assays with the mutant haploid strains. Interestingly, *smc4-9A* showed no growth defects at restrictive temperature compared to *smc4-7A*. Unexpectedly, when both sets of mutations were combined in *smc4-16A*, the *smc4-9A* phenotype fully rescued the growth defects observed in *smc4-7A* (Figure 7A).

Robellet et al. previously showed that the Smc4-NT is phosphorylated early in mitosis, whereas Smc-7A-NT experiences no phosphorylation-induced gel retardation throughout the cell cycle (64). There appears to be a preliminary level of phosphorylation present at the beginning of the cell cycle in wild-type Smc4-NT, indicated by a "fuzzy" Western blot band at T=0 as opposed to a clean single band for Smc4-7A-NT at the same time point (Figure 7B). We wondered if removal of the mass spectrometry-identified phosphorylation sites in Smc4-9A-NT would impact this initial level of phosphorylation. We transformed plasmids expressing either Smc4-9A-NT or Smc4-16A-NT into *cdc15-2* strains for use in phosphorylation time course assays. The use of strains with the temperature sensitive *cdc15-2* allele allowed us to evaluate the phosphorylation

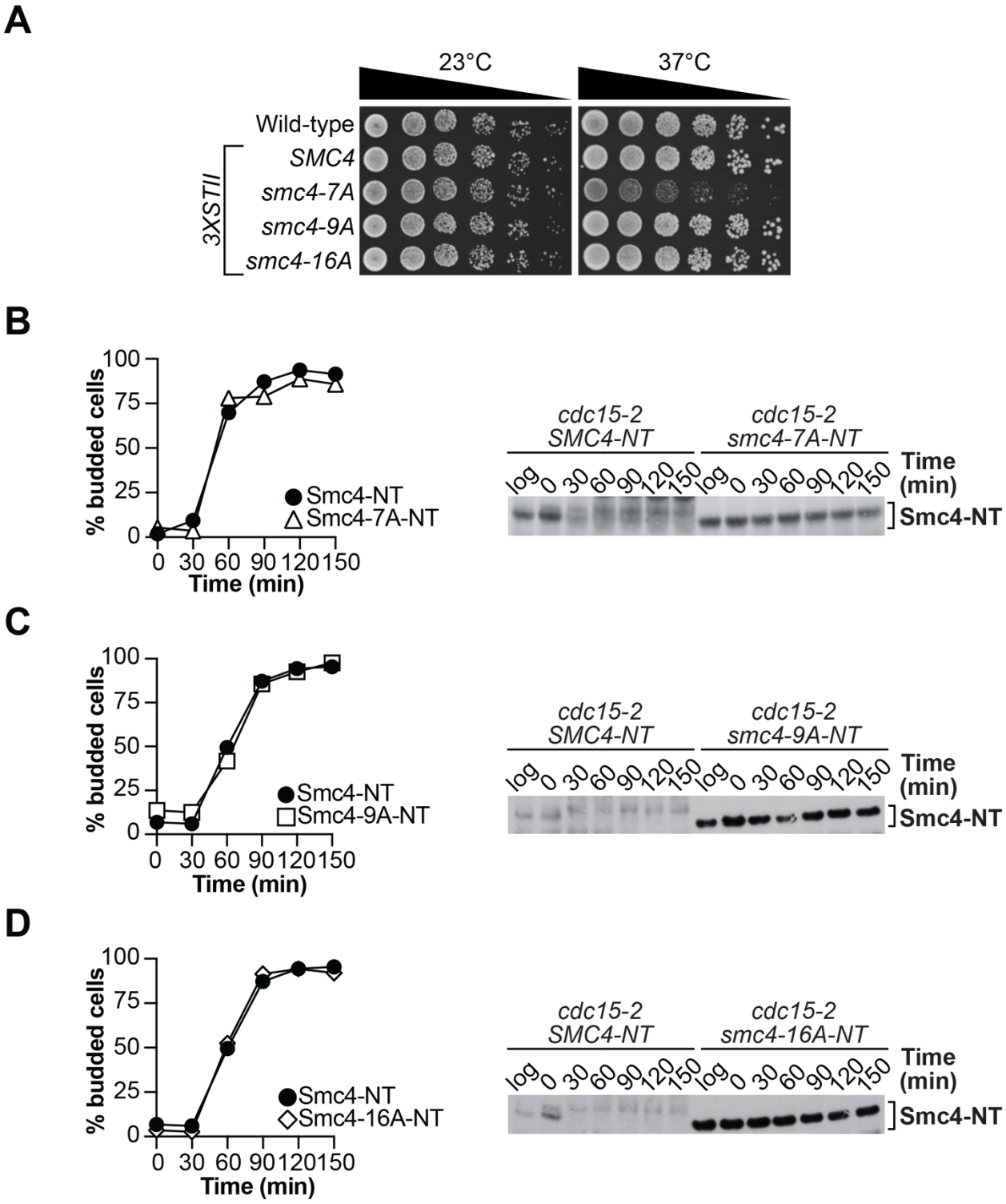

Figure 7. Abrogation of putative Cdk1 phosphorylation sites in the Smc4-NT affects yeast growth and cell cycle dependent phosphorylation of the Smc4-NT. **(A)** Growth phenotype of haploid yeast strains containing the *smc4-7A*, *smc4-9A*, and *smc4-16A* mutations. Five-fold serial dilutions of *MAT***a** wild-type (untagged), Strep-tagged wild-type (*SMC4-3xSTII*), and Strep-tagged phospho-mutant *smc4* strains were spotted on solid medium. Strains were grown at 23°C and 37°C for 36 hours and 30

hours, respectively, to evaluate sensitivity of growth to temperature, n=3. Time course analyses of Smc4-NT phosphorylation in the presence and absence of **(B)** minimal consensus Cdk1 sites (Smc4-7A-NT), **(C)** mass spectrometry-identified Cdk1 phosphorylation sites (Smc4-9A-NT), and **(D)** minimal consensus and mass spectrometry-identified Cdk1 phosphorylation sites (Smc4-16A-NT). Cells expressing wild-type or phospho-mutant Smc4-NT were arrested in G1 using α-factor and released at restrictive temperature (37°C). Samples were taken at 30-minute intervals to evaluate cell cycle-dependent phosphorylation-induced gel retardation (right). Representative budding index of cells throughout time course experiment corresponding to blot is shown on the left.

state throughout the duration of one cell cycle, as this allele is defective in mitotic exit at a restrictive temperature of 37°C. We used alpha factor to arrest these strains in the G1 stage of the cell cycle at a permissive temperature of 23°C. Cell cycle arrest was confirmed by evaluating the morphological changes of cells until most of the cell population adopted a "shmoo" morphology. Cells were then released from cell cycle arrest at a restrictive temperature, and time points were collected at regular intervals. To verify the phosphorylation status of the Smc4-NT, we ran cell lysates on Phos-Tag SDS-PAGE gels, which allow for increased separation of phosphorylated vs unphosphorylated species of the same protein relative to regular SDS-PAGE (129). Surprisingly, while demonstrating no discernable growth defects in yeast, Smc4-9A-NT appeared to show a complete loss of detectable phosphorylation throughout the cell cycle (Figure 7C). Smc4-16A-NT also experienced a loss of detectable phosphorylation-induced gel retardation resembling that of Smc4-9A-NT (Figure 7D). These results suggest that the mass spectrometry-identified sites are *in vivo* phosphorylation sites in the Smc4-NT, that contribute to the phosphorylation-dependent regulatory mechanism of the Smc4-NT. That removal of these sites alone is sufficient to show complete loss of detectable phosphorylation of the Smc4-NT suggests that regulation of the Smc4-NT may not be exclusively done by Cdk1, but by various kinases whose activity is spatiotemporally regulated during the cell cycle.

Smc4-NT phospho-mutants demonstrate different affinities for ssDNA

We wondered whether removal of the minimal consensus Cdk1 or mass spectrometry-identified phosphorylation sites from the Smc4-NT would affect its affinity for ssDNA. To test the importance of these sites for DNA binding through EMSA, we overexpressed and purified Smc4-7A-NT (Figure 8A), Smc4-9A-NT (Figure 8B), and Smc4-16A-NT (Figure 8C) in *E. coli*. We used the same workflow as optimized with wild-type Smc4-NT protein (Figure 6B). We incubated the mutant Smc4-NT proteins with ssDNA in EMSAs to establish the baseline DNA binding activity of the mutants and determine if DNA binding activity was reduced with the elimination of key residues. It is important to note that the ssDNA binding affinity for each mutant was evaluated alongside wild-type protein on the same agarose gel, with equilibrated salt concentrations and identical parameters. As such, though the exact binding at each molar excess point for wild-type protein varies across different gels and on different mutant binding curves, this measure should be taken as a relative value that serves as a comparison point for each mutant. From the resulting Hill plots, we discovered that relative to wild-type protein ($K_D \approx$ 5326-fold excess), Smc4-7A-NT exhibited slightly more affinity for ssDNA ($K_D \approx$ 3854-fold excess), though the binding at any molar excess point was not statistically significant compared to wild-type protein (Figure 8D). In contrast, Smc4-9A-NT exhibited slightly lower affinity for ssDNA ($K_D \approx$ 4582-fold excess) compared to wild-type protein ($K_D \approx$ 3314-fold excess), though again, this was not statistically significant (Figure 8E). When both sets of mutations were combined in Smc4-16A-NT, the mutant showed visibly more binding to ssDNA compared to wild-type protein ($K_D \approx$ 2832-fold excess for Smc4-16A-NT and $K_D \approx$ 5688-fold excess for wild-type protein) (Figure 8F). None of the mutants showed significantly different binding at any molar excess point relative to wild-type protein.

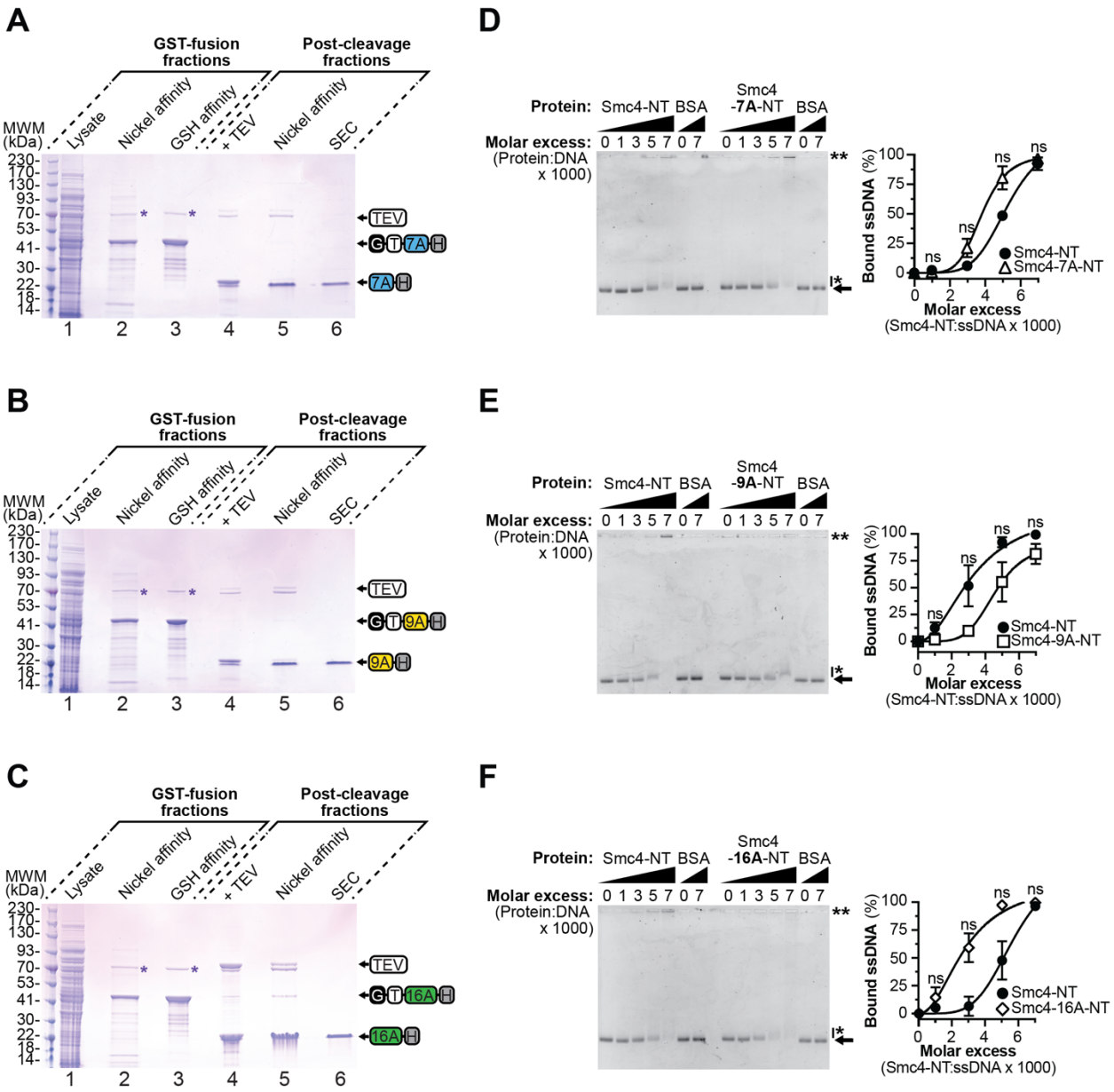

Figure 8. Purified Smc4-NT phospho-mutant proteins bind ssDNA with slight differences to wild-type protein. Representative gels showing a summary of chromatography steps used to obtain purified **(A)** Smc4-7A-NT, **(B)** Smc4-9A-NT, and **(C)** Smc4-16A-NT proteins. The positions of recombinant HaloTEV protease, uncleaved GST-tagged proteins, and TEV-cleaved proteins are indicated on the right. In the fusion proteins, "T" refers to a TEV cleavage site flanked by flexible linkers between the GST tag and the Smc4-NT. Asterisks (*) on gel indicate a contaminant band that co-migrates at the same molecular weight as HaloTEV protease, present in the purification samples prior to and following the addition of HaloTEV protease. EMSA gels (left) and binding curves (right) with increasing molar concentrations of wild-type Smc4-NT compared to **(D)** Smc4-7A-NT, **(E)** Smc4-9A-NT, and **(F)** Smc4-16A-NT mutant proteins. Increasing molar amounts of protein were incubated with 0.2nM ssDNA and resolved by gel electrophoresis. ssDNA was visualized using SYBR

Gold nucleic acid stain. BSA control reaction contains DNA substrate incubated with an equivalent amount of BSA to the highest molar excess of Smc4-NT used. Arrow (←) points to free DNA, single asterisk (*) indicates partially bound DNA, and double asterisk (**) shows fully bound DNA. Band intensity of free DNA was calculated using ImageJ and subtracted from 100% free DNA to determine amount of bound ssDNA at each molar excess point of Smc4-NT. Nonlinear regression was performed to determine the specific binding of the Smc4-NT using Hill slope. Data was quantified using Image J and shows an average +/- SEM of n=3 (D) and n=4 (E, F). Statistical significance was calculated with two-tailed, paired t-tests to compare mutant Smc4-NT to wild-type Smc4-NT DNA binding at each molar excess point; ns = not significant.

Taken together, these results suggest that at baseline, the residues thought to be putative phosphorylation sites do not directly confer DNA binding activity to the Smc4-NT.

Phosphorylation of the Smc4-NT abrogates DNA binding activity

Having established that the Smc4-NT has baseline DNA binding activity, we next wanted to investigate the effects of Cdk1 phosphorylation on the affinity of the Smc4-NT for ssDNA. We used yeast Cdc28-Clb2 to phosphorylate the Smc4-NT *in vitro*; the presence of phosphorylated Smc4-NT was confirmed by gel retardation of the substrate after electrophoresis (Figure 9A, reaction B). We also heat-denatured Cdc28-Clb2 to abrogate its kinase activity and incubated inactivated Cdc28-Clb2 with Smc4-NT in the presence of ATP, to further confirm that any changes in electrophoretic behaviour of the Smc4-NT were indeed due to phosphorylation by Cdc28-Clb2 (Figure 9A, reaction D). Additionally, we set up a series of identical reactions without any ATP, to investigate whether merely the presence of Cdc28-Clb2 alone would be enough to impact the DNA binding activity of the Smc4-NT (Figure 9A, reactions A'-E').

We discovered that phosphorylation of wild-type Smc4-NT by Cdc28-Clb2 completely abrogated its affinity for ssDNA (Figure 9C, lanes 6-8). Interestingly, when inactivated Cdc28-Clb2 was combined with Smc4-NT in the presence of ATP, we observed more DNA binding

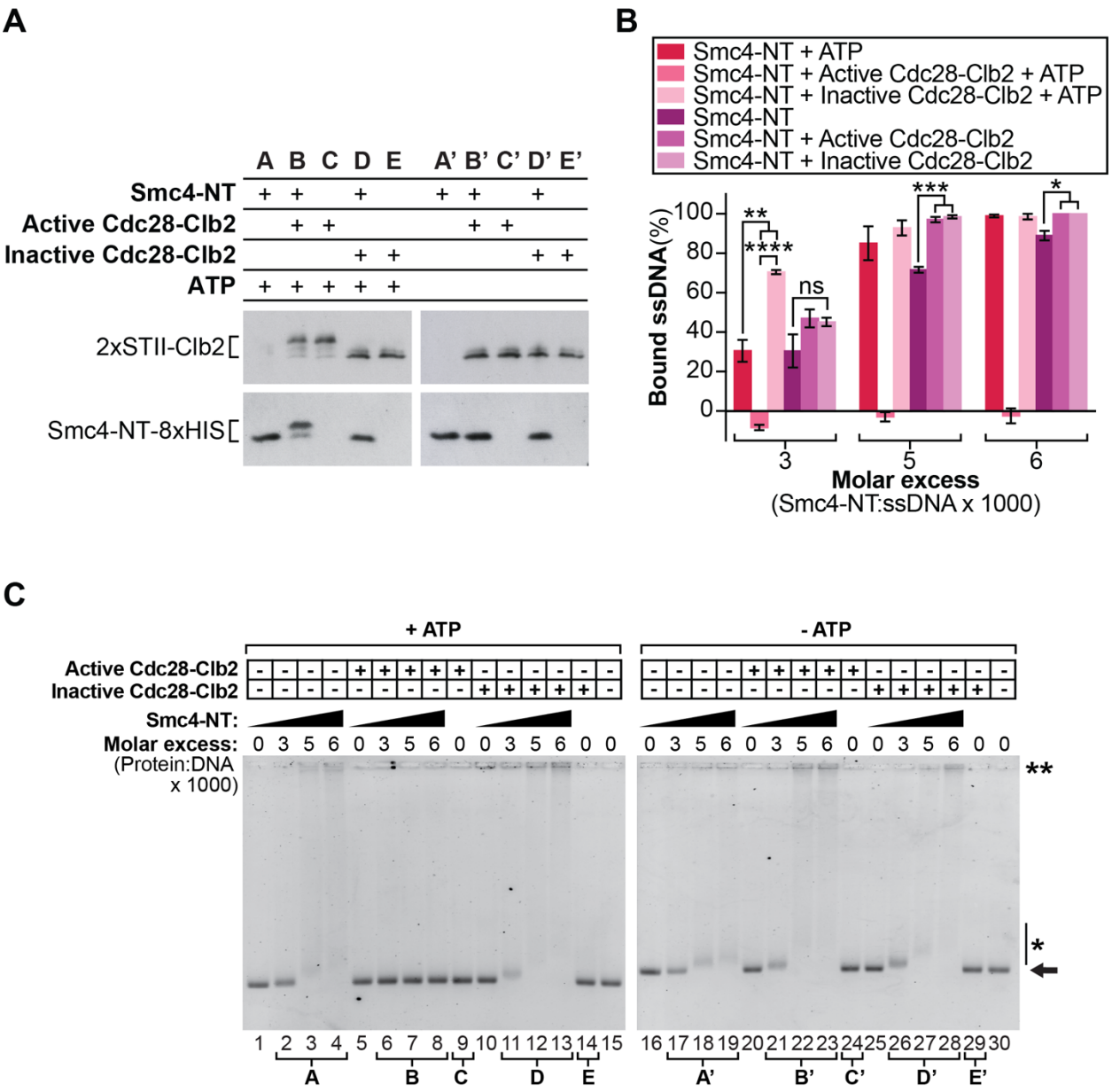

Figure 9. Cdc28-Clb2 modulates Smc4-NT affinity for DNA. (A) *In vitro* kinase assays of Smc4-NT with active and denatured Cdc28-Clb2, in the presence (reactions A-E) and absence (reactions A'-E') of ATP. Purified Smc4-NT protein was incubated alone (A, A'), with active Cdc28-Clb2 (B, B') or with heat-inactivated Cdc28-Clb2 (D, D'). Negative control reactions for DNA binding were set up with just active Cdc28-Clb2 (C, C') or inactive Cdc28-Clb2 (E, E'). After incubation, proteins were separated on a 14% SDS-polyacrylamide gel and transferred to a nitrocellulose membrane probed for the Smc4-NT or Clb2 subunit using α-His or α-Strep antibodies, respectively. All panels for western blot were run on one blot but are presented in separate panels to match the loading order of reactions in EMSAs. **(B)** Quantification of bound ssDNA at each molar excess point of Smc4-NT for all conditions. Band intensity of free DNA was calculated using ImageJ and subtracted from 100% free DNA to determine amount of bound ssDNA for each molar excess point of Smc4-NT.

Data shows an average +/- SEM of n=3. Statistical significance was calculated by repeated measures one-way ANOVA tests to compare all column means; no symbol = statistics not calculated; ns = not significant; *p<0.05; **p<0.01; ***p<0.001; ****p<0.0001. **(C)** EMSA with Smc4-NT protein from *in vitro* kinase assays. EMSAs with increasing molar concentrations of Smc4-NT, incubated alone or with active or inactive Cdc28-Clb2 in the presence (left) or absence (right) of ATP. Kinase reactions were used at indicated molar excesses in EMSA reactions with a constant amount of 0.2nM ssDNA. Protein-DNA complexes were separated on a 1% agarose gel and visualized with SYBR Gold nucleic acid stain. Reactions C, C', E' and E' contain only active or denatured Cdc28-Clb2 and serve as negative controls for DNA binding. Arrow (←) points to free DNA, single asterisk (*) indicates partially bound DNA, and double asterisk (**) shows fully bound DNA. All wells were equalized for salt concentration including carryover from kinase reactions.

compared to Smc4-NT alone (Figure 9C, lanes 2-4 vs lanes 11-13). Quantification of DNA binding at 3000-fold molar excess of protein: DNA in the presence of ATP showed a significant contrast between Smc4-NT affinity for ssDNA in different conditions (Figure 9B). We did not observe any DNA binding in reactions that contained only active or inactive kinase without Smc4-NT, indicating that this change in DNA binding affinity was indeed due to modulation of the Smc4-NT and not due to intrinsic binding activity of Cdc28-Clb2 (Figure 9C, lanes 9 and 14, respectively).

We used the ATP-free reactions to determine whether the presence of Cdc28-Clb2 alone would be enough to modulate the affinity of Smc4-NT for DNA. Interestingly, removal of ATP from the kinase reactions prevented phosphorylation of Smc4-NT but still influenced its affinity for ssDNA. We found that compared to binding by the Smc4-NT alone, the mere presence of Cdc28-Clb2 in the reaction, whether active or inactive, caused a "super-shift" in DNA binding by the Smc4-NT (Figure 9C, lanes 17-19 vs lanes 21-23 for active kinase and lanes 26-28 for inactive kinase). Again, this phenotype was not recapitulated upon incubation of the kinase alone with ssDNA substrate (Figure 9C, lanes 24 and 29). This "super-shift" was quantifiably observable at the 5000- and 6000-fold molar excess of protein: DNA, where there was a significant difference between the DNA binding of Smc4-NT alone vs. when combined with active or inactive kinase

(Figure 9B). To ensure that the observed increase in binding was not due to stabilization of the Smc4-NT by a large protein complex, we performed control "kinase assays" in which we combined Smc4-NT with BSA protein instead of Cdc28-Clb2 prior to incubation with ssDNA. This set of assays did not generate the same "super-shifts" (data not shown). Such a DNA binding "super-shift" was observed when Smc4-NT was combined with active or inactive Cdc28-Clb2, suggesting that Cdc28-Clb2 binds the Smc4-NT to further retard the migration of the Smc4-NT-DNA complex through the gel. As heat-denaturing Cdc28-Clb2 did not hinder this "super-shift", the interaction between the Smc4-NT and Cdc28-Clb2 may be mediated by the interaction of a specific sequence of residues between the two proteins.

Smc4-NT phospho-mutants show phosphorylation-dependent DNA binding differences

Having established that phosphorylation of the Smc4-NT modulates its affinity for ssDNA through EMSA, we wondered how phosphorylation of mutant Smc4-NT proteins lacking putative phosphorylation sites would influence their ability to bind DNA. We used only active Cdc28-Clb2 to repeat the kinase assays coupled to EMSAs as performed with wild-type Smc4-NT protein, in the presence and absence of ATP (Figure 10).

We discovered that Smc4-7A-NT, lacking the minimal consensus Cdk1 phosphorylation sites, did not experience a change in electrophoretic behaviour after incubation with Cdc28-Clb2 and ATP (Figure 10A, left). This may not necessarily mean that Smc4-7A-NT is not phosphorylated by Cdc28-Clb2 at all, but does indicate that the extent of detectable phosphorylation is decreased upon removal of these key sites. In line with this assumption, Smc4-7A-NT protein incubated with ssDNA in the presence of Cdc28-Clb2 and ATP did not show phosphorylation-dependent DNA binding defects (Figure 10A, right). However, in both ATP and

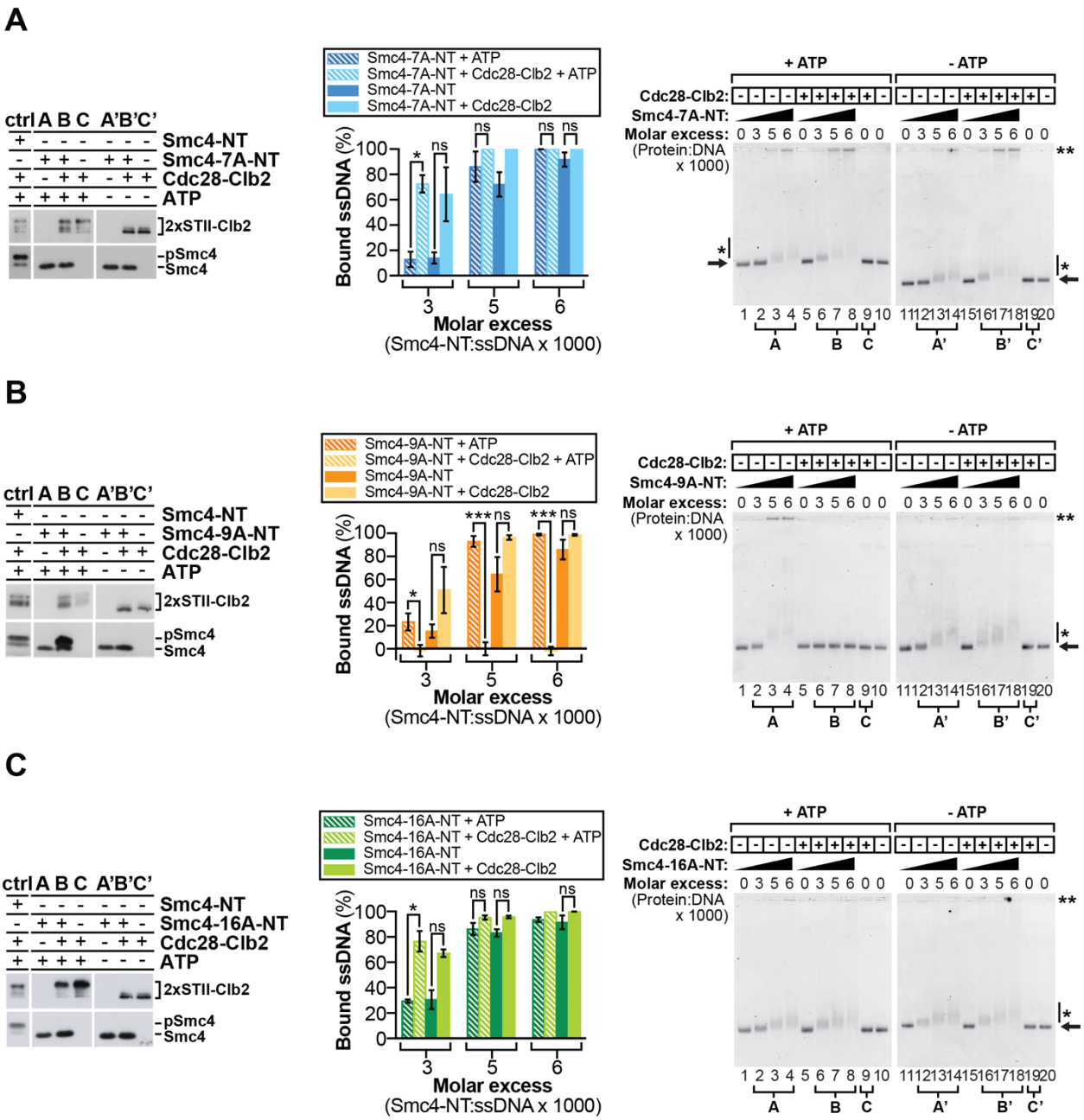

Figure 10. Removal of minimal consensus Cdk1 phosphorylation sites in the Smc4-NT abrogates phosphorylation-dependent DNA binding defects. *In vitro* kinase assays **(left)** of **(A)** Smc4-7A-NT, **(B)** Smc4-9A-NT, and **(C)** Smc4-16A-NT with active Cdc28-Clb2, in the presence (reactions A-C) and absence (reactions A'-C') of ATP. Purified mutant Smc4-NT proteins were incubated alone (A, A') or with active Cdc28-Clb2 (B, B'). Negative control reactions for DNA binding were set up with only Cdc28-Clb2 (C, C'). Wild-type Smc4-NT was phosphorylated alongside each mutant (ctrl) to confirm Cdc28-Clb2 enzyme efficiency. Kinase reaction completion was validated by immunoblot analysis of Smc4-NT proteins to verify presence of kinase and phosphorylated or unphosphorylated Smc4-NT protein. For each assay, all panels for western blot were run on one blot but are presented as shown in separate panels to

match the loading order of reactions in EMSAs. Quantification of bound ssDNA at each molar excess point **(middle)** of **(A)** Smc4-7A-NT, **(B)** Smc4-9A-NT, and **(C)** Smc4-16A-NT for all conditions. Band intensity of free DNA was calculated using ImageJ and subtracted from 100% free DNA to determine amount of bound ssDNA at each molar excess point of Smc4-NT. Data shows an average +/- SEM of n=3. Statistical significance was calculated with two-tailed, paired t-tests to compare the DNA binding of Smc4-NT alone to the presence of Cdc28-Clb2 in ATP and ATP-free conditions; no symbol = statistics not calculated; ns = not significant; *$p<0.05$; ***$p<0.001$. EMSAs **(right)** with increasing molar concentrations of **(A)** Smc4-7A-NT, **(B)** Smc4-9A-NT, and **(C)** Smc4-16A-NT proteins from *in vitro* kinase assays in the presence (left) or absence (right) of ATP. Kinase reactions were used at indicated molar excesses for EMSA reactions with a constant amount of 0.2nM ssDNA. Protein-DNA complexes were separated on 1% agarose gels and visualized with SYBR Gold nucleic acid stain. Reactions C and C' contain only Cdc28-Clb2 and serve as negative controls for DNA binding. Arrow (←) points to free DNA, single asterisk (*) indicates partially bound DNA, and double asterisk (**) shows fully bound DNA. All wells were equalized for salt concentration including carryover from kinase reactions.

ATP-free conditions, the presence of Cdc28-Clb2 caused a DNA binding "super-shift" when Smc4-7A-NT was combined with ssDNA (Figure 10A, center, right). This reinforces the idea that Cdc28-Clb2 and Smc4-NT do not interact solely due to phosphorylation, but that there is a physical interaction between the two proteins mediated by a linear sequence of residues.

Next, we tested the affinity of Smc4-9A-NT for ssDNA when combined with Cdc28-Clb2, with and without ATP. We found that Smc4-9A-NT still showed phosphorylation-induced gel migration retardation (Figure 10B, left). This is likely due to the presence of the minimal Cdk1 consensus phosphorylation sites in this mutant that are responsible for the major detectable phosphorylation-induced band shift of the protein. Interestingly, phosphorylation of Smc4-9A-NT by Cdc28-Clb2 completely abrogated DNA binding activity, and the presence of Cdc28-Clb2 without ATP was enough to generate a DNA binding "super-shift" (Figure 10B, center, right). As this mutant does not lack the minimal consensus Cdk1 phosphorylation sites, these sites could still be phosphorylated by Cdc28-Clb2 *in vitro* and exert influence on Smc4-9A-NT's DNA binding activity. Importantly, the phosphorylation of Smc4-9A-NT by Cdc28-Clb2 was conducted in an

isolated, reconstituted, *in vitro* environment, where Cdc28-Clb2 and ssDNA were added sequentially to Smc4-9A-NT. The lack of phosphorylation sites in Smc4-9A-NT still modulated the phosphorylation status of the Smc4-NT *in vivo*, as seen in Figure 7C, suggesting that these sites may be targets for other kinases, a possibility we will explore further later on.

When both sets of mutations were combined in Smc4-16A-NT, Cdc28-Clb2 did not appear to phosphorylate the Smc4-NT in the presence of ATP, likely due to the lack of the minimal consensus Cdk1 phosphorylation sites (Figure 10C, left). The DNA binding phenotype after incubation with kinase also most closely resembled that of Smc4-7A-NT, where there were no DNA binding defects after incubation with Cdc28-Clb2 and ATP, and a DNA binding "super-shift" in the presence of Cdc28-Clb2 alone (Figure 10, middle, right). Altogether, these results suggest that the sites absent in Smc4-7A-NT are more directly targeted by Cdk1 *in vitro* in yeast, whereas the sites lacking in Smc4-9A-NT could be targets for other kinases or not as preferentially phosphorylated by Cdc28-Clb2 *in vitro*. Thus, removal of phosphorylation sites in Smc4-7A-NT abrogates any phosphorylation-dependent DNA binding defects in the Smc4-NT, whereas removal of the Smc4-9A-NT sites is insufficient to prevent DNA binding defects, indicating that DNA binding by the Smc4-NT is regulated in a phosphorylation-dependent manner.

Deletion of CK2 affects viability of yeast and in vivo phosphorylation of the Smc4-NT

It has previously been shown that condensin is regulated by many mitotic kinases such as Cdc5 and Ipl1, in addition to Cdk1(104). However, recent evidence has shown that condensin also plays a role in regulating interphase chromatin structure, despite not being as directly implicated as other interphase regulators (55, 92, 106, 115). Of particular interest, CK2 plays an important role in negatively regulating interphase condensin (62, 112).

As removal of the mass spectrometry-identified phosphorylation sites in the Smc4-NT abrogated phosphorylation of the Smc4-NT in a cell cycle dependent manner (Figure 7C), but did not fully abrogate phosphorylation of the Smc4-NT *in vitro* (Figure 10B), we hypothesized that these sites may serve as secondary, inhibitory phospho-sites that are targeted by a different kinase. Specifically, we wondered if the Smc4-NT is regulated in a multistep phosphorylation mechanism in which it is activated by Cdk1 phosphorylation and inhibited by CK2 phosphorylation prior to the onset of mitosis. To investigate this possibility, we deleted the beta regulatory subunits of CK2 (i.e., Ckb1 and Ckb2) in *SMC4*, *smc4-7A*, *smc4-9A*, and *smc4-16A* strains, as deletion of the alpha subunits of CK2 results in lethality (130). We observed that the phenotype of *ckb1Δckb2Δ* was dominant over each of the phenotypes for *smc4-7A*, *smc4-9A*, and *smc4-16A* individually (Figure 11A). Specifically, while *smc4-7A* appeared to be fully rescued by *ckb1Δckb2Δ*, the phenotypes of *smc4-9A ckb1Δckb2Δ* and *smc4-16A ckb1Δckb2Δ* were slightly temperature sensitive relative to *smc4-9A* and *smc4-16A* alone. Rescue of a temperature sensitive *smc4* mutant by deletion of *CKB1* and *CKB2* has also previously been shown in *S. pombe*, where the growth defects in *cut3-477* mutants were circumvented by individual deletion of *CKB1* or *CKB2* (111). Additionally, deletion of *CKB1* and *CKB2* did not appear to affect the abundance of Smc4 proteins through immunoblot analysis (Figure 11B). It has previously been shown that Smc4-7A is less abundant than wild-type Smc4, but the reduction of protein levels of Smc4-7A is not responsible for observable growth defects (64).

We next wondered how deletion of Ckb1 and Ckb2 would affect the phosphorylation of the Smc4-NT throughout the cell cycle. We crossed the strains used in phosphorylation time courses with *ckb1Δckb2Δ* strains, performed phosphorylation time course assays, and separated lysates on Phos-Tag gels to visualize their phospho-shifts. We had initially hypothesized that the

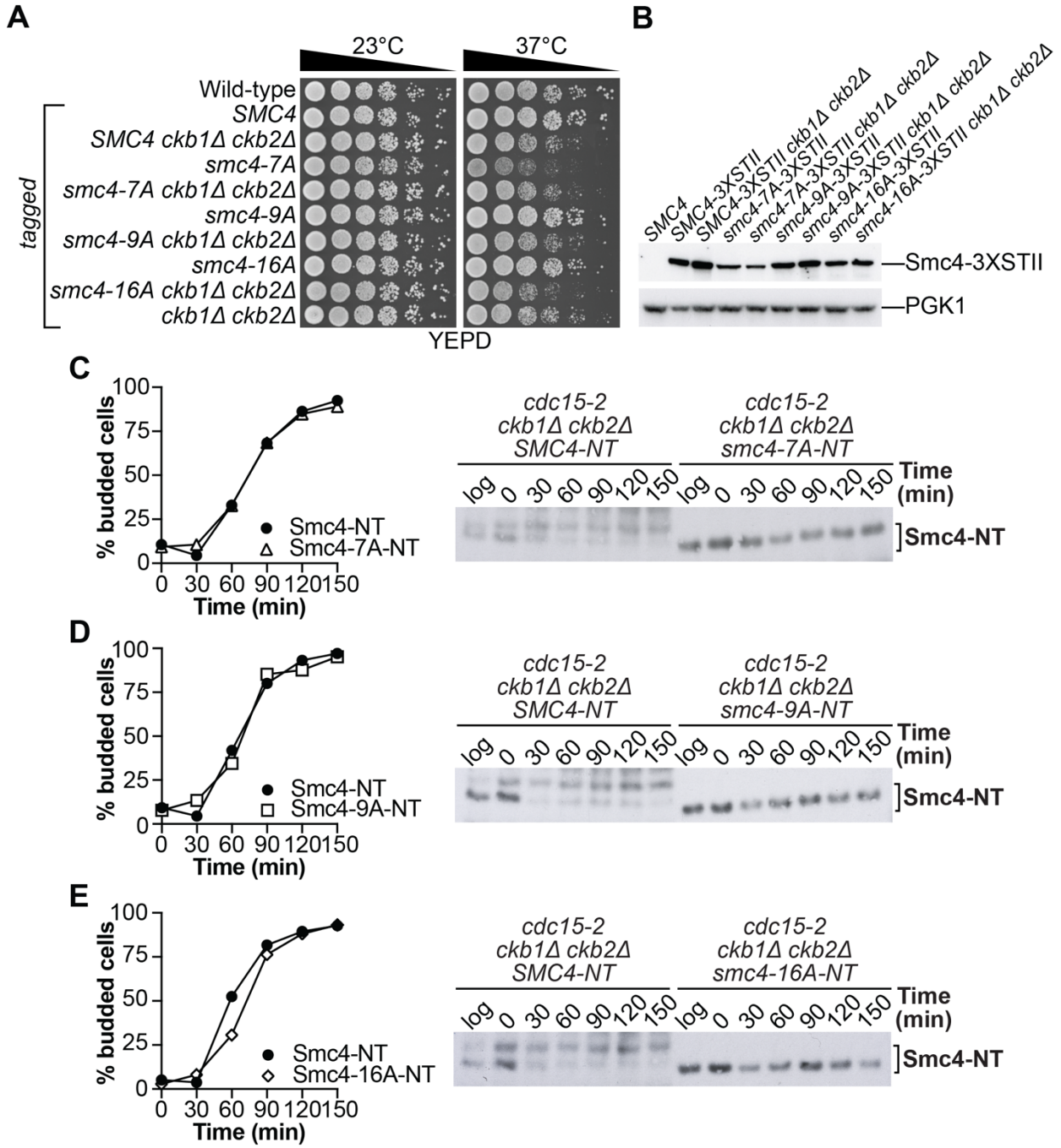

Figure 11. Deletion of beta regulatory subunits of CK2 affects cell viability and cell cycle dependent phosphorylation of Smc4-NT. (A) Deletion of *CKB1* and *CKB2* has a dominant growth phenotype over all other mutations. Five-fold serial dilutions of *MAT***a** haploid strains were spotted on solid medium and grown at 23°C and 37°C for 30 hours or 36 hours to evaluate sensitivity of growth to temperature, n=3. All strains bracketed with "tagged" are tagged with 3xSTII at the C-terminus of *SMC4*. **(B)** Immunoblot probed with α-Strep shows that all Smc4 mutant proteins are expressed in yeast. Phosphorylation time courses comparing Smc4-NT phosphorylation in a strain lacking Ckb1 and Ckb2, combined with the absence of **(C)** minimal consensus Cdk1 sites (Smc4-7A-NT), **(D)** mass spectrometry-identified Cdk1

phosphorylation sites (Smc4-9A-NT), and **(E)** minimal consensus and mass spectrometry-identified Cdk1 phosphorylation sites (Smc4-16A-NT). Cells expressing wild-type or phospho-mutant Smc4-NT in a *cdc15-2 ckb1Δ ckb2Δ* background were arrested in G1 with α-factor and released at a restrictive temperature of 37°C. Samples were taken at 30-minute intervals to evaluate cell cycle-dependent phosphorylation-induced gel retardation (right). Representative budding index of cells throughout time course experiment corresponding to blot is shown on the left.

mass spectrometry-identified phosphorylation sites were responsible for the initial level of phosphorylation that can be observed at T = 0 in wild-type Smc4-NT, and that removal of these sites would not cause a complete loss of phosphorylation in Smc4-9A-NT as seen in Smc4-7A-NT (Figure 7B). However, surprisingly, Smc4-9A-NT and Smc4-16A-NT both experienced what appeared to be a complete loss of phosphorylation throughout the cell cycle, and no observable preliminary phosphorylation at T = 0 (Figure 7C, D). Thus, we did not expect that deletion of *CKB1* and *CKB2* would have more stringent impacts on phosphorylation through immunoblot analysis than we had already seen, as was proven to be the case for Smc4-7A-NT (Figure 11C), Smc4-9A-NT (Figure 11D), and Smc4-16A-NT (Figure 11E). However, when observing the phosphorylation of wild-type Smc4-NT throughout the cell cycle in strains lacking Ckb1 and Ckb2, it appeared as though the Smc4-NT was present mainly as 2 distinct bands, one unphosphorylated band, and one phosphorylated band. This contrasts wild-type Smc4-NT's electrophoretic behaviour in a strain containing Ckb1 and Ckb2, where phosphorylation presented as more of a "smear" rather than in distinct forms (Figure 11C vs 7B, Smc4-NT). Thus, the absence of a "smear" could indicate that phosphorylation by CK2 is responsible for the "fuzzy" band that appears at T=0 in wild-type Smc4-NT protein. Furthermore, it appears as though in a strain lacking Ckb1 and Ckb2, wild-type Smc4-NT protein stayed partially unphosphorylated throughout the cell cycle, as demonstrated by the "unphosphorylated" band present at every time point. Taken together, we propose that the mass spectrometry-identified phosphorylation sites may remain

residually phosphorylated at the onset of a new cell cycle, where Cdk1 phosphorylation of the Smc4-NT occurs before dephosphorylation of the sites that have been inhibitorily phosphorylated by CK2 during interphase.

The Smc4-NT is phosphorylated by CK2 in vitro

Having determined that deletion of the beta regulatory subunits of CK2 appeared to have effects on the cell cycle dependent phosphorylation of the Smc4-NT *in vivo*, we next sought to determine whether the Smc4-NT is directly phosphorylated by CK2 *in vitro*. We first attempted to verify the phosphorylation status of the Smc4-NT by incubating it with human CK2 in the presence of ATP and running the reaction mixture on a 14% agarose gel. This technique has successfully been used to show phosphorylation of the Smc4-NT by Cdk1 through the appearance of a phosphorylation-induced band shift of the Smc4-NT (64) (Figure 9A). We were unable to detect phosphorylation of the Smc4-NT through this method (data not shown), so we moved to an alternate approach using a phosphoprotein-specific fluorescent stain. We set up kinase reactions with purified Smc4-NT and CK2 and ran a polyacrylamide gel which was stained with Pro-Q Diamond Phosphoprotein gel stain. This phosphoprotein-specific stain selectively targets phosphorylated residues, presenting a convenient alternative to the use of radiolabelled ATP to verify kinase reactions (131). To confirm the efficacy of the kinase reaction and the Pro-Q Diamond stain, we also phosphorylated Smc4-NT with Cdc28-Clb2 as a positive control and used bacterially purified Smc4-NT as a negative control. We observed that Pro-Q Diamond stained both kinase reaction lanes and did not stain the lane containing the substrate only control, indicating that the Smc4-NT is phosphorylated by CK2 *in vitro* (Figure 12A). To further validate that the signal detected was indeed due to phosphorylated residues only, we stained the gel with SYPRO

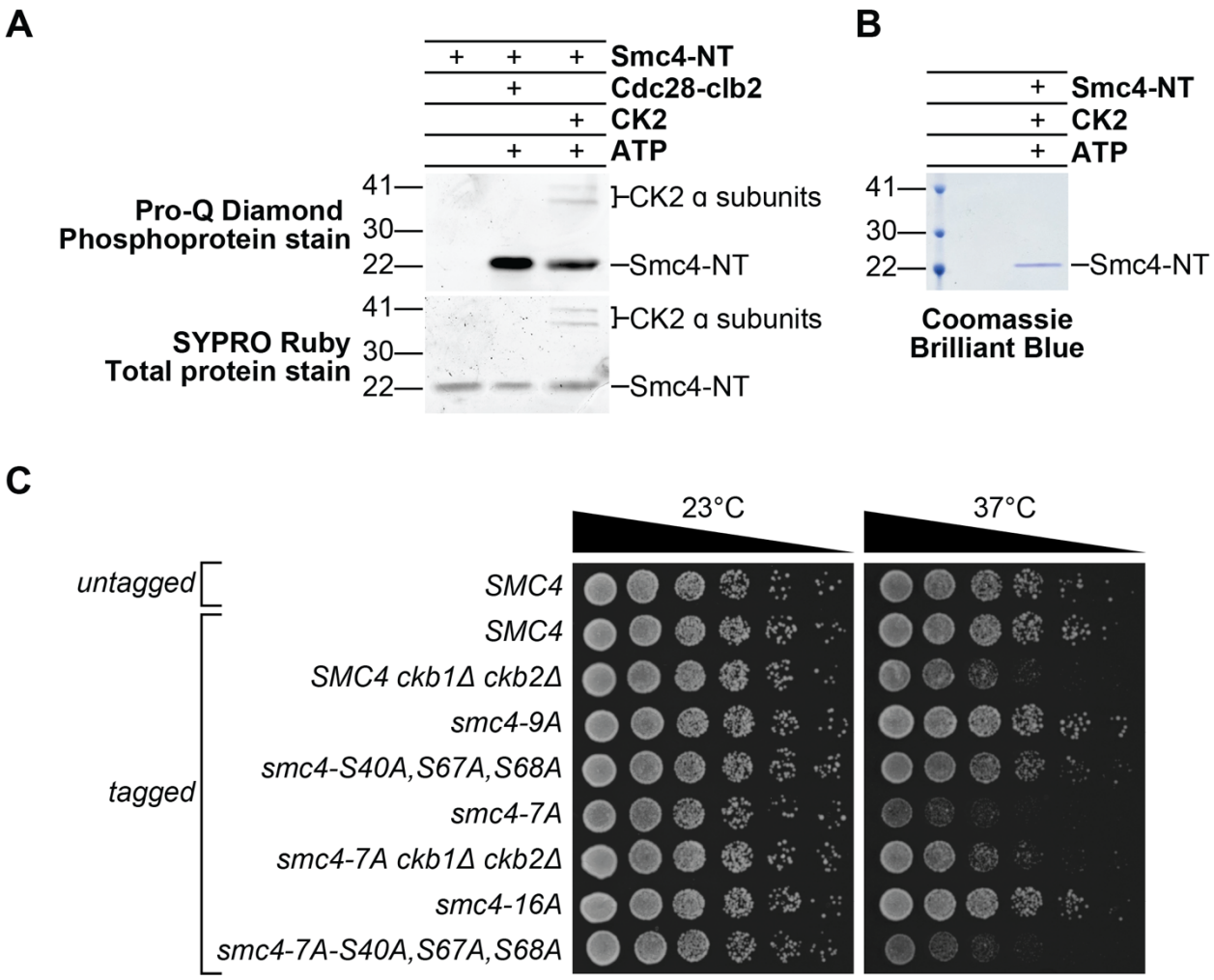

Figure 12. CK2 phosphorylates the Smc4-NT *in vitro*. (A) *In vitro* kinase reactions incubating purified Smc4-NT alone (1st lane, negative control), with Cdc28-Clb2 (2nd lane, positive control) or with CK2 (3rd lane). After incubation, proteins were separated on a 4-12% SDS-polyacrylamide gel and stained with Pro-Q Diamond phosphoprotein stain (top) followed by SYPRO Ruby total protein stain (bottom). **(B)** *In vitro* kinase reaction of Smc4-NT with CK2 was separated on a 4-12% SDS-polyacrylamide gel and revealed by Coomassie staining; band was excised and sent for mass spectrometry analysis. **(C)** Removal of only mass spectrometry-identified CK2 phosphorylation sites is not sufficient to rescue the growth defects observed in *smc4-7A*. Mass spectrometry-detected CK2 phosphorylation sites in the Smc4-NT were mutated in *SMC4* and *smc4-7A*. Five-fold serial dilutions of *MAT**a*** haploid untagged wild-type and tagged wild-type and mutant *SMC4* strains were spotted on solid medium and grown at 23°C and 37°C for 30 hours or 36 hours to evaluate sensitivity of growth to temperature, n=3. Tagged strains have a 3xStrep tag at the C-terminus of Smc4.

Ruby total protein fluorescent stain. We observed an equivalent amount of protein in all lanes, including the no kinase control lane. Thus, we determined that the Smc4-NT is phosphorylated by

CK2 *in vitro*. We ran the same CK2-phosphorylated Smc4-NT protein on a gel that was stained with Coomassie Brilliant Blue, excised the band, and sent it for mass spectrometry analysis to identify phosphorylated residues (Figure 12B).

The general minimal consensus motif for CK2 is S/T-X-X-E/D, though variations of this sequence, such as S/T-X-E/D and S/T-E/D, can also be phosphorylated (132). Mass spectrometry analysis of CK2-phosphorylated Smc4-NT identified a potential phosphorylation site at S40, which falls into the S-E potential phosphorylation sequence for CK2. Also identified as a potential phosphorylation site was S67 or S68, the former of which initiates the sequence S-S-G-E, following the ideal minimal consensus motif for CK2. The first mass spectrometry analysis of Cdc28-Clb2-phosphorylated Smc4-NT also identified S68 as a putative phosphorylation site. We wondered whether removal of these 3 sites would be sufficient to recapitulate the rescue of *smc4-7A* by *smc4-9A*. We thus created S40A, S67A, and S68A mutations in *SMC4* as well as in *smc4-7A* and tested whether these mutants had growth defects at restrictive temperature.

We observed that *smc4-S40A, S67A, S68A* showed very slight growth defects at a nonpermissive temperature of 37°C; these effects were not as prominent as the defects seen in *ckb1Δ ckb2Δ*, but were more severe than *smc4-9A,* which showed no temperature-dependent growth defects (Figure 12C). Furthermore, combining these 3 mutations with *smc4-7A* did not rescue its growth defects, in contrast to the effects seen in *smc4-16A* or after the deletion of *CKB1* and *CKB2*. Taken together, these results show that removal of mass spectrometry-identified CK2 phosphorylation sites in the Smc4-NT are not sufficient to rescue the growth defects observed in *smc4-7A*, indicating there may be more sites targeted by CK2 in the Smc4-NT.

The cyclin binding motifs in the Smc4-NT mediate its interaction with Cdc28-Clb2

Based on results obtained through EMSAs, phosphorylation of the Smc4-NT by Cdc28-Clb2 abrogates DNA binding of the Smc4-NT. However, when Smc4-NT is combined with active Cdc28-Clb2 in the absence of ATP, or with heat-inactivated Cdc28-Clb2, there is an apparent increase in DNA binding by the Smc4-NT. This binding does not appear to be due to stabilization of the protein by nature of a large protein complex, indicating that there may be a physical interaction between Cdc28-Clb2 and Smc4-NT that is mediated by a linear stretch of residues.

We first attempted to detect this interaction through pulldown assays in which tagged Cdc28-Clb2 was bound to beads and incubated with His-tagged Smc4-NT (data not shown). However, even upon the addition of ssDNA to help mediate or trigger the reaction, we were unable to detect a direct interaction between Cdc28-Clb2 and Smc4-NT. The major limitation of this experiment is that it is generally used to characterize strong or stable protein interactions. As such, if the interaction between Cdc28-Clb2 and Smc4-NT is transient or weak, or is mediated by other proteins or PTMs, it would not necessarily be detected through such a pulldown assay. We moved to a biological approach to try to detect an interaction between the Smc4-NT and Cdc28-Clb2. Substrates of CDK-cyclin complexes often contain RxL docking motifs that interact with the hydrophobic patches of cyclins to mediate CDK targeting to their substrates (99). The Smc4-NT contains two RxL motifs, RKL (residues 62-64) and RRL (residues 120-122). We wondered whether ablation of the two RxL docking motifs in the Smc4-NT would prevent Cdc28-Clb2 from targeting the Smc4-NT, as it has previously been shown that removal of the RxL motifs from the Smc4-NT reduced the extent of its cell cycle-dependent phosphorylation (64).

We attempted to create haploid yeast strains containing *smc4-rxlA* mutations by introducing the mutant allele into a wild-type diploid yeast strain for genomic integration at one

allele only and creating haploid strains by tetrad spore dissection. However, tetrad spore dissections of *SMC4/smc4-rxlA* strains showed a non-Mendelian segregation pattern of 3:1 viable spores, possibly due to errors in meiosis (Figure 13A). Haploid strains isolated from these tetrads showed differential temperature sensitivities despite having the same sequenced genotype at the Smc4-NT (data not shown). We also observed diploid strains that appeared to be temperature sensitive, but when dissected, did not result in temperature sensitive haploid strains (data not shown). To determine the true phenotype of *smc4-rxlA*, we transformed full length *smc4-rxlA* under the natural *SMC4* promoter into the *URA3* locus of the highly temperature sensitive *smc4-22* strain (77). As the *smc4-22* mutant is viable at 23°C but nonviable at 37°C, the true phenotype of *smc4-rxlA* would be revealed at 37°C. We observed that at 37°C, *smc4-rxlA* rescued the growth defects caused by *smc4-22* (Figure 13B). This indicates that *smc4-rxlA* expresses a functional copy of Smc4 and does not have dominant growth defects. We also transformed *smc4-rxlA* into the *URA3* locus of a strain with wild-type *SMC4* at its endogenous locus and did not observe any dominant growth defects in this strain at restrictive temperature (Figure 13B). Furthermore, immunoblot analysis showed that Smc4-rxlA protein was expressed from the *URA3* locus in strains with endogenous *SMC4* or *smc4-22*, albeit at a slightly lower level than wild-type Smc4 protein (Figure 13C). Taken together, these results indicate that ablation of the RxL motifs in Smc4-NT does not result in dominant effects on cell viability and protein expression.

As Robellet et al. showed the importance of the RxL motifs in regulating the cell cycle-dependent phosphorylation of the Smc4-NT, we wondered whether removal of these motifs would impact the DNA binding activity of the Smc4-NT (64). We purified Smc4-rxlA-NT protein by expressing GST-Smc4-rxlA-NT-8xHIS in *E. coli* and performing 4 consecutive rounds of purification as described earlier (Figure 6B, Figure 13D). Unexpectedly, despite the rescue of

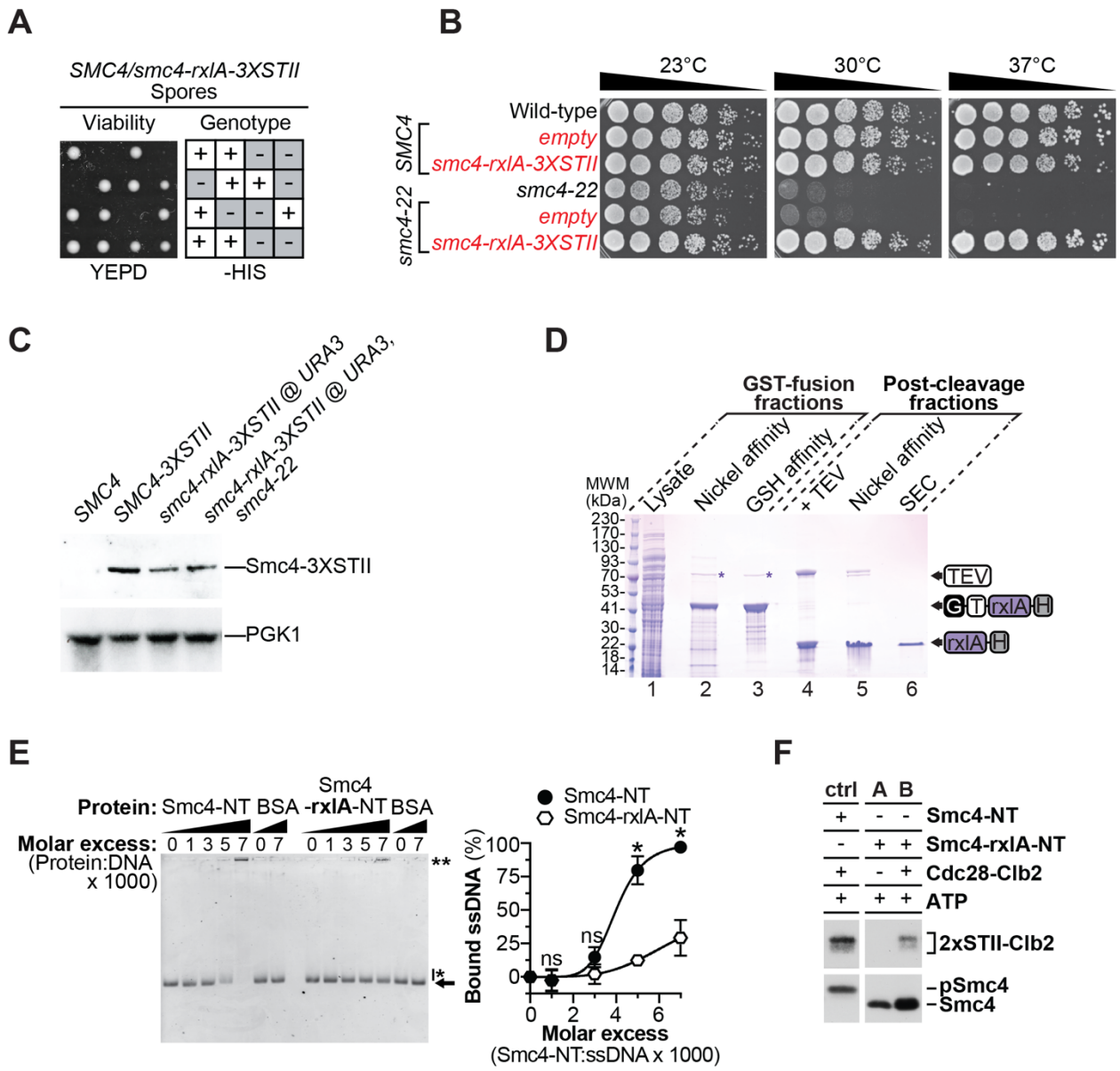

Figure 13. Mutation of cyclin binding motifs in the Smc4-NT generates functional Smc4 protein with severe DNA binding defects. (A) Tetrad spore dissection of *SMC4/smc4-rxlA-3xSTII* has a non-Mendelian segregation pattern. The genotype of spores was determined by evaluating growth on SC-HIS plates using the *HIS3* marker associated with the *smc4-rxlA* allele; + indicates wild-type *SMC4*. **(B)** The *smc4-rxlA-3xSTII* gene integrated at the *URA3* locus of *smc4-22* rescues the growth phenotype associated with *smc4-22* and shows no dominant growth defects when integrated at the *URA3* locus of a wild-type yeast strain. Five-fold serial dilutions of the *MAT***a** haploid strains were spotted on solid medium. Strains were grown at 23°C and 37°C for 30 hours or 36 hours days to evaluate sensitivity of growth to temperature, n = 3. Strains labelled "empty" or "*smc4-rxlA-3xSTII*" are transformed with an empty *YIplac211* vector or *YIplac211-Psmc4-smc4-rxlA-3xSTII* (under the natural *SMC4* promoter) at the *URA3* locus. **(C)** Immunoblot analysis shows that Smc4-rxlA-3xSTII protein is expressed when integrated at the *URA3* locus of yeast. **(D)** Representative gels

showing a summary of chromatography steps used to obtain purified Smc4-rxlA-NT protein. The positions of recombinant HaloTEV protease, uncleaved GST-tagged Smc4-rxlA-NT protein, and pure Smc4-rxlA-NT protein are indicated on the right. In the fusion protein, "T" refers to a TEV cleavage site flanked by flexible linkers between the GST tag and Smc4-rxlA-NT. Asterisks (*) on gel indicate a contaminant band that co-migrates at the same molecular weight as HaloTEV protease, present in the purification samples prior to and following the addition of HaloTEV protease. **(E)** EMSA gel (left) and binding curve (right) with wild-type Smc4-NT compared to Smc4-rxlA-NT mutant protein. Increasing molar amounts of proteins as indicated were incubated with 0.2nM linearized ssDNA and resolved by agarose gel electrophoresis. ssDNA was visualized using SYBR Gold nucleic acid stain. BSA control reaction contains DNA substrate incubated with an equivalent amount of BSA to the highest molar excess of Smc4-NT used. Arrow (←) points to free DNA, single asterisk (*) indicates partially bound DNA, and double asterisk (**) shows fully bound DNA. Salt concentrations were equalized between proteins. For binding curve, band intensity of free DNA was calculated using ImageJ and subtracted from 100% free DNA to determine amount of bound ssDNA for each molar excess point. Nonlinear regression was performed to determine the specific binding of the Smc4-NT using Hill slope; data shows an average +/- SEM of n=3. Statistical significance was calculated with two-tailed, paired t-tests to compare the DNA binding of Smc4-rxlA-NT to that of wild-type Smc4-NT at each molar excess point; no symbol = statistics not calculated; ns = not significant; **$p<0.01$. **(F)** Cdc28-Clb2 cannot efficiently phosphorylate Smc4-rxlA-NT *in vitro*. Purified Smc4-rxlA-NT was incubated alone (A) or with active Cdc28-Clb2 and ATP (B). Relative to phosphorylated wild-type Smc4-NT, Smc4-rxlA-NT does not show phosphorylation-induced gel migration retardation. Control reaction was run on the same blot as reactions A and B.

smc4-22 by *smc4-rxlA*, removal of the putative cyclin docking motifs in the Smc4-NT almost completely abrogated its DNA binding activity ($K_D \approx$ 4002-fold excess for Smc4-NT vs. $K_D \approx$ 6771-fold excess for Smc4-rxlA-NT; Figure 13E). Despite the absence of kinase activity in this assay, at baseline, Smc4-rxlA-NT had severely limited DNA binding activity *in vitro* despite acting as a functional copy of Smc4 *in vivo*. Additionally, Cdc28-Clb2 was unable to efficiently phosphorylate Smc4-rxlA-NT *in vitro* (Figure 13F). We propose that the RxL docking motifs in the Smc4-NT mediate its interaction with Cdc28-Clb2, and that this interaction plays an important role in regulating Cdc28-Clb2 phosphorylation of the Smc4-NT in the context of DNA binding.

Discussion

Smc4-NT has affinity for ssDNA

The unique N-terminal extension of the Smc4 subunit of condensin is essential for viability in yeast, suggesting it plays an important role in the regulation of condensin function (64). We established that the Smc4-NT has DNA binding activity, as is consistent with the mode of action of condensin (Figure 6D, E) (33, 34, 77–79).

We chose ssDNA for our assays as unpublished work from our laboratory has shown that the Smc4-NT binds ssDNA with higher affinity than dsDNA, which has also been shown to be the case for the hinge and ATPase head regions of Smc4 (33, 77). Importantly, the ΦX174 Virion ssDNA substrate we used in EMSAs was much larger in size compared to the Smc4-NT protein: ~170kDa relative to ~25 kDa, respectively. This would suggest thousands of possible binding sites on every DNA substrate, in contrast to substrates such as oligonucleotides which would represent a model of only one binding site per molecule. We chose to use ssDNA as our substrate to provide insights on DNA binding by the Smc4-NT that could be relevant to the context of the cell (i.e., large stretches of DNA), but easily measured using experimental parameters (i.e., not so large that massive amounts of DNA were required to observe binding shifts). As such, a large fold excess of Smc4-NT was required to affect the migration of the DNA. This is consistent with the observation that other DNA binding regions, such as the Smc2/4 heterodimer, require high molar ratios of protein to DNA base pairs regardless of plasmid size to induce a shift (78).

We wanted to investigate the DNA binding activity of the disordered Smc4-NT as it has been well established that intrinsically disordered proteins often possess DNA binding activity (65). Proteome-wide analysis of Cdk1 substrates has shown that intrinsically disordered regions are often rich in phosphorylation sites (93). While the exact location of these phospho-sites is not

conserved, the clustering of several Cdk1 sites in particular regions or proteins indicates biological function for these regions that was selected for throughout evolution (94). Thus, it can be no coincidence that the Smc4-NT, a region essential for cell survival and rich in Cdk1 phosphorylation sites, has DNA binding activity and is part of a complex responsible for restructuring DNA. Establishing the baseline DNA binding activity of the Smc4-NT allowed us to study how the Smc4-NT and its interaction with different proteins help to regulate the function of condensin.

Purified Smc4-NT construct eluted from the gel filtration column as a single peak corresponding to a molecular mass of approximately 66 kDa compared to globular mass standards (Figure S2). This is far larger than the calculated molecular mass of a monomeric Smc4-NT construct, which is about 20 kDa. This is likely due to the predicted disordered nature of the Smc4-NT, as size exclusion chromatography is sensitive to macromolecule shape. Since the protein mass standards used for calibration of the column were globular in shape, the relative elution size of the Smc4-NT cannot accurately be determined using these standards (133). As the protein elutes as a strong, single peak and runs at the calculated size on an SDS-PAGE gel, it is highly likely that the Smc4-NT exists in monomeric form. Further analysis of the protein, for example, by multi-angle light scattering, would more conclusively confirm this notion.

Comparing the wild-type protein to the mutant proteins, all eluted at approximately the same size, thus, the induced mutations did not affect the solubility or stability of the proteins, even though polar residues (serine and threonine) were mutated to non-polar (alanine) residues. The Smc4-NT is predicted to be a disordered region, so changing the polarity of certain amino acids did not have a significant effect on protein folding as the protein does not have a stable three-dimensional shape (64). We observed a slight increase in the DNA binding activity of the Smc4-NT upon the removal of all 16 putative phosphorylation sites (Figure 8F). It has been shown that

in chicken CAP-D3 of condensin II, a threonine to alanine mutation of a putative Cdk1 site resulted in hypercondensation of chromosomes but had no effects on cell survival (134). It was proposed that CAP-D3 plays a role in regulating condensin by limiting its binding to chromosomes. It has also been suggested that for condensin to compact chromatin, it must experience lower levels of binding with DNA when active than when inactive (135). That the abrogation of 16 putative phosphorylation sites in the Smc4-NT led to increases in DNA binding would support the hypothesis that these residues may play a role in minimizing the interaction of Smc4-NT, a part of condensin, with DNA. This *in vitro* assay evaluated the binding of purified, unphosphorylated proteins, so removal of specific residues allowed us to discern the baseline role they play before modification by phosphorylation. This suggests that while phosphorylation may act in regulating DNA binding of the Smc4-NT, phosphorylation at key sites is not what directly confers DNA binding activity to the Smc4-NT. A PhD student in our laboratory, Alyssa Pastic, is currently investigating several key DNA binding motifs in the Smc4-NT.

Removal of putative Cdk1 phosphorylation sites in vivo

Mass spectrometry analysis was performed by phosphorylating purified Smc4-NT and Smc4-7A-NT with purified Cdc28-Clb2, separating the reactions on a gel, and excising the bands corresponding to Smc4-NT and Smc4-7A-NT. Both samples were sent for mass spectrometry analysis and nine non-S/T-P phosphorylation sites were detected across both proteins. While there are many limitations of *in vitro* experiments, the use of an *in vitro* system for this assay offered the advantage of allowing us to study the activity of only Cdc28-Clb2 on Smc4-NT, in an isolated system without interference from other kinases.

It has been shown that Cdk1 can phosphorylate non-S/T-P motifs *in vitro* (87, 88). It is possible that in the reconstituted system we used for our kinase assays, that Cdc28-Clb2 acted on the Smc4-NT in a way that would not have been measurable in a cellular context. We posit that while Cdk1 has preference for the minimal consensus S/T-P motif, when all minimal consensus sites are mutated (Smc4-7A-NT), Cdk1 can act on non-consensus sites, such as the nine mass spectrometry-identified sites. We hypothesize that normally, the nine mass spectrometry-identified sites are phosphorylated by CK2 to inhibit the activity of the Smc4-NT. While the sites absent in Smc4-7A-NT may be the primary level of regulation and the main targets for Cdk1, perhaps the sites removed in Smc4-9A-NT get phosphorylated as a "backup" when the minimal consensus Cdk1 sites are not present or are blocked, as a compensatory mechanism by Cdk1 in the absence of CK2. It has been shown that CK2 phosphorylation appears to be dominant over Cdk1 phosphorylation (62), but when CK2 is not present in the system and there are no consensus sites to be targeted, perhaps Cdk1 tries to compensate for its loss by phosphorylating sites that are normally targeted by CK2. Phosphorylation by Cdk1 rather than CK2 could lead to these sites triggering "activation" of condensin rather than their normal function of inhibition.

We were surprised that abrogation of the nine mass spectrometry-identified phosphorylation sites rescued the growth defects observed upon the ablation of the seven minimal consensus Cdk1 sites in the Smc4-NT (Figure 7A). Upon initial observation that *smc4-9A* had no temperature sensitive growth defects, it appeared as though these sites were not essential to the regulation of the Smc4-NT. The presence of the seven minimal consensus Cdk1 phosphorylation sites seemed to be sufficient to allow yeast to persist in the absence of the mass spectrometry-identified sites. However, removal of the nine mass spectrometry-identified sites led to a complete loss of phosphorylation of the Smc4-NT throughout the cell cycle, despite normal cell cycle

progression kinetics (Figure 7C). This indicates that abrogation of these sites does affect the phospho-regulation of the Smc4-NT, which we propose occurs in a stepwise mechanism we delve into further below. Consistent with this, while *smc4-16A* appeared to have no temperature sensitive growth defects, it also experienced a complete abrogation of cell cycle dependent phosphorylation despite normal cell cycle progression (Figure 7A, 7D). Likely, the reversal of growth defects from *smc4-7A* in *smc4-16A* is due to cell division that persists despite defects in chromosome morphology. This could be due to nonspecific phosphorylation events caused by the absence of key targets for Cdk1 and CK2. Emerging evidence shows that *SMC4* may act as a tumour prognostic marker as it is overexpressed in many diseases characterized by erroneous cell division, such as cancers (136). Thus, while ablation of mass spectrometry-identified phosphorylation sites does not appear to cause growth defects in yeast, the loss of cell cycle-dependent phosphorylation in these mutants indicates errors in the regulation of Smc4. This may be due to a loss of all potential target sites for Cdk1 as well as CK2, leading to cell cycle progression despite defects in condensin regulation.

This is further reinforced by the yeast strains where we deleted potential phospho-sites in *SMC4* and the regulatory subunits of CK2 (Figure 11A). The absence of CK2 activity fully rescued the growth defects observed upon abrogation of the minimal consensus Cdk1 sites (*smc4-7A ckb1Δ ckb2Δ* vs. *smc4-7A*). Perhaps this improvement in growth can be explained by Cdk1 acting to phosphorylate the nine mass spectrometry-identified sites, normally phosphorylated by CK2. The inactivation of CK2 would lead to other targets of this kinase not getting adequately phosphorylated, leading to the slight growth defects observed in *ckb1Δ ckb2Δ* relative to wild-type yeast. In *smc4-9A ckb1Δ ckb2Δ*, we observed relatively healthy yeast, with minimal growth defects at restrictive temperature. This could be due to regular phosphorylation of the minimal consensus

sites in Smc4-NT by Cdk1, but the complete loss of CK2 activity due to deletion of the kinase as well as its target sites in Smc4-NT. In *smc4-16A ckb1Δ ckb2Δ*, we see slightly more growth defects at restrictive temperature relative to *smc4-9A ckb1Δ ckb2Δ*, due to a complete loss of putative phosphorylation sites and one of 2 major regulatory kinases. This indicates that despite the presence of Cdk1, the combination of the ablation of phosphorylation sites in Smc4 and deletion of CK2 has drastic impacts on the cell. Importantly, the deletion of *CKB1* and *CKB2* likely had more severe effects on cell growth than simply the removal of phosphorylation sites in the Smc4-NT, as CK2 has other targets within the cell that are affected by its inactivity.

Interestingly, we found that deletion of Ckb1 and Ckb2 resulted in a partially unphosphorylated species of wild-type Smc4-NT persisting throughout the cell cycle (Figure 7B vs 11C, Smc4-NT). Additionally, rather than appearing as a "smear" of several differentially phosphorylated species of Smc4-NT, wild-type Smc4-NT appeared to be present in 2 distinct forms, one appearing to be phosphorylated, and the other unphosphorylated. This could mean that CK2 phosphorylation serves to "prime" the Smc4-NT for phosphorylation by Cdk1. While we believe that phosphorylation by CK2 is inhibitory whereas Cdk1 phosphorylation is activatory, there could be a certain level of phosphorylation by each kinase required to modulate not only DNA binding of the Smc4-NT, but the overall activity of condensin. Treatment of later time points with a phosphatase, such as lambda phosphatase, will confirm the presence of different phosphorylated forms of the Smc4-NT.

The effects of phosphorylation by Cdk1 on DNA binding by the Smc4-NT

As it is known that chromosome condensation events are triggered by Cdk1 and that the Smc4-NT is a key target for Cdk1 modification, we next investigated the effects of Cdk1

phosphorylation on DNA binding by the Smc4-NT (Figure 9). We observed that phosphorylation by Cdc28-Clb2 led to almost a complete abrogation of DNA binding by the Smc4-NT. This is consistent with work on other DNA binding proteins, where it has been proposed that phosphorylation of key proteins is essential to reduce interaction with DNA. For example, a lamin protein, LAP2α, is also differentially phosphorylated in interphase and mitosis by different kinases, the main mitotic regulator being Cdk1. Mutation of a key phospho-site of this protein to alanine causes the protein to be unable to dissociate from chromosomes during mitosis, suggesting that phosphorylation is important for decreasing DNA binding affinity (137). Furthermore, Doughty et al. suggested that condensin must dissociate from chromosomes following mitosis to enable efficient cell cycle progression (135). Cell cycle-dependent phosphorylation of the Smc4-NT showed increased phosphorylation in a time-dependent manner, suggesting that through mitotic progression, Smc4-NT may reduce either its own interaction with DNA, or the interaction of condensin with DNA.

Furthermore, we observed that phosphorylation at the minimal consensus Cdk1 sites specifically is what reduces DNA binding activity of the Smc4-NT. Smc4-9A-NT protein still showed phosphorylation-dependent gel retardation and DNA binding defects similar to wild-type Smc4-NT protein (Figure 10B). However, Smc4-7A-NT protein as well as Smc4-16A-NT protein did not appear to be phosphorylated through immunoblot analysis, nor did they experience any loss in DNA binding activity after Cdk1 phosphorylation (Figures 10A, 10C). In our kinase assays with Smc4-9A-NT, in which the minimal consensus Cdk1 sites were present and the only kinase activity came from Cdk1, the combination of Cdk1 and its ideal target sequence came to the forefront as the main regulatory mechanism. Of important note, these experiments were conducted in an *in vitro* environment using only Cdk1 with no interference from CK2. CK2 has been shown

to act on IDPRs and assist in their binding to DNA, RNA and other proteins, and has also been shown to be a major regulator for condensin (62, 138). Despite observing phosphorylation of the Smc4-9A-NT *in vitro*, this mutant still appears to show a complete loss of cell cycle dependent phosphorylation *in vivo* (Figure 10B, 7C). This would imply a specific sequence of phosphorylation events, where the activity of CK2 dominates lower levels of Cdk1 until a key threshold of Cdk1 activity is reached. Following priming of Cdk1 phosphorylation, CK2 phosphorylation would be removed by key phosphatases. For re-entry into interphase, Smc4-NT residues already phosphorylated by either Cdk1 or other kinases that act later in mitosis could help to prime the activity of CK2.

CK2 phosphorylation of the Smc4-NT could inhibit condensin function

Mass spectrometry analysis of CK2-phosphorylated Smc4-NT identified 3 potential phosphorylation sites. However, alanine mutations at these sites (S40, S67, S68) in the Smc4-NT resulted in slight temperature sensitive growth defects in yeast and was unable to rescue the growth defects observed in *smc4-7A*. As with any mass spectrometry experiment conducted in an *in vitro* system, there are many limitations. In this analysis, we phosphorylated bacterially expressed Smc4-NT, which should not have any baseline phosphorylation, with purified human CK2. As CK2 is a conserved eukaryotic kinase, we would expect it to phosphorylate yeast Smc4-NT if target sites exist. The major limitation is that in an *in vitro* experiment conducted with purified proteins, it would be impossible to detect phosphorylation that is dependent on other PTMs or phosphorylation by other kinases. If the Smc4-NT is spatiotemporally regulated by a multi-kinase, stepwise mechanism of phosphorylation, phosphorylation of a purified protein by a purified kinase

would not recapitulate *in vivo* phenotypes. It will also be important to confirm whether the whole condensin complex from *Saccharomyces cerevisiae* is phosphorylated by CK2 *in vitro*.

Evidently, a key experiment would be to test the DNA binding activity of the Smc4-NT after CK2 phosphorylation, which could lead to one of two outcomes. Ideally, if CK2 phosphorylation has the opposite effect of Cdk1 phosphorylation, (i.e., it increases the affinity of the Smc4-NT for ssDNA or has no effects), this would support the notion that inhibitory phosphorylation by CK2 counteracts its activation by Cdk1. Alternatively, and more likely, CK2 phosphorylation may also decrease the Smc4-NT's affinity for ssDNA; CK2 phosphorylation of nucleosome protein CBX2 has been shown to attenuate its DNA binding activity through EMSA (139). We would then posit that the reason these kinases have opposite effects is due to the spatiotemporal regulation of their activity.

RxL motifs on the Smc4-NT permit dynamic docking of Cdc28-Clb2

Our EMSA experiments were designed in such a way that Cdc28-Clb2 was not removed from the reaction mixture prior to use in EMSAs. As such, we thought it would be important to investigate the effects of the presence of Cdc28-Clb2 on DNA binding by the Smc4-NT in ATP-free conditions, where kinase was present, but unable to phosphorylate the Smc4-NT.

We observed that Cdc28-Clb2 interaction with the Smc4-NT generated a DNA binding "super-shift" independent of Cdc28-Clb2 structure (Figure 9C). "Super-shift" assays are a powerful tool that can help identify unknown proteins that bind DNA in a given reaction mixture (140). They are generally performed by including an antibody that recognizes a specific protein of interest in an EMSA reaction. The antibody binds to its target, forming a larger complex with the protein of interest, and this results in an even larger mobility shift than when the protein of interest

is incubated with the DNA substrate by itself. In our experiment, the unintentional generation of a "super-shift" suggests that Cdc28-Clb2 interacts with Smc4-NT to form a complex. The Smc4-NT is predicted to be disordered, and as this "super-shift" is observed when Cdc28-Clb2 is active or heat-denatured, the interaction between the two proteins may be due to a linear sequence of residues between both proteins. We hypothesized that this interaction is mediated by the RxL motifs in the Smc4-NT, which have been shown to be essential for cell cycle-dependent phosphorylation of the Smc4-NT (64).

Ablation of RxL motifs in an exogenous copy of *SMC4* was able to rescue the temperature-dependent growth defects observed in the very sick *smc4-22* allele. While there are two RxL motifs in the Smc4-NT, there are several more RxL motifs in the rest of the full-length Smc4 protein. As such, if RxL motifs confer an important role in mediating the interaction between Smc4 and Cdc28-Clb2, the presence of other motifs in the rest of the sequence may compensate for the removal of the 2 within the Smc4-NT. As condensin does not act as a single molecule, but rather several condensins are known to associate with the same region of chromatin, the *in vivo* viability tests could be showing the effects brought upon by different condensin molecules with varying levels of activity (40, 141).

While we observed that mutation of the Smc4-NT RxL cyclin binding motifs did not result in dominant growth defects in yeast, ablation of these motifs completely abrogated DNA binding activity of the Smc4-NT *in vitro*. The role of the RxL motifs is to allow for interactions between cyclins and substrates of CDKs that target them, but typically these motifs are more prominent in S phase targets. LxF motifs have recently been shown to play a role in substrate recognition by M phase Cdk-cyclin complexes, but the Smc4-NT does not contain any such motifs. In drosophila, RxL motif mediated Cdk phosphorylation inhibits the DNA binding activity of the ORC *in vitro*,

yet the complex is able to maintain association with chromatin under high Cdk1 activity (142). It was posited that this DNA association is due to other factors, such as phosphatases that overcome phosphorylation, or that high affinity for DNA is only required at certain periods of the cell cycle. Since removal of the RxL motifs has such striking effects on the baseline DNA binding of the Smc4-NT, their presence may be essential for the regulation of the Smc4-NT. Absence of the RxL motifs recapitulates the DNA binding phenotype of Cdc28-Clb2-phosphorylated Smc4-NT, as in, there is nearly no detectable DNA binding. Smc4-rxlA-NT does not appear to be phosphorylated by Cdc28-Clb2 *in vitro*, likely due to Cdc28-Clb2 being unable to dock on and specifically target its substrate. If Cdc28-Clb2 docking to the Smc4-NT is completely inhibited, cell cycle progression may be severely limited. While the exact role of the RxL motifs in regulating condensin function remains elusive, further exploration of docking motifs may assist in a deeper understanding of the spatiotemporal regulation of condensin activity.

Possible charge-based interaction between Smc4-NT and ssDNA

If all forms of phosphorylation play a role in diminishing the affinity of the Smc4-NT for ssDNA, it would be tempting to speculate that Smc4-NT binding to DNA is regulated by electrostatic charge. The phosphate backbone of DNA backbone is negatively charged, approximately half of which is neutralized by core histones (14). Some of the remaining negative charge is further neutralized by other factors, such as histone H1, as well as histone modifications (22). RNA has also been shown to play a role in regulating DNA charge by neutralizing positively charged histone tails to reduce electrostatic compaction of DNA and promote open chromatin structure, facilitating transcription (18). Nucleosome electrostatics show that the net charge of chromatin remains negative despite some charge neutralization by various factors (143). The DNA

binding activity of the Smc4-NT is supported by studies which show that several intrinsically disordered proteins can bind DNA despite lacking a well-characterized three-dimensional structure (65, 68, 74). It has also been shown that DNA-binding proteins tend to have disordered tails that act as a subdomain to engage in nonspecific interactions with DNA, often as a result of their positive charge (74). The Smc4-NT, interestingly, is slightly positively charged at neutral pH, even when all 16 putative Cdk1 phosphorylation sites are mutated to alanine. The addition of negatively charged phosphate groups to the protein would severely impact the charge of the Smc4-NT, making it extremely negatively charged and thus electrostatically repulsive to the negatively charged chromatin backbone. It will be important to observe how the binding affinity of Smc4-NT to linear DNA compares to its binding to chromatin, with all the molecular scaffolding that assists in its compaction.

Phosphorylation inducing a "disorder to order" transition of the Smc4-NT

During interactions with DNA, disordered proteins are posited to undergo a "disorder to order" transition to improve the specificity of DNA binding. These disordered regions may have been evolutionarily selected to have a charge pattern that optimizes DNA search (65). A structural comparison can also be made between condensin and the CFTR, another ATPase protein regulated by the phosphorylation of its disordered regulatory "R" region of about 200 residues (144). Cryo-EM structures of ATP bound and ATP-free CFTR protein reveal that when non-phosphorylated, the "R" region inhibits channel activity by interacting with its nucleotide binding domains and preventing heterodimerization (145). Phosphorylation of the R region removes it from the dimer interface, allowing channel activity to resume (146).

Crystal structures of the ATP bound and ATP-free SMC head domains of condensin show no large conformational differences, but this does not negate the possibility that large structural rearrangements occur when the SMC heads are bound to other subunits of condensin (61). Crosslinking experiments of chicken condensin have proposed that when not actively engaged on mitotic chromosomes, condensin may adopt a closed structure rather than remaining an open ring (147). Combining the features of IDPRs possessing DNA binding activity with the structurally similar ATPase protein CFTR, condensin activity could be regulated by Smc4-NT phosphorylation as follows. During interphase, when condensin does not play a major role in regulating chromosome architecture, the Smc4-NT could be inhibitorily phosphorylated by CK2 to hold a conformation that keeps it inside the ring structure of condensin. Subsequent dephosphorylation of CK2 target sites and phosphorylation by Cdk1 could result in a more "folded" state of Smc4-NT, allowing it to exit the condensin ring and for chromatin to pass through. Shaltiel et al. proposed that condensin loop extrusion is driven by a "hold and feed" mechanism where DNA is actively fed into the condensin ring structure (148). Structural mapping of condensin chambers that would be able to accommodate the DNA backbone to feed it into condensin show several chambers generated by different condensin subunits, but due to the lack of known structure of the Smc4-NT, it is omitted from these analyses (149). Since, phosphorylated Smc4-NT has lower affinity for DNA than non-phosphorylated Smc4-NT, the phosphorylated, "active" state could induce a structural conformation allowing the Smc4-NT to act as a latch to enclose a DNA double helix and feed it into the condensin ring structure, without directly binding to DNA. Understanding the structural changes that occur upon Smc4-NT phosphorylation by Cdk1 and CK2 would validate the role of the Smc4-NT in actively feeding DNA into the condensin ring.

Conclusions and Next Steps

We have established that the Smc4-NT has DNA binding activity *in vitro*. It will be important to translate this to an *in vivo* setting, which could be done through chromatin immunoprecipitation assays. We could evaluate the enrichment at chromatin regions of condensin lacking the minimal consensus or mass spectrometry-identified phosphorylation sites of the Smc4-NT. If phosphorylation by Cdk1 plays a role in for reducing the affinity of condensin for chromatin, we would expect to see more condensin enrichment in the minimal consensus site mutant.

It will also be essential to understand how removal of putative phosphorylation sites of the Smc4-NT affects chromosome morphology through fluorescence *in situ* hybridization (FISH) of the rDNA locus. rDNA endures dramatic reorganization in normal cells during mitosis to transform from an uncondensed 'puff' configuration into a condensed 'loop' configuration (150). This change in configuration signifies the compaction of chromatin, so cells incapable of chromosome condensation will retain their ‘puff’ configuration (151). Robellet et al. have previously shown that the temperature sensitive *smc4-7A* experiences defects in chromosome morphology through FISH assays (64). Since we observe no growth defects in *smc4-16A*, which still lacks the minimal consensus Cdk1 sites that confer temperature sensitivity to *smc4-7A*, it will be important to evaluate chromosome morphology of this mutant to determine if cell growth persists despite major chromosome condensation defects.

While our experiments were conducted primarily in yeast, human Smc4-NT contains minimal consensus Cdk1 sites, suggesting that the function of the region may be conserved across different species (52). Alternatively, the human CAP-D2 and CAP-D3 subunits of condensin I and II, respectively, possess conserved, metazoan-specific C-terminal extensions thought to play the same role as the Smc4-NT in yeast. These extension also contain several minimal consensus Cdk1

phosphorylation sites (51). Specifically, it has been suggested that the phosphorylation of the CAP-D3 C-terminus of condensin II in humans may be responsible for initiating chromosome condensation, indicating an equivalent function to that of the Smc4-NT in yeast (51).

Despite several regions in the Smc4 protein having DNA binding activity, the clustered phospho-sites in the N-terminus of the protein lead us to believe that this region may play a unique role in modulating DNA binding by condensin. We believe that phosphorylation at these key sites acts as an essential trigger for the initiation of chromosome condensation. Building on the hypothesis of Bazile et al. (52) and expanding on the work of Robellet et al. (64), we propose that the activation of condensin occurs as follows (Figure 14). During interphase, the Smc4-NT is inactivated by CK2 phosphorylation, which is dominant over low levels of phosphorylation by Cdk1 (62). This phosphorylation may cause the Smc4-NT to adopt a conformation that blocks the opening of the condensin ring, preventing active loop extrusion. When CK2 is not present, for example, in the mutants we created, Cdk1 may try to compensate for the loss of CK2 activity by phosphorylating Smc4-NT sites it does not ordinarily target. At the G2/M transition, phosphatases such as PP6 may act to remove phosphorylated residues (113). Concurrently, Cdk1 phosphorylation of the Smc4-NT at the onset of mitosis, perhaps primed by low levels of CK2 phosphorylation, may cause Smc4-NT to exit the opening of the condensin ring. This specific, "activatory" phosphorylation could be mediated by docking of Cdc28-Clb2 at the RxL motifs of the Smc4-NT. The resulting conformational change would limit the interaction of the Smc4-NT with DNA and subsequently activate condensin for chromosome condensation. The adopted conformation may allow the Smc4-NT to function as a latch for chromatin, actively feeding it into the condensin ring structure. As proposed by Bazile et al., there are likely other kinases implicated in maintaining condensin activity throughout mitosis (52). It is possible that phosphorylation at

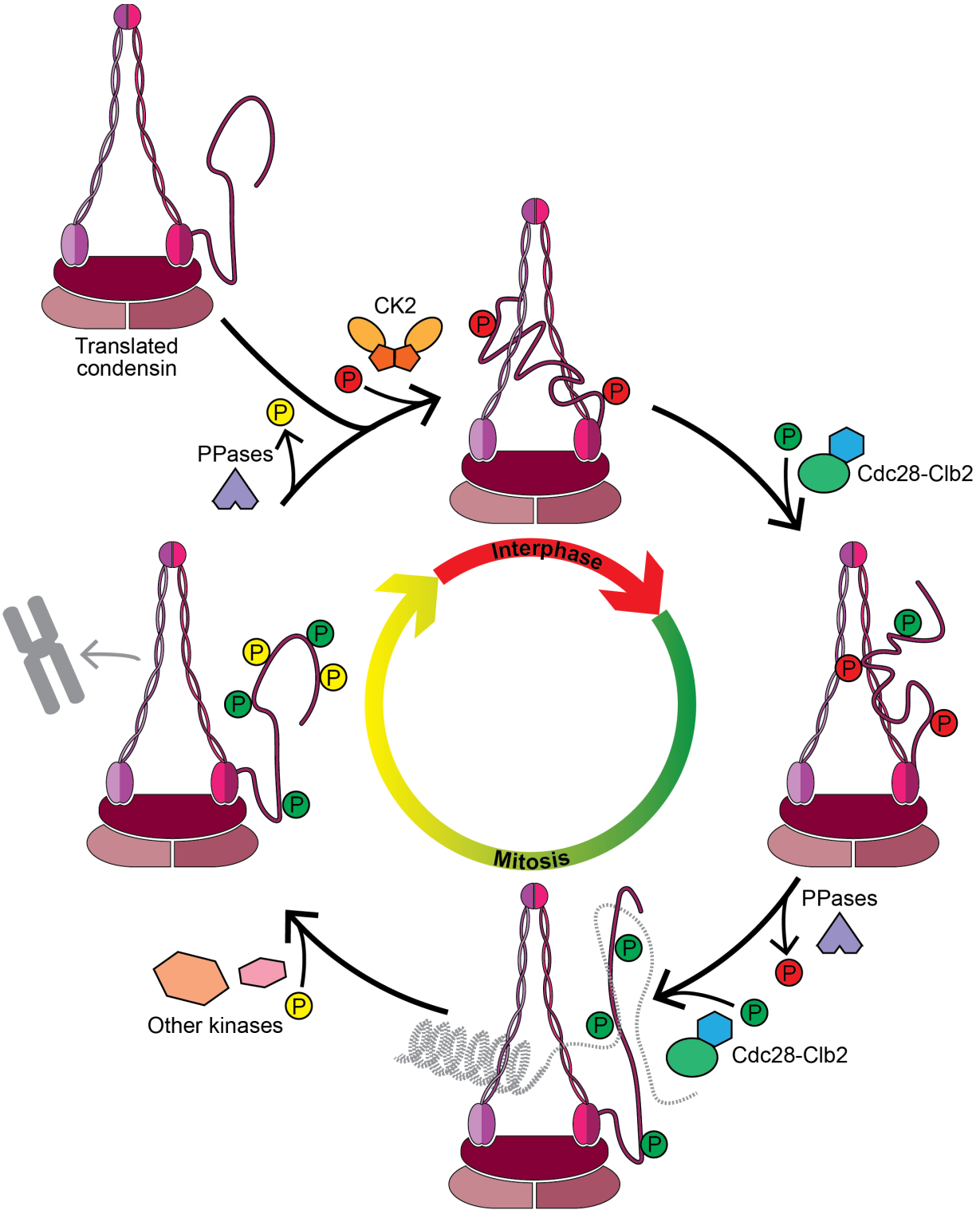

Figure 14. Proposed mechanism of condensin regulation by Smc4-NT phosphorylation. After condensin is translated and throughout interphase, phosphorylation of the Smc4-NT by CK2 maintains condensin in an inactive state (top). At the onset of mitosis, the presence of CK2-mediated phosphorylated residues

primes phosphorylation by Cdc28-Clb2 (right). CK2 phosphorylation is subsequently removed by various phosphatases as Cdc28-Clb2 phosphorylation continues, fully activating condensin and allowing it to associate with chromatin and begin loop extrusion (bottom). Other kinases maintain the activation of condensin to generate fully resolved chromosomes (left).

the nine mass spectrometry-identified sites in the Smc4-NT prevents cell cycle progression by inhibition of condensin function, and removal of all 16 sites phosphorylation sites in the Smc4-NT allows for condensation and segregation despite defects in chromosome morphology.

Condensin dysregulation has been shown to be associated with several diseases characterized by erroneous cell division, including conditions of the nervous system (152). Of all condensin subunits, Smc4 is of particular interest as mutations in this gene are enriched in the tumour genome (153). Further analysis of this region and its role in chromosome morphogenesis presents a promising avenue for understanding the specifics of the mitotic process, currently a big unknown in the scientific field.

References

1. Antonin, W., and Neumann, H. (2016) Chromosome condensation and decondensation during mitosis. *Curr Opin Cell Biol*. **40**, 15–22
2. Paweletz, N. (2001) Walther Flemming: Pioneer of mitosis research. *Nat Rev Mol Cell Biol*. 10.1038/35048077
3. Paulson, J. R., Hudson, D. F., Cisneros-Soberanis, F., and Earnshaw, W. C. (2021) Mitotic chromosomes. *Semin Cell Dev Biol*. **117**, 7–29
4. Ravi, M., Ramanathan, S., and Krishna, K. (2020) Factors, mechanisms and implications of chromatin condensation and chromosomal structural maintenance through the cell cycle. *J Cell Physiol*. 10.1002/jcp.29038
5. Dekker, B., and Dekker, J. (2022) Regulation of the mitotic chromosome folding machines. *Biochemical Journal*. **479**, 2153–2173
6. Arata, Y., and Takagi, H. (2019) Quantitative Studies for Cell-Division Cycle Control. *Front Physiol*. 10.3389/fphys.2019.01022
7. Sherr, C. J. (1994) G1 phase progression: Cycling on cue. *Cell*. **79**, 551–555
8. Pederson, T. (2003) Historical review: An energy reservoir for mitosis, and its productive wake. *Trends Biochem Sci*. **28**, 125–129
9. Laskey, R. A., Fairman, M. P., and Blow, J. J. (1989) S Phase of the Cell Cycle. *Science (1979)*. **246**, 609–614
10. Kousholt, A., Menzel, T., and Sørensen, C. (2012) Pathways for Genome Integrity in G2 Phase of the Cell Cycle. *Biomolecules*. **2**, 579–607

11. Adler, S. O., Spiesser, T. W., Uschner, F., Münzner, U., Hahn, J., Krantz, M., and Klipp, E. (2022) A yeast cell cycle model integrating stress, signaling, and physiology. *FEMS Yeast Res*. 10.1093/femsyr/foac026

12. McIntosh, J. R. (2016) Mitosis. *Cold Spring Harb Perspect Biol*. **8**, a023218

13. Batty, P., and Gerlich, D. W. (2019) Mitotic Chromosome Mechanics: How Cells Segregate Their Genome. *Trends Cell Biol*. **29**, 717–726

14. Maeshima, K., Imai, R., Tamura, S., and Nozaki, T. (2014) Chromatin as dynamic 10-nm fibers. *Chromosoma*. **123**, 225–37

15. Baldi, S., Korber, P., and Becker, P. B. (2020) Beads on a string—nucleosome array arrangements and folding of the chromatin fiber. *Nat Struct Mol Biol*. **27**, 109–118

16. Bustin, M., Catez, F., and Lim, J.-H. (2005) The Dynamics of Histone H1 Function in Chromatin. *Mol Cell*. **17**, 617–620

17. Peterson, C. L., and Laniel, M.-A. (2004) Histones and histone modifications. *Current Biology*. **14**, R546–R551

18. Dueva, R., Akopyan, K., Pederiva, C., Trevisan, D., Dhanjal, S., Lindqvist, A., and Farnebo, M. (2019) Neutralization of the Positive Charges on Histone Tails by RNA Promotes an Open Chromatin Structure. *Cell Chem Biol*. 10.1016/j.chembiol.2019.08.002

19. Sanborn, A. L., Rao, S. S. P., Huang, S.-C., Durand, N. C., Huntley, M. H., Jewett, A. I., Bochkov, I. D., Chinnappan, D., Cutkosky, A., Li, J., Geeting, K. P., Gnirke, A., Melnikov, A., McKenna, D., Stamenova, E. K., Lander, E. S., and Aiden, E. L. (2015) Chromatin extrusion explains key features of loop and domain formation in wild-type and engineered genomes. *Proceedings of the National Academy of Sciences*. 10.1073/pnas.1518552112

20. Shaffer, L., and Theisen, A. (2010) Disorders caused by chromosome abnormalities. *Appl Clin Genet*. 10.2147/TACG.S8884

21. Koshland, D., and Strunnikov, A. (1996) Mitotic Chromosome Condensation. *Annu Rev Cell Dev Biol*. **12**, 305–333

22. Ohta, S., Bukowski-Wills, J. C., Sanchez-Pulido, L., Alves, F. de L., Wood, L., Chen, Z. A., Platani, M., Fischer, L., Hudson, D. F., Ponting, C. P., Fukagawa, T., Earnshaw, W. C., and Rappsilber, J. (2010) The Protein Composition of Mitotic Chromosomes Determined Using Multiclassifier Combinatorial Proteomics. *Cell*. 10.1016/j.cell.2010.07.047

23. Hirano, T., and Mitchison, T. J. (1994) A heterodimeric coiled-coil protein required for mitotic chromosome condensation in vitro. *Cell*. **79**, 449–458

24. Shintomi, K., Inoue, F., Watanabe, H., Ohsumi, K., Ohsugi, M., and Hirano, T. (2017) Mitotic chromosome assembly despite nucleosome depletion in Xenopus egg extracts. *Science (1979)*. **356**, 1284–1287

25. Belmont, A. S., Braunfeld, M. B., Sedat, J. W., and Agard, D. A. (1989) Large-scale chromatin structural domains within mitotic and interphase chromosomes in vivo and in vitro. *Chromosoma*. **98**, 129–143

26. Hirano, T., Kobayashi, R., and Hirano, M. (1997) Condensins, Chromosome Condensation Protein Complexes Containing XCAP-C, XCAP-E and a Xenopus Homolog of the Drosophila Barren Protein. *Cell*. **89**, 511–521

27. Hirota, T., Gerlich, D., Koch, B., Ellenberg, J., and Peters, J. M. (2004) Distinct functions of condensin I and II in mitotic chromosome assembly. *J Cell Sci*. 10.1242/jcs.01604

28. Uhlmann, F. (2016) SMC complexes: From DNA to chromosomes. *Nat Rev Mol Cell Biol*. 10.1038/nrm.2016.30

29. Hirano, T. (2012) Condensins: universal organizers of chromosomes with diverse functions. *Genes Dev*. **26**, 1659–1678

30. Hirano, T. (2016) Condensin-Based Chromosome Organization from Bacteria to Vertebrates. *Cell*. 10.1016/j.cell.2016.01.033

31. Freeman, L., Aragon-Alcaide, L., and Strunnikov, A. (2000) The Condensin Complex Governs Chromosome Condensation and Mitotic Transmission of Rdna. *Journal of Cell Biology*. **149**, 811–824

32. Schmiesing, J. A., Gregson, H. C., Zhou, S., and Yokomori, K. (2000) A Human Condensin Complex Containing hCAP-C–hCAP-E and CNAP1, a Homolog of *Xenopus* XCAP-D2, Colocalizes with Phosphorylated Histone H3 during the Early Stage of Mitotic Chromosome Condensation. *Mol Cell Biol*. **20**, 6996–7006

33. Griese, J. J., and Hopfner, K. P. (2011) Structure and DNA-binding activity of the Pyrococcus furiosus SMC protein hinge domain. *Proteins: Structure, Function and Bioinformatics*. 10.1002/prot.22903

34. Griese, J. J., Witte, G., and Hopfner, K.-P. (2010) Structure and DNA binding activity of the mouse condensin hinge domain highlight common and diverse features of SMC proteins. *Nucleic Acids Res*. **38**, 3454–3465

35. Onn, I., Aono, N., Hirano, M., and Hirano, T. (2007) Reconstitution and subunit geometry of human condensin complexes. *EMBO J*. **26**, 1024–1034

36. Cuylen, S., Metz, J., and Haering, C. H. (2011) Condensin structures chromosomal DNA through topological links. *Nat Struct Mol Biol*. **18**, 894–901

37. Yoshimura, S. H., Hizume, K., Murakami, A., Sutani, T., Takeyasu, K., and Yanagida, M. (2002) Condensin Architecture and Interaction with DNA. *Current Biology*. **12**, 508–513

38. Cutts, E. E., and Vannini, A. (2020) Condensin complexes: understanding loop extrusion one conformational change at a time. *Biochem Soc Trans*. 10.1042/BST20200241

39. Terakawa, T., Bisht, S., Eeftens, J. M., Dekker, C., Haering, C. H., and Greene, E. C. (2017) The condensin complex is a mechanochemical motor that translocates along DNA. *Science (1979)*. **358**, 672–676

40. Sakai, Y., Mochizuki, A., Kinoshita, K., Hirano, T., and Tachikawa, M. (2018) Modeling the functions of condensin in chromosome shaping and segregation. *PLoS Comput Biol*. **14**, e1006152

41. Ganji, M., Shaltiel, I. A., Bisht, S., Kim, E., Kalichava, A., Haering, C. H., and Dekker, C. (2018) Real-time imaging of DNA loop extrusion by condensin. *Science (1979)*. 10.1126/science.aar7831

42. Banigan, E. J., van den Berg, A. A., Brandão, H. B., Marko, J. F., and Mirny, L. A. (2020) Chromosome organization by one-sided and two-sided loop extrusion. *Elife*. 10.7554/eLife.53558

43. Kim, E., Kerssemakers, J., Shaltiel, I. A., Haering, C. H., and Dekker, C. (2020) DNA-loop extruding condensin complexes can traverse one another. *Nature*. 10.1038/s41586-020-2067-5

44. Sun, M., Amiri, H., Tong, A. B., Shintomi, K., Hirano, T., Bustamante, C., and Heald, R. (2023) Monitoring the compaction of single DNA molecules in Xenopus egg extract in real time. *Proceedings of the National Academy of Sciences*. 10.1073/pnas.2221309120

45. Golfier, S., Quail, T., Kimura, H., and Brugués, J. (2020) Cohesin and condensin extrude DNA loops in a cell cycle-dependent manner. *Elife*. 10.7554/eLife.53885

46. Hirano, T. (2005) SMC proteins and chromosome mechanics: from bacteria to humans. *Philosophical Transactions of the Royal Society B: Biological Sciences*. **360**, 507–514

47. Petrushenko, Z. M., She, W., and Rybenkov, V. V. (2011) A new family of bacterial condensins. *Mol Microbiol*. **81**, 881–896

48. Green, L. C., Kalitsis, P., Chang, T. M., Cipetic, M., Kim, J. H., Marshall, O., Turnbull, L., Whitchurch, C. B., Vagnarelli, P., Samejima, K., Earnshaw, W. C., Choo, K. H. A., and Hudson, D. F. (2012) Contrasting roles of condensin I and II in mitotic chromosome formation. *J Cell Sci*. 10.1242/jcs.097790

49. Petrova, B., Dehler, S., Kruitwagen, T., Hériché, J.-K., Miura, K., and Haering, C. H. (2013) Quantitative Analysis of Chromosome Condensation in Fission Yeast. *Mol Cell Biol*. **33**, 984–998

50. Bhalla, N., Biggins, S., and Murray, A. W. (2002) Mutation of YCS4, a Budding Yeast Condensin Subunit, Affects Mitotic and Nonmitotic Chromosome Behavior. *Mol Biol Cell*. **13**, 632–645

51. Abe, S., Nagasaka, K., Hirayama, Y., Kozuka-Hata, H., Oyama, M., Aoyagi, Y., Obuse, C., and Hirota, T. (2011) The initial phase of chromosome condensation requires Cdk1-mediated phosphorylation of the CAP-D3 subunit of condensin II. *Genes Dev*. 10.1101/gad.2016411

52. Bazile, F., St-Pierre, J., and D'Amours, D. (2010) Three-step model for condensin activation during mitotic chromosome condensation. *Cell Cycle*. 10.4161/cc.9.16.12620

53. Gerlich, D., Hirota, T., Koch, B., Peters, J.-M., and Ellenberg, J. (2006) Condensin I Stabilizes Chromosomes Mechanically through a Dynamic Interaction in Live Cells. *Current Biology*. **16**, 333–344

54. Thadani, R., Kamenz, J., Heeger, S., Muñoz, S., and Uhlmann, F. (2018) Cell-Cycle Regulation of Dynamic Chromosome Association of the Condensin Complex. *Cell Rep*. 10.1016/j.celrep.2018.04.082

55. Zhang, T., Paulson, J. R., Bakhrebah, M., Kim, J. H., Nowell, C., Kalitsis, P., and Hudson, D. F. (2016) Condensin I and II behaviour in interphase nuclei and cells undergoing premature chromosome condensation. *Chromosome Research*. **24**, 243–269

56. Weyburne, E., and Bosco, G. (2021) Cancer-associated mutations in the condensin II subunit CAPH2 cause genomic instability through telomere dysfunction and anaphase chromosome bridges. *J Cell Physiol*. **236**, 3579–3598

57. Woodward, J., Taylor, G. C., Soares, D. C., Boyle, S., Sie, D., Read, D., Chathoth, K., Vukovic, M., Tarrats, N., Jamieson, D., Campbell, K. J., Blyth, K., Acosta, J. C., Ylstra, B., Arends, M. J., Kranc, K. R., Jackson, A. P., Bickmore, W. A., and Wood, A. J. (2016) Condensin II mutation causes T-cell lymphoma through tissue-specific genome instability. *Genes Dev*. **30**, 2173–2186

58. Kokkinidis, M., Glykos, N. M., and Fadouloglou, V. E. (2020) Catalytic activity regulation through post-translational modification: the expanding universe of protein diversity, pp. 97–125, 10.1016/bs.apcsb.2020.05.001

59. Ramazi, S., and Zahiri, J. (2021) Post-translational modifications in proteins: resources, tools and prediction methods. *Database*. 10.1093/database/baab012

60. Takemoto, A., Kimura, K., Yokoyama, S., and Hanaoka, F. (2004) Cell Cycle-dependent Phosphorylation, Nuclear Localization, and Activation of Human Condensin. *Journal of Biological Chemistry*. **279**, 4551–4559

61. Piazza, I., Haering, C. H., and Rutkowska, A. (2013) Condensin: crafting the chromosome landscape. *Chromosoma*. **122**, 175–190

62. Takemoto, A., Kimura, K., Yanagisawa, J., Yokoyama, S., and Hanaoka, F. (2006) Negative regulation of condensin I by CK2-mediated phosphorylation. *EMBO J*. **25**, 5339–5348

63. Hassler, M., Shaltiel, I. A., Kschonsak, M., Simon, B., Merkel, F., Thärichen, L., Bailey, H. J., Macošek, J., Bravo, S., Metz, J., Hennig, J., and Haering, C. H. (2019) Structural Basis of an Asymmetric Condensin ATPase Cycle. *Mol Cell*. **74**, 1175-1188.e9

64. Robellet, X., Thattikota, Y., Wang, F., Wee, T. L., Pascariu, M., Shankar, S., Bonneil, Eé., Brown, C. M., and D'amours, D. (2015) A high-sensitivity phospho-switch triggered by Cdk1 governs chromosome morphogenesis during cell division. *Genes Dev*. **29**, 426–439

65. Vuzman, D., and Levy, Y. (2012) Intrinsically disordered regions as affinity tuners in protein-DNA interactions. *Mol Biosyst*. 10.1039/c1mb05273j

66. Mollica, L., Bessa, L. M., Hanoulle, X., Jensen, M. R., Blackledge, M., and Schneider, R. (2016) Binding mechanisms of intrinsically disordered proteins: Theory, simulation, and experiment. *Front Mol Biosci*. 10.3389/fmolb.2016.00052

67. Wright, P. E., and Dyson, H. J. (2015) Intrinsically disordered proteins in cellular signalling and regulation. *Nat Rev Mol Cell Biol*. 10.1038/nrm3920

68. Vuzman, D., Azia, A., and Levy, Y. (2010) Searching DNA via a "Monkey Bar" Mechanism: The Significance of Disordered Tails. *J Mol Biol*. 10.1016/j.jmb.2009.11.056

69. Iakoucheva, L. M. (2004) The importance of intrinsic disorder for protein phosphorylation. *Nucleic Acids Res*. **32**, 1037–1049

70. Bah, A., and Forman-Kay, J. D. (2016) Modulation of Intrinsically Disordered Protein Function by Post-translational Modifications. *Journal of Biological Chemistry*. **291**, 6696–6705

71. Liu, N., Guo, Y., Ning, S., and Duan, M. (2020) Phosphorylation regulates the binding of intrinsically disordered proteins via a flexible conformation selection mechanism. *Commun Chem*. **3**, 123

72. Bah, A., Vernon, R. M., Siddiqui, Z., Krzeminski, M., Muhandiram, R., Zhao, C., Sonenberg, N., Kay, L. E., and Forman-Kay, J. D. (2015) Folding of an intrinsically disordered protein by phosphorylation as a regulatory switch. *Nature*. **519**, 106–109

73. Darling, A. L., and Uversky, V. N. (2018) Intrinsic disorder and posttranslational modifications: The darker side of the biological dark matter. *Front Genet*. 10.3389/fgene.2018.00158

74. Vuzman, D., and Levy, Y. (2010) DNA search efficiency is modulated by charge composition and distribution in the intrinsically disordered tail. *Proc Natl Acad Sci U S A*. 10.1073/pnas.1011775107

75. Kimura, K., and Hirano, T. (1997) ATP-dependent positive supercoiling of DNA by 13S condensin: A biochemical implication for chromosome condensation. *Cell*. 10.1016/S0092-8674(00)80524-3

76. Kimura, K., Cuvier, O., and Hirano, T. (2001) Chromosome Condensation by a Human Condensin Complex inXenopus Egg Extracts. *Journal of Biological Chemistry*. **276**, 5417–5420

77. Palou, R., Dhanaraman, T., Marrakchi, R., Pascariu, M., Tyers, M., and D'Amours, D. (2018) Condensin ATPase motifs contribute differentially to the maintenance of chromosome morphology and genome stability. *PLoS Biol*. 10.1371/journal.pbio.2003980

78. Stray, J. E., and Lindsley, J. E. (2003) Biochemical Analysis of the Yeast Condensin Smc2/4 Complex. *Journal of Biological Chemistry*. **278**, 26238–26248

79. Stray, J. E., Crisona, N. J., Belotserkovskii, B. P., Lindsley, J. E., and Cozzarelli, N. R. (2005) The Saccharomyces cerevisiae Smc2/4 Condensin Compacts DNA into (+) Chiral Structures without Net Supercoiling. *Journal of Biological Chemistry*. **280**, 34723–34734

80. Piazza, I., Rutkowska, A., Ori, A., Walczak, M., Metz, J., Pelechano, V., Beck, M., and Haering, C. H. (2014) Association of condensin with chromosomes depends on DNA binding by its HEAT-repeat subunits. *Nat Struct Mol Biol*. **21**, 560–568

81. Akai, Y., Kanai, R., Nakazawa, N., Ebe, M., Toyoshima, C., and Yanagida, M. (2014) ATPase-dependent auto-phosphorylation of the open condensin hinge diminishes DNA binding. *Open Biol*. **4**, 140193

82. Thattikota, Y., Tollis, S., Palou, R., Vinet, J., Tyers, M., and D'Amours, D. (2018) Cdc48/VCP Promotes Chromosome Morphogenesis by Releasing Condensin from Self-Entrapment in Chromatin. *Mol Cell*. 10.1016/j.molcel.2018.01.030

83. Ubersax, J. A., Woodbury, E. L., Quang, P. N., Paraz, M., Blethrow, J. D., Shah, K., Shokat, K. M., and Morgan, D. O. (2003) Targets of the cyclin-dependent kinase Cdk1. *Nature*. **425**, 859–864

84. Brown, N. R., Korolchuk, S., Martin, M. P., Stanley, W. A., Moukhametzianov, R., Noble, M. E. M., and Endicott, J. A. (2015) CDK1 structures reveal conserved and unique features of the essential cell cycle CDK. *Nat Commun*. **6**, 6769

85. Enserink, J. M., and Kolodner, R. D. (2010) An overview of Cdk1-controlled targets and processes. *Cell Div*. 10.1186/1747-1028-5-11

86. Malumbres, M. (2014) Cyclin-dependent kinases. *Genome Biol*. **15**, 122

87. Shah, O. J., Ghosh, S., and Hunter, T. (2003) Mitotic Regulation of Ribosomal S6 Kinase 1 Involves Ser/Thr, Pro Phosphorylation of Consensus and Non-consensus Sites by Cdc2. *Journal of Biological Chemistry*. **278**, 16433–16442

88. Suzuki, K., Sako, K., Akiyama, K., Isoda, M., Senoo, C., Nakajo, N., and Sagata, N. (2015) Identification of non-Ser/Thr-Pro consensus motifs for Cdk1 and their roles in mitotic regulation of C2H2 zinc finger proteins and Ect2. *Sci Rep*. **5**, 7929

89. Skoufias, D. A., Indorato, R.-L., Lacroix, F., Panopoulos, A., and Margolis, R. L. (2007) Mitosis persists in the absence of Cdk1 activity when proteolysis or protein phosphatase activity is suppressed. *Journal of Cell Biology*. **179**, 671–685

90. Wittenberg, C., and Reed, S. I. (1989) Conservation of function and regulation within the Cdc28/cdc2 protein kinase family: characterization of the human Cdc2Hs protein kinase in Saccharomyces cerevisiae. *Mol Cell Biol*. **9**, 4064 LP – 4068

91. Kimura, K., Hirano, M., Kobayashi, R., and Hirano, T. (1998) Phosphorylation and Activation of 13S Condensin by Cdc2 in Vitro. *Science (1979)*. **282**, 487–490

92. Ono, T., Fang, Y., Spector, D. L., and Hirano, T. (2004) Spatial and temporal regulation of condensins I and II in mitotic chromosome assembly in human cells. *Mol Biol Cell*. 10.1091/mbc.E04-03-0242

93. Holt, L. J., Tuch, B. B., Villén, J., Johnson, A. D., Gygi, S. P., and Morgan, D. O. (2009) Global Analysis of Cdk1 Substrate Phosphorylation Sites Provides Insights into Evolution. *Science (1979)*. **325**, 1682–1686

94. Chang, E. J., Begum, R., Chait, B. T., and Gaasterland, T. (2007) Prediction of Cyclin-Dependent Kinase Phosphorylation Substrates. *PLoS One*. **2**, e656

95. Kõivomägi, M., Valk, E., Venta, R., Iofik, A., Lepiku, M., Morgan, D. O., and Loog, M. (2011) Dynamics of Cdk1 Substrate Specificity during the Cell Cycle. *Mol Cell*. **42**, 610–623

96. Loog, M., and Morgan, D. O. (2005) Cyclin specificity in the phosphorylation of cyclin-dependent kinase substrates. *Nature*. **434**, 104–108

97. Schulman, B. A., Lindstrom, D. L., and Harlow, E. (1998) Substrate recruitment to cyclin-dependent kinase 2 by a multipurpose docking site on cyclin A. *Proceedings of the National Academy of Sciences*. **95**, 10453–10458

98. Örd, M., Puss, K. K., Kivi, R., Möll, K., Ojala, T., Borovko, I., Faustova, I., Venta, R., Valk, E., Kõivomägi, M., and Loog, M. (2020) Proline-Rich Motifs Control G2-CDK Target Phosphorylation and Priming an Anchoring Protein for Polo Kinase Localization. *Cell Rep*. **31**, 107757

99. Wohlschlegel, J. A., Dwyer, B. T., Takeda, D. Y., and Dutta, A. (2001) Mutational Analysis of the Cy Motif from p21 Reveals Sequence Degeneracy and Specificity for Different Cyclin-Dependent Kinases. *Mol Cell Biol*. **21**, 4868–4874

100. Wilmes, G. M., Archambault, V., Austin, R. J., Jacobson, M. D., Bell, S. P., and Cross, F. R. (2004) Interaction of the S-phase cyclin Clb5 with an “RXL” docking sequence in the initiator protein Orc6 provides an origin-localized replication control switch. *Genes Dev*. **18**, 981–991

101. Takeda, D. Y., Wohlschlegel, J. A., and Dutta, A. (2001) A Bipartite Substrate Recognition Motif for Cyclin-dependent Kinases. *Journal of Biological Chemistry*. **276**, 1993–1997

102. Örd, M., Venta, R., Möll, K., Valk, E., and Loog, M. (2019) Cyclin-Specific Docking Mechanisms Reveal the Complexity of M-CDK Function in the Cell Cycle. *Mol Cell*. **75**, 76-89.e3

103. Philip, J., Örd, M., Silva, A., Singh, S., Diffley, J. F., Remus, D., Loog, M., and Ikui, A. E. (2022) Cdc6 is sequentially regulated by PP2A-Cdc55, Cdc14, and Sic1 for origin licensing in S. cerevisiae. *Elife*. 10.7554/eLife.74437

104. St-Pierre, J., Douziech, M., Bazile, F., Pascariu, M., Bonneil, É., Sauvé, V., Ratsima, H., and D'Amours, D. (2009) Polo Kinase Regulates Mitotic Chromosome Condensation by Hyperactivation of Condensin DNA Supercoiling Activity. *Mol Cell*. 10.1016/j.molcel.2009.04.013

105. D'Ambrosio, C., Schmidt, C. K., Katou, Y., Kelly, G., Itoh, T., Shirahige, K., and Uhlmann, F. (2008) Identification of cis -acting sites for condensin loading onto budding yeast chromosomes. *Genes Dev*. **22**, 2215–2227

106. Wallace, H. A., and Bosco, G. (2013) Condensins and 3D Organization of the Interphase Nucleus. *Curr Genet Med Rep*. 10.1007/s40142-013-0024-4

107. Aono, N., Sutani, T., Tomonaga, T., Mochida, S., and Yanagida, M. (2002) Cnd2 has dual roles in mitotic condensation and interphase. *Nature*. **417**, 197–202

108. Litchfield, D. W. (2003) Protein kinase CK2: structure, regulation and role in cellular decisions of life and death. *Biochemical Journal*. **369**, 1–15

109. Meggio, F., and Pinna, L. A. (2003) One-thousand-and-one substrates of protein kinase CK2? *The FASEB Journal*. **17**, 349–368

110. Hanna, D. E., Rethinaswamy, A., and Glover, C. V. C. (1995) Casein Kinase II Is Required for Cell Cycle Progression during G1 and G2/M in Saccharomyces cerevisiae. *Journal of Biological Chemistry*. **270**, 25905–25914

111. Kim, H. S., Mukhopadhyay, R., Rothbart, S., Silva, A., Vanoosthuyse, V., Radovani, E., Kislinger, T., Roguev, A., Ryan, C., Xu, J., Jahari, H., Hardwick, K., Greenblatt, J., Krogan, N., Fillingham, J., Strahl, B., Bouhassira, E., Edelmann, W., and Keogh, M. C. (2014) Identification of a BET Family Bromodomain/Casein Kinase II/TAF-Containing Complex as a Regulator of Mitotic Condensin Function. *Cell Rep*. 10.1016/j.celrep.2014.01.029

112. Rusin, S. F., Adamo, M. E., and Kettenbach, A. N. (2017) Identification of Candidate Casein Kinase 2 Substrates in Mitosis by Quantitative Phosphoproteomics. *Front Cell Dev Biol*. **5**, 97

113. Rusin, S. F., Schlosser, K. A., Adamo, M. E., and Kettenbach, A. N. (2015) Quantitative phosphoproteomics reveals new roles for the protein phosphatase PP6 in mitotic cells. *Sci Signal*. **8**, rs12–rs12

114. St-Denis, N., Gabriel, M., Turowec, J. P., Gloor, G. B., Li, S. S.-C., Gingras, A.-C., and Litchfield, D. W. (2015) Systematic investigation of hierarchical phosphorylation by protein kinase CK2. *J Proteomics*. **118**, 49–62

115. Dowen, J. M., Bilodeau, S., Orlando, D. A., Hübner, M. R., Abraham, B. J., Spector, D. L., and Young, R. A. (2013) Multiple Structural Maintenance of Chromosome Complexes at Transcriptional Regulatory Elements. *Stem Cell Reports*. **1**, 371–378

116. Duina, A. A., Miller, M. E., and Keeney, J. B. (2014) Budding yeast for budding geneticists: A primer on the Saccharomyces cerevisiae model system. *Genetics*. 10.1534/genetics.114.163188

117. Neiman, A. M. (2011) Sporulation in the Budding Yeast Saccharomyces cerevisiae. *Genetics*. **189**, 737–765

118. Hartwell, L. H. (1967) Macromolecule synthesis in temperature-sensitive mutants of yeast. *J Bacteriol*. 10.1128/jb.93.5.1662-1670.1967

119. Edgar, R. S., and Lielausis, I. (1964) Temperature-Sensitive Mutants of Bacteriophage T4d: Their Isolation and Genetic Characterization. *Genetics*. **49**, 649–62

120. Kalderon, D., Roberts, B. L., Richardson, W. D., and Smith, A. E. (1984) A short amino acid sequence able to specify nuclear location. *Cell*. **39**, 499–509

121. Guthrie, C., and Fink, G. R. (1991) Guide to yeast genetics and molecular biology. in *Methods in Enzymology*, Academic Press, San Diego, 10.2307/3760517

122. Schiestl, R. H., and Gietz, R. D. (1989) High efficiency transformation of intact yeast cells using single stranded nucleic acids as a carrier. *Curr Genet*. **16**, 339–346

123. Gietz, R. D., Schiestl, R. H., Willems, A. R., and Woods, R. A. (1995) Studies on the transformation of intact yeast cells by the LiAc/SS-DNA/PEG procedure. *Yeast*. **11**, 355–360

124. Foiani, M., Marini, F., Gamba, D., Lucchini, G., and Plevani, P. (1994) The B subunit of the DNA polymerase alpha-primase complex in Saccharomyces cerevisiae executes an essential function at the initial stage of DNA replication. *Mol Cell Biol*. **14**, 923–933

125. Schneider, C. A., Rasband, W. S., and Eliceiri, K. W. (2012) NIH Image to ImageJ: 25 years of image analysis. *Nat Methods*. **9**, 671–675

126. Shevchenko, A., Tomas, H., Havli, J., Olsen, J. V, and Mann, M. (2006) In-gel digestion for mass spectrometric characterization of proteins and proteomes. *Nat Protoc*. **1**, 2856–2860

127. Vinckier, N. K., Chworos, A., and Parsons, S. M. (2011) Improved isolation of proteins tagged with glutathione S-transferase. *Protein Expr Purif*. **75**, 161–164

128. Lanz, M. C., Yugandhar, K., Gupta, S., Sanford, E. J., Faça, V. M., Vega, S., Joiner, A. M. N., Fromme, J. C., Yu, H., and Smolka, M. B. (2021) In-depth and 3-dimensional exploration of the budding yeast phosphoproteome. *EMBO Rep*. **22**, e51121

129. Kinoshita, E., Kinoshita-Kikuta, E., and Koike, T. (2009) Separation and detection of large phosphoproteins using Phos-tag SDS-PAGE. *Nat Protoc*. **4**, 1513–1521

130. Bidwai, A. P., Hanna, D. E., and Glover, C. V. (1992) Purification and characterization of casein kinase II (CKII) from delta cka1 delta cka2 Saccharomyces cerevisiae rescued by Drosophila CKII subunits. The free catalytic subunit of casein kinase II is not toxic in vivo. *Journal of Biological Chemistry*. **267**, 18790–18796

131. Martin, K., Steinberg, T. H., Cooley, L. A., Gee, K. R., Beechem, J. M., and Patton, W. F. (2003) Quantitative analysis of protein phosphorylation status and protein kinase activity on microarrays using a novel fluorescent phosphorylation sensor dye. *Proteomics*. **3**, 1244–1255

132. St-Denis, N., Gabriel, M., Turowec, J. P., Gloor, G. B., Li, S. S.-C., Gingras, A.-C., and Litchfield, D. W. (2015) Systematic investigation of hierarchical phosphorylation by protein kinase CK2. *J Proteomics*. **118**, 49–62

133. Some, D., Amartely, H., Tsadok, A., and Lebendiker, M. (2019) Characterization of Proteins by Size-Exclusion Chromatography Coupled to Multi-Angle Light Scattering (SEC-MALS). *Journal of Visualized Experiments*. 10.3791/59615

134. Bakhrebah, M., Zhang, T., Mann, J. R., Kalitsis, P., and Hudson, D. F. (2015) Disruption of a Conserved CAP-D3 Threonine Alters Condensin Loading on Mitotic Chromosomes Leading to Chromosome Hypercondensation. *Journal of Biological Chemistry*. **290**, 6156–6167

135. Doughty, T. W., Arsenault, H. E., and Benanti, J. A. (2016) Levels of Ycg1 Limit Condensin Function during the Cell Cycle. *PLoS Genet*. **12**, e1006216

136. Zhao, Z., Wang, X., Ding, Y., Cao, X., and Zhang, X. (2023) SMC4, a novel tumor prognostic marker and potential tumor therapeutic target. *Front Oncol*. 10.3389/fonc.2023.1117642

137. Gajewski, A., Csaszar, E., and Foisner, R. (2004) A Phosphorylation Cluster in the Chromatin-binding Region Regulates Chromosome Association of LAP2α. *Journal of Biological Chemistry*. **279**, 35813–35821

138. Zhang, L., Zhang, D., Liu, D., Li, Y., Li, H., Xie, Y., Wang, Z., Hansen, B. O., and Olsson, S. (2020) Conserved Eukaryotic Kinase CK2 Chaperone Intrinsically Disordered Protein Interactions. *Appl Environ Microbiol*. 10.1128/AEM.02191-19

139. Kawaguchi, T., Machida, S., Kurumizaka, H., Tagami, H., and Nakayama, J. (2017) Phosphorylation of CBX2 controls its nucleosome-binding specificity. *The Journal of Biochemistry*. **162**, 343–355

140. Hellman, L. M., and Fried, M. G. (2007) Electrophoretic mobility shift assay (EMSA) for detecting protein–nucleic acid interactions. *Nat Protoc*. **2**, 1849–1861

141. Kinoshita, K., Tsubota, Y., Tane, S., Aizawa, Y., Sakata, R., Takeuchi, K., Shintomi, K., Nishiyama, T., and Hirano, T. (2022) A loop extrusion–independent mechanism contributes to condensin I–mediated chromosome shaping. *Journal of Cell Biology*. 10.1083/jcb.202109016

142. Remus, D., Blanchette, M., Rio, D. C., and Botchan, M. R. (2005) CDK Phosphorylation Inhibits the DNA-binding and ATP-hydrolysis Activities of the Drosophila Origin Recognition Complex. *Journal of Biological Chemistry*. **280**, 39740–39751

143. Gebala, M., Johnson, S. L., Narlikar, G. J., and Herschlag, D. (2019) Ion counting demonstrates a high electrostatic field generated by the nucleosome. *Elife*. 10.7554/eLife.44993

144. Bozoky, Z., Krzeminski, M., Chong, P. A., and Forman-Kay, J. D. (2013) Structural changes of CFTR R region upon phosphorylation: a plastic platform for intramolecular and intermolecular interactions. *FEBS J.* **280**, 4407–4416

145. Zhang, Z., and Chen, J. (2016) Atomic Structure of the Cystic Fibrosis Transmembrane Conductance Regulator. *Cell*. **167**, 1586-1597.e9

146. Zhang, Z., Liu, F., and Chen, J. (2018) Molecular structure of the ATP-bound, phosphorylated human CFTR. *Proceedings of the National Academy of Sciences*. **115**, 12757–12762

147. Barysz, H., Kim, J. H., Chen, Z. A., Hudson, D. F., Rappsilber, J., Gerloff, D. L., and Earnshaw, W. C. (2015) Three-dimensional topology of the SMC2/SMC4 subcomplex from chicken condensin I revealed by cross-linking and molecular modelling. *Open Biol*. 10.1098/rsob.150005

148. Shaltiel, I. A., Datta, S., Lecomte, L., Hassler, M., Kschonsak, M., Bravo, S., Stober, C., Ormanns, J., Eustermann, S., and Haering, C. H. (2022) A hold-and-feed mechanism drives directional DNA loop extrusion by condensin. *Science (1979)*. **376**, 1087–1094

149. Lee, B.-G., Merkel, F., Allegretti, M., Hassler, M., Cawood, C., Lecomte, L., O'Reilly, F. J., Sinn, L. R., Gutierrez-Escribano, P., Kschonsak, M., Bravo, S., Nakane, T., Rappsilber, J., Aragon, L., Beck, M., Löwe, J., and Haering, C. H. (2020) Cryo-EM structures of holo condensin reveal a subunit flip-flop mechanism. *Nat Struct Mol Biol*. **27**, 743–751

150. Lavoie, B. D., Hogan, E., and Koshland, D. (2004) In vivo requirements for rDNA chromosome condensation reveal two cell-cycle-regulated pathways for mitotic chromosome folding. *Genes Dev*. 10.1101/gad.1150404

151. Guacci, V., Hogan, E., and Koshland, D. (1994) Chromosome condesation and sister chromatid pairing in budding yeast. *Journal of Cell Biology*. 10.1083/jcb.125.3.517

152. Pang, D., Yu, S., and Yang, X. (2022) A mini-review of the role of condensin in human nervous system diseases. *Front Mol Neurosci*. 10.3389/fnmol.2022.889796

153. Woodward, J., Taylor, G. C., Soares, D. C., Boyle, S., Sie, D., Read, D., Chathoth, K., Vukovic, M., Tarrats, N., Jamieson, D., Campbell, K. J., Blyth, K., Acosta, J. C., Ylstra, B., Arends, M. J., Kranc, K. R., Jackson, A. P., Bickmore, W. A., and Wood, A. J. (2016) Condensin II mutation causes T-cell lymphoma through tissue-specific genome instability. *Genes Dev*. 10.1101/gad.284562.116

Appendix

Supplementary Tables

Table S1. Yeast strains used in this study.

Figure	Name	Relevant Genotype
Fig. 7A	D4107	*MAT***a** *SMC4*
	D3272	*MAT***a** *SMC4::3xSTII::HIS3MX6*
	D2563	*MAT***a** *smc4-7A::3xSTII::HIS3MX6*
	D7546	*MAT***a** *smc4-9A::3xSTII::HIS3MX6*
	D7550	*MAT***a** *smc4-16A::3xSTII::HIS3MX6*
Fig. 7B	D3265	*MAT***a** *SMC4::3xSTII::HIS3MX6 YCG1::3xFLAG::kanMX6 cdc15-2 [YCplac111-Smc4-NT::NLS::13xMYC]*
	D3267	*MAT***a** *smc4-7A::3xSTII::HIS3MX6 YCG1::3xFLAG::kanMX6 cdc15-2 [YCplac111-smc4-7A-NT::NLS::13xMYC]*
Fig. 7C	D3265	*MAT***a** *SMC4::3xSTII::HIS3MX6 YCG1::3xFLAG::kanMX6 cdc15-2 [YCplac111-Smc4-NT::NLS::13xMYC]*
	D7500	*MAT***a** *YCG1::3xFLAG::kanMX6 cdc15-2 [YCplac111-smc4-9A-NT::NLS::13xMYC]*
Fig. 7D	D3265	*MAT***a** *SMC4::3xSTII::HIS3MX6 YCG1::3xFLAG::kanMX6 cdc15-2 [YCplac111-Smc4-NT::NLS::13xMYC]*
	D7501	*MATa YCG1::3xFLAG::kanMX6 cdc15-2 [YCplac111-smc4-16A-NT::NLS::13xMYC]*
Fig. 11A	D4107	*MAT***a** *SMC4*
	D3272	*MAT***a** *SMC4::3xSTII::HIS3MX6*
	D3662	*MAT***a** *SMC4::3xSTII::HIS3MX6 ckb1::URA3MX6 ckb2::TRP1*
	D2563	*MAT***a** *smc4-7A::3xSTII::HIS3MX6*
	D3666	*MAT***a** *smc4-7A::3xSTII::HIS3MX6 ckb1::URA3MX6 ckb2::TRP1*
	D7546	*MAT***a** *smc4-9A::3xSTII::HIS3MX6*
	D7647	*MAT***a** *smc4-9A::3xSTII::HIS3MX6 ckb1::URA3MX6 ckb2::TRP1*
	D7550	*MAT***a** *smc4-16A::3xSTII::HIS3MX6*
	D7653	*MAT***a** *smc4-16A::3xSTII::HIS3MX6 ckb1::URA3MX6 ckb2::TRP1*
	D3660	*MAT***a** *ckb1::URA3MX6 ckb2::TRP1*
Fig. 11B	D4107	*MAT***a** *SMC4*
	D3272	*MAT***a** *SMC4::3xSTII::HIS3MX6*
	D3662	*MAT***a** *SMC4::3xSTII::HIS3MX6 ckb1::URA3MX6 ckb2::TRP1*
	D2563	*MAT***a** *smc4-7A::3xSTII::HIS3MX6*
	D3666	*MAT***a** *smc4-7A::3xSTII::HIS3MX6 ckb1::URA3MX6 ckb2::TRP1*
	D7546	*MAT***a** *smc4-9A::3xSTII::HIS3MX6*
	D7647	*MAT***a** *smc4-9A::3xSTII::HIS3MX6 ckb1::URA3MX6 ckb2::TRP1*
	D7550	*MAT***a** *smc4-16A::3xSTII::HIS3MX6*
	D7653	*MAT***a** *smc4-16A::3xSTII::HIS3MX6 ckb1::URA3MX6 ckb2::TRP1*
Fig. 11C	D7997	*MAT***a** *SMC4::3xSTII::HIS3MX6 YCG1::3xFLAG::kanMX6 cdc15-2 ckb1::URA3MX6 ckb2::TRP1 [YCplac111-Smc4-NT::NLS::13xMYC]*
	D8002	*MAT***a** *smc4-7A::3xSTII::HIS3MX6 YCG1::3xFLAG::kanMX6 cdc15-2 ckb1::URA3MX6 ckb2::TRP1 [YCplac111-smc4-7A-NT::NLS::13xMYC]*
Fig. 11D	D7997	*MAT***a** *SMC4::3xSTII::HIS3MX6 YCG1::3xFLAG::kanMX6 cdc15-2 ckb1::URA3MX6 ckb2::TRP1 [YCplac111-Smc4-NT::NLS::13xMYC]*
	D8099	*MAT***a** *YCG1::3xFLAG::kanMX6 cdc15-2 ckb1::URA3MX6 ckb2::TRP1 [YCplac111-smc4-9A-NT::NLS::13xMYC]*
Fig. 11E	D7997	*MAT***a** *SMC4::3xSTII::HIS3MX6 YCG1::3xFLAG::kanMX6 cdc15-2 ckb1::URA3MX6 ckb2::TRP1 [YCplac111-Smc4-NT::NLS::13xMYC]*
	D8225	*MAT***a** *YCG1::3xFLAG::kanMX6 cdc15-2 ckb1::URA3MX6 ckb2::TRP1 [YCplac111-smc4-16A-NT::NLS::13xMYC]*

Fig. 12C	D4107	*MAT**a** SMC4*
	D3272	*MAT**a** SMC4::3xSTII::HIS3MX6*
	D3662	*MAT**a** SMC4::3xSTII::HIS3MX6 ckb1::URA3MX6 ckb2::TRP1*
	D7546	*MAT**a** smc4-9A::3xSTII::HIS3MX6*
	D8733	*MAT**a** smc4-S40A,S67A,S68A::3xSTII::HIS3MX6*
	D2653	*MAT**a** smc4-7A::3xSTII::HIS3MX6*
	D3666	*MAT**a** smc4-7A::3xSTII::HIS3MX6 ckb1::URA3MX6 ckb2::TRP1*
	D7550	*MAT**a** smc4-16A::3xSTII::HIS3MX6*
	D8736	*MAT**a** smc4-7A[S40A,S67A,S68A]::3xSTII::HIS3MX6*
Fig. 13A	D4094	*MAT**a** /MAT**α** SMC4/smc4-rxlA::3xSTII::HIS3MX6*
Fig. 13B	D4107	*MAT**a** SMC4*
	D2430	*MAT**a** ura3-1::YIplac211::URA3*
	D7983	*MAT**a** ura3-1::Psmc4-smc4-rxlA::3xSTII::HIS3MX6::URA3*
	D1821	*MAT**a** smc4-22::HIS3MX6*
	D2021	*MAT**a** smc4-22::HIS3MX6 ura3-1::YIplac211::URA3*
	D7926	*MAT**a** smc4-22::HIS3MX6 ura3-1:: Psmc4-smc4-rxlA::3xSTII::HIS3MX6::URA3*
Fig. 13C	D4107	*MAT**a** SMC4*
	D3272	*MAT**a** SMC4::3xSTII::HIS3MX6*
	D7983	*MAT**a** ura3-1::Psmc4-smc4-rxlA::3xSTII::HIS3MX6::URA3*
	D7926	*MAT**a** smc4-22::HIS3MX6 ura3-1:: Psmc4-smc4-rxlA::3xSTII::HIS3MX6::URA3*

Supplementary Figures

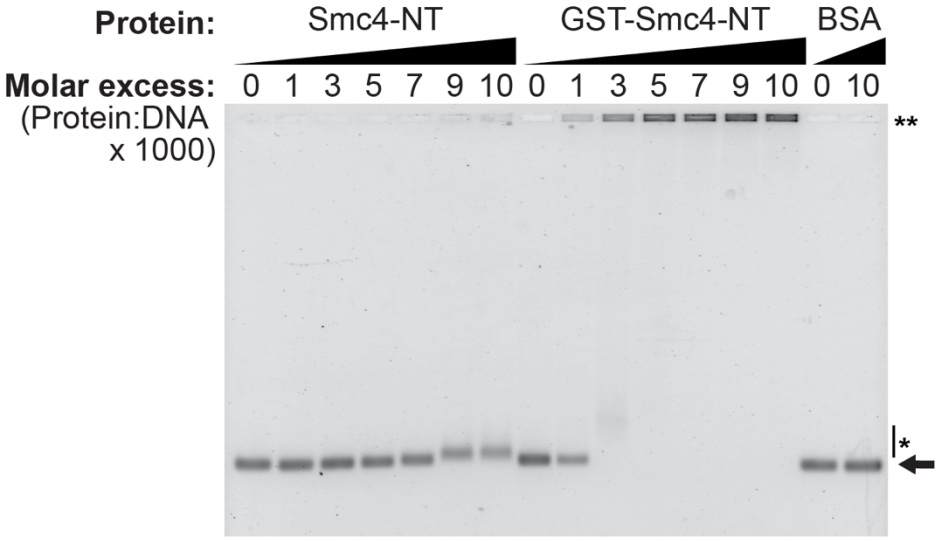

Figure S1. GST tag interferes with Smc4-NT DNA binding. EMSA with increasing molar concentrations of Smc4-NT or GST-Smc4-NT protein relative to 0.2nM ssDNA. DNA-protein complexes were resolved on a 1% agarose gel and visualized using SYBR Gold nucleic acid stain. BSA control lane shows a reaction of DNA substrate incubated with BSA at the highest equivalent molar excess to Smc4-NT. Arrow (←) points to free DNA, single asterisk (*) indicates partially bound DNA, and double asterisk (**) shows fully bound DNA.

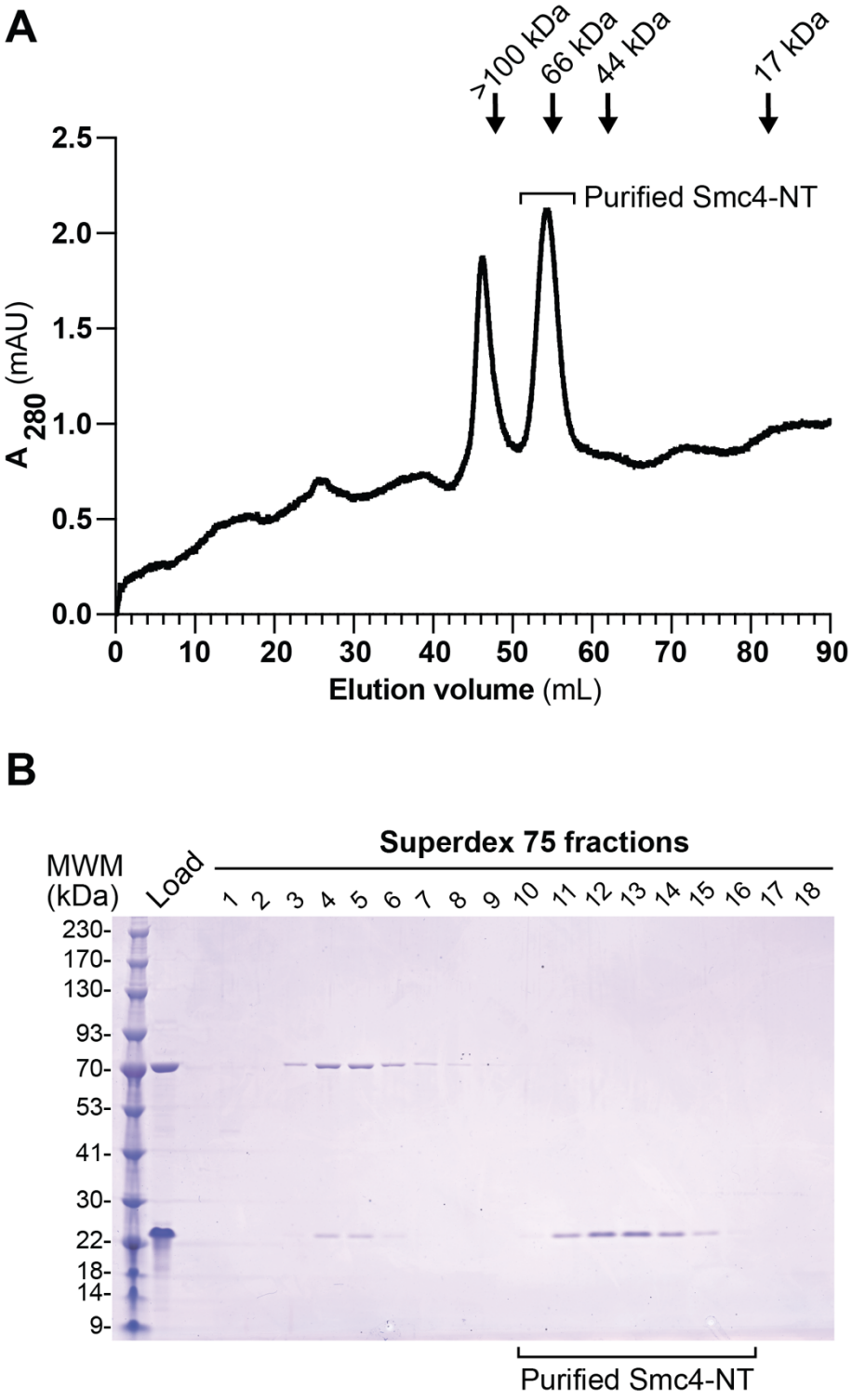

Figure S2. Apparent mass of Smc4-NT is higher than the calculated molecular weight of the protein construct. (A) The elution profile of the Smc4-NT protein from the last step of protein purification, gel filtration using Superdex 75 column, shows one major peak corresponding to Smc4-NT and one major peak corresponding to a contaminant. (B) Coomassie-stained gel showing collected elution fractions from

Superdex 75 that cover the region of both peaks. Load indicates concentrated sample from previous round of purification that was injected onto column. Fractions containing pure protein that were pooled and concentrated for further analysis are bracketed.